UNIVERSITY OF OKLAHOMA

GRADUATE COLLEGE

COMPARATIVE STUDY OF PROPRIETARY AND NON-PROPRIETARY ULTRA-HIGH PERFORMANCE CONCRETE AS PARTIAL-DEPTH JOINT REPLACEMENT

A THESIS

SUBMITTED TO THE GRADUATE FACULTY

in partial fulfillment of the requirements for the

Degree of

MASTER OF SCIENCE

By

KIM SEREY VUTH CHEA
Norman, Oklahoma
2020

COMPARATIVE STUDY OF PROPRIETARY AND NON-PROPRIETARY ULTRA-HIGH PERFORMANCE CONCRETE AS PARTIAL-DEPTH JOINT REPLACEMENT

A THESIS APPROVED FOR THE
SCHOOL OF CIVIL ENGINEERING AND ENVIRONMENTAL SCIENCE

BY THE COMMITTEE CONSISTING OF

Dr. Royce Floyd, PE, Chair

Dr. Jeffery Volz, PE, SE

Dr. P. Scott Harvey, PE

I would like to dedicate this thesis to my parents, Sereyrath Thon and Pheakdei Chea, for their unconditional love, inspiration, support, and always believing in me.

Acknowledgement

First and foremost, I would like to thank to express my gratitude to my advisor, Dr. Royce Floyd, for his unwavering support, for his patience, guidance, and confidence in me. I would also like to thank Dr. Jeffery Volz and Dr. P. Scott Harvey for providing guidance as committee members.

I am grateful to the team of undergraduate and graduate researchers and others that helped me throughout completing this thesis. Especially, a massive thank you to Mike Schmitz, Trevor Looney, Jacob Choate, Stephen Roswurm, Conor Casey, Mujtaba Ahmadi, and Phuoc Huynh. I would also like to thank ODOT for funding this project, Lafarge North America for donating Ductal®, and Dolese Bros. Co. for donating cement, aggregate, and Glenium.

Last but not least, I would like to thank my friends, and family for supporting me throughout this process. I would not be here today if it were not for their love and motivation.

Table of Contents

List of Tables

List of Figures

Abstract

Ultra-High Performance Concrete (UHPC) is a special type of concrete that has unique properties that are desirable for various types of construction projects. The most common form of UHPC used in the field is a proprietary UHPC product, which is much more costly than normal strength conventional concrete. Due to the expensive nature of the proprietary UHPC, research studies have been conducted to produce comparatively more affordable alternative non-proprietary UHPC made from local and readily available materials. This paper presents comparative studies of proprietary and non-proprietary UHPC as partial-depth bridge joint replacement. The proprietary UHPC product used in this study is manufactured by LafargeHolcim under the name Ductal® and the non-proprietary UHPC is the J3 mix developed previously at the University of Oklahoma. The nature of this study was comparative, hence all methods and tests performed were similar to previous studies conducted at the University of Oklahoma.

Having reviewed relevant literature, six pairs of slab specimens were cast using normal-strength conventional concrete before joining each pair with a half-depth, heat cured UHPC joint once the conventional concrete slabs achieved the design strength. Three joint specimens were constructed using both proprietary and non-proprietary UHPC. These half-depth jointed slab specimens were tested both statically to failure and cyclically using service level loads. This research produced encouraging results regarding the UHPC alternative. All slab specimens exceeded the calculated failure load for a monolithic normal-strength concrete slab potentially due to the supplementary strength provided by the UHPC joint. The cracking loads for half-depth specimens were lower than those of full-depth specimens from previous research. In addition, the

half-depth J3 specimens had smaller cracking loads compared to the Ductal® half-depth specimens. All half-depth specimens produced a comparable performance to full-depth specimens regarding flexural capacity. For cyclic testing, there was limited change in stiffness over time unless the maximum cyclic load was increased. The conclusions made from this study indicate that the non-proprietary UHPC alternative, J3, is a suitable repair material for bridge joints and can achieve similar performance to proprietary UHPC for certain applications.

1) Introduction

Bridges are essential components of a nation's transportation system. They are constructed to provide passages over obstacles such as other roads, railroads, rivers, creeks, or streams. They also provide links between roads to help reduce congested traffic. These bridges are commonly built from two most common construction materials, steel and concrete. The importance of bridges is unquestionable, and they need to be carefully looked after, maintained, and repaired to prolong their lifespan and usage. Unfortunately, a recent study conducted by the American Society of Civil Engineers (ASCE) in 2017 concludes that 8.8% of all bridges in the United States are structurally deficient. According to Infrastracture.org, the grade for America Infrastructure is a "D+". In support of this claim, ASCE in 2012 gave a rating of "C+" to all the bridge infrastructure. Some of these deficient bridges need to be rebuilt or repaired. However, government funding has been limited and improvement of the deficient bridges' quality is slow. This challenge also allows Departments of Transportation (DOTs) of various states an opportunity to be creative and cost effective. Studies have been conducted to find solutions for bridge repairs and construction that are cheaper and more affordable, but maintain adequate, or improved, performance and longevity. Failed expansion joints are a major issue for bridges in Oklahoma. According to Peters (2018), at that time there were 47 miles of failed expansion joints in Oklahoma.

This research study assessed the feasibility of using Ultra-High Performance Concrete (UHPC) as a repair material for bridges in Oklahoma and performance of one specific UHPC joint detail. UHPC is a type of concrete that has special properties such as very high compressive strength (21.7 ksi defined by the Federal Highway Administration), excellent durability, high post-cracking tensile strength (0.72 ksi defined by the Federal Highway Administration), and

various advantageous properties that can be utilized as connections and in bridge repairs. Despite its high cost compared to most types of concrete, there is potentially a benefit when used in small quantities for applications such as bridge joints or repairs. Its high durability allows for long-lasting structures in comparison to conventional concrete. This allows for decreasing the volume and frequency of repairs and maintenance throughout the life span of a structure. Since UHPC is a considerably new material and its applications are still limited, further studies are needed to identify how to best utilize its excellent properties and for which applications it would be most suitable.

1.1) Purpose of This Research

In Oklahoma, the Oklahoma Department of Transportation (ODOT) is funding research related to the use of UHPC in bridge expansion joint rehabilitation and replacement. Most readily available UHPC materials are prepackaged proprietary formulations. The most common product is manufactured by LafargeHolcim under the name Ductal®. However, this product is very expensive. Alternative UHPC mix designs made from available local materials are becoming more common and ODOT has expressed interest in a locally available mix design. The main purpose of this study is to compare the performance of a common proprietary and locally developed non-proprietary UHPC used as a half-depth expansion joint replacement subjected to flexural and cyclic loads. There are obvious benefits of implementing half-depth joints instead of full depth joints. Half-depth joints require less volume of UHPC and this helps reduce expenditures on materials. Another benefit is that half-depth joints' formwork is more easily constructed on bridges that cross rivers or streams since the slab can act. The results of this study of the half-depth joint is compared with previous research conducted at the University of

Oklahoma by Funderburg (2018) and Coleman (2018). These previous studies were based on full-depth UHPC joint with a similar design.

1.2) General Overview

UHPC applications only made great strides commercially recently. UHPC became commercially available in the United States in the year 2000 and its applications have expanded ever since (Graybeal 2014). UHPC consists of 4 main constituents, which are dry components, chemical admixtures, water, and steel fiber reinforcement (Graybeal 2011). Dry components make up the majority of UHPC constituents. Generally, portland cement, silica fume, and fine aggregates are the primary dry components. However, small coarse aggregates and supplementary cementitious materials can also be included in some UHPC mixture designs. UHPC has a water-to-cementitious materials ratio less than 0.25 and, and a high percentage of steel fiber reinforcement. As a repair material, UHPC has demonstrated its capability in helping deteriorated conventional concrete structures that face issues such as cracking, low durability, and freeze-thaw degradation. The advantages of UHPC include high compressive strength, excellent durability, high flowability, negligible permeability, and self-consolidation.

UHPC construction is generally similar to conventional concrete with slight adjustments. The mixing procedure requires higher energy input and a longer mixing time. However, a conventional concrete mixer can still be used as long as the mixing time is increased to input the required energy. UHPC takes longer to set than most types of concrete. Hence, heat curing is often used to shorten the set time and allow for the concrete to exponentially increase its compressive strength in a shorter time period. Generally, a compressive strength of 14 ksi is considered sufficient for the concrete to be put in service as it reaches an acceptable hydration level (Graybeal 2011). Because of its advanced properties, modified quality control testing

procedures are required for UHPC. For instance, a load rate of 150 psi/s is more applicable for compressive strength tests rather than the typical range of 28 to 42 psi/s for conventional concrete (Graybeal 2011). In addition, mortar flow tests are considered more suitable than slump tests due to the self-consolidating properties of UHPC.

1.3) Previous Implementation

UHPC has only been commercially available in the United States for about 20 years. Despite its relatively new arrival, its applications have been prevalent in tee beams, girders, and joints between deck panels (Graybeal 2013). UHPC applications in new structures are more popular than usage as a repair material in the rehabilitation of aging structures. Extensive studies have focused on the feasibility of using UHPC in joints between precast members. However, there are limited studies on UHPC applications as repair materials. Future studies should continue to emphasize the feasibility of using UHPC to prevent and sustain aging structures from deteriorating.

1.4) Research Conducted

To achieve the stated goals and objectives, this research focused on determining the flexural capacity and analyzing the effect of fatigue loading on flexural strength over time through the application of static and cyclic loads on full-scale slab specimens. The slab specimens were constructed from two panels of conventional concrete joined by a half-depth UHPC joint. The slab specimens are representative of a bridge with joints repaired with UHPC. There were 6 total slab specimens constructed for the research. Three slab specimens were constructed with a joint using non-proprietary UHPC named J3 with the mix design developed by Looney et al. (2019). Three slab specimens were constructed with a joint using proprietary UHPC, which was manufactured by LafargeHolcim under the name Ductal®. Four slab

specimens were tested statically with two specimens each from the J3 and Ductal® joints. Two slab specimens were tested cyclically with one specimen each from the J3, and Ductal® joints.

1.5) Goals and Objectives

One goal of this research was to explore the possibility of using alternative UHPC mix designs that are more affordable and practical for construction and repair. Another goal was to analyze performance of a half-depth detail for bridge deck expansion joint replacement and compare the results with tests of full-depth joints as well as examine the practicality of implementing UHPC for joint repair in Oklahoma. The following are the main objectives for this study:

a) Replicate large-scale testing from previous research for half-depth slab joints and compare the results to the study of full-depth slab joints (Funderburg 2018 and Coleman 2018)
b) Compare the results of proprietary and non-proprietary half-depth UHPC joints and determine if non-proprietary UHPC can provide similar or better performance than proprietary UHPC
c) Provide recommendations to ODOT on use of non-proprietary UHPC for future construction or repair

2) Literature Review

2.1) Overview

This section provides summaries of relevant literature that relates to the application of UHPC, both proprietary and non-proprietary mix designs, for bridge deck and beam repairs. UHPC has been studied extensively to determine its suitability for repairs and other special usage. The results have been promising and additional studies are and will be conducted to further expand its applications. UHPC is well known for its high compressive strength, use of steel fibers, and its darker grey color compared to conventional portland cement concrete. There are four main material components that UHPC is composed of. These include fine sand, steel fibers, superplasticizer (High Range Water Reducer), and cementitious materials. Silica fume is almost always included in addition to traditional portland cement. Additional supplementary cementitious materials or fillers such as fly ash, slag cement, limestone powder, or ground quartz are added to achieve required performance. No coarse aggregate is included and components such as steel fibers, and superplasticizer are not typically found in conventional concrete; hence, the characteristics of UHPC such as flow (slump test) and consolidation are different from conventional concrete. The high cost of prepackaged (proprietary) mixtures has prompted various studies to focus on local and lower-cost UHPC mixtures. Its high durability and excellent bond strength also encourage more studies on connections and repairs using UHPC. It is important to stress that UHPC is still a relatively new discovery, and most of its application is for high-strength, flexible, or aesthetically pleasing architectural structures. However, UHPC usage is increasing, more research is being conducted, and the material further developed. The following sections discuss previous studies and findings that help narrow the current research

focus. Figure 1 shows UHPC transported to a site for field casting and placement. Figure 2 depicts the longitudinal connections using UHPC after field-casting.

Figure 1: Field-casting and placement of UHPC (Graybeal 2010)

Figure 2: Longitudinal connections using UHPC (Graybeal 2010)

2.2) Alternative UHPC Mix Designs

Alternatives to proprietary UHPC are desired due to the high cost of prepackaged mixtures and the desired flexibility of local mix designs. The development of non-proprietary UHPC has been steady to produce a desirable performance at a lower cost. Looney et al. (2019) tested various mixes to determine the effect of multiple variables on performance of UHPC and identify a mix design meeting the required material properties. One of the most important factors that influence UHPC performance is water-cementitious materials ratio. Others are particle packing and cementitious material reactivity. Yu et al. (2014) concluded that the low water/binder ratio and relatively large cement content produces a small degree of hydration. Cheaper filler materials such as limestone and quartz powder can be used to improve workability and enhance the efficiency of steel fibers and binder (Yu et al. 2014). Superplasticizers also play an important role and could affect the water-cementitious materials ratio. The purpose of superplasticizers is to reduce the amount of water required for adequate workability and help optimize particle packing. Wang et al. (2017) concluded that high water to binder and superplasticizer dosage lead to high flowability and decrease the yield stress. Supplementary cementitious materials such as silica fume increase the bond strength and density of the cement paste. Looney et al. (2019) also discuss the importance of heat curing to increase the early age strength of UHPC. They determined an optimum time to cure the specimen of 36 hours at 194°F (90°C), which produced the same compressive strength as at 28 days without heat curing. The non-proprietary UHPC developed by Looney et al. (2019) did not achieve or surpass the compressive strength value (21.7 ksi) defined by the Federal Highway Administration (FHWA) definition for UHPC, but exhibited other properties meeting the FHWA definition. Table 1 indicates the non-proprietary J3 UHPC mix design developed by Looney et al. (2019).

Table 1: Non-proprietary J3 UHPC, mix proportions by weight (Looney et al. 2019)

Material	Amount per yd^3
Fine Masonry Sand	1966 lb
Slab	590 lb
Silica Fume	197 lb
Type 1 Portland Cement	1180 lb
Water	393 lb
Steel Fiber	265 lb
Glenium 7920	18 oz./cwt

2.3) Steel Fiber Reinforcement

The benefit of including small steel fibers in UHPC is the increase in ductility and post-cracking tensile strength. Most UHPC mixes contain 1% to 3% steel fibers by volume to obtain desired mechanical properties. In general, the higher the fiber percent, the greater the strength. The influence of superplasticizers, water-cement ratio, and casting methods can affect the outcome of the steel fibers on mechanical properties. Wang et al. (2017) indicate that the fibers need to be dispersed throughout the specimen and evenly distributed to provide the greatest benefit. To achieve the even distribution, all the fibers must be fully submerged, and the matrix must have adequate flowability and viscosity to suspend the fibers. Wang et al. (2017) conclude that the increase of fiber percentage from 1% to 3% "reflect worse dispersion of steel fibers in UHPC." They theorize that it is caused by the lack of cement paste for covering the surface of each fiber and lower mobility of steel fibers in the mixtures. Despite the strength correlating with

percent of fibers, a moderate percent of fiber (1% to 3%) is desired for workability purposes. Figure 3 shows the most common type of steel fiber reinforcement.

Figure 3: Typical steel fiber reinforcement (Graybeal 2014)

2.4) Surface Preparation and Bond Angle

The ability of UHPC to bond to conventional concrete will depend on surface preparation along with properties of the UHPC. The greater the bond strength, the better the performance, which can reduce the chance of needing further repair in the future. Surface preparation is essential for adequate bond between two structures. Murugesan (2014) states that "To improve the bond strength, it is common to increase the roughness of the substrate surface." Besides the roughness and bonding agents, temperature and humidity can also influence the bond strength. Before connecting UHPC to a substrate surface, the surface needs to be roughened, pre-wetted, and cured sufficiently. Murugesan (2014) also indicates that the curing process plays an important role because the bond strength between concrete layers can be increased if the

compressive strength of the concrete increases. Julio et al. (2004) indicate that sand-blasting and wet-jetting also known as wet abrasive blast are the best surface preparation methods. Several tests can be used to determine the bond strength. These include the pull-off test, direct tension test, split cylinder test, direct shear test, and slant shear test. Graybeal (2014) specifies that pre-wetting the precast concrete interface to a saturated surface dry (SSD) condition before casting UHPC will improve bonding. A study by Tayeh et al. (2013) indicated that the bond strength between normal concrete and UHPC is "stronger than the cracking strength of normal concrete". Tayeh et al. (2013) also agree with Julio et al. (2004) that sand-blasting provides the best surface preparation for achieving the highest bond strength. Figure 4 shows an exposed aggregate surface finish commonly used for new construction.

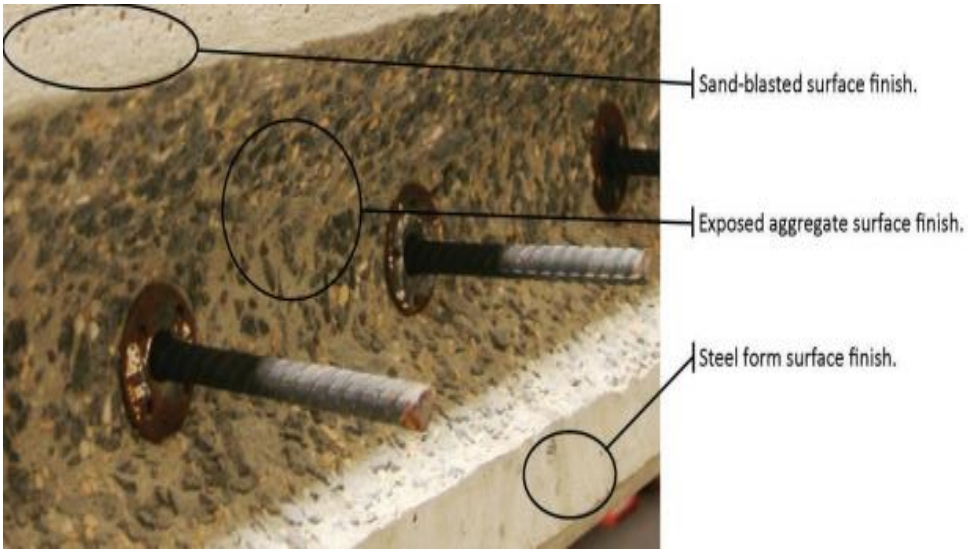

Figure 4: Exposed aggregate surface finish on a precast concrete component (Graybeal 2014)

2.5) Material Fatigue and S-N Curve

When a material is subjected to varied stress over time, it will fail below its ultimate strength. This phenomenon is known as material fatigue, which has tremendous impact on bridge

design. The constant movement of vehicles on top of the bridge as well as dynamic loads applied on the bridge deck slabs could impact the lifespan and its longevity (Zhang et al., 2018). The structural failure tends to occur at a lower ultimate strength, which potentially costs valuable property and human lives. The mechanism of how material fatigue occurs is due to the formation and propagation of cracks. Firstly, cracks form due to the concentration of stress, which in turn causes the crack to grow larger until critical fracture occurs. Determining the likelihood of how a material or structure fails in fatigue is accomplished by running a fatigue test. Fatigue tests can be performed on a specimen through a constant amplitude of stress through multiple test cycles and counting the number of cycles until it is fractured. The test can be repeated by applying variety of stress ranges to accumulate enough data for plotting. By plotting the stress versus the number of cycles to failure, the material failure stress can be determined from the best fit curve, which is also known as S-N curve. Graybeal (2010) performed cyclic tests on UHPC bridge deck connections to determine the structural response measured by electronic gauges and to examine fatigue performance for the overall slab joint. Each specimen consisted of two precast concrete panels connected by a proprietary UHPC joint. At least 2 million cycles of sinusoidal cyclic load ranging from 2 to 16 kips (cracking load was 16 kips) were applied on 4 specimens and only one specimen exhibited structural cracking. Graybeal (2010) concluded that the support conditions and loading conditions for the cyclic test produced stresses “more severe than would traditionally be observed in a concrete bridge deck under similar magnitude wheel loads.” The conclusions from instrumental configurations will be explained and shown in the following section.

2.6) Previous Studies on UHPC Slab Joints

Previous research on UHPC joints, including static and cyclic tests, was conducted by Graybeal (2010). Six UHPC slab joint specimens were constructed and tested in both transverse and longitudinal connection configurations. The specimens would undergo cyclic testing of at least 2 million cycles loaded below the cracking strength, and then followed by at least 5 million cycles to a load higher than the cracking strength. The specimen would be loaded statically until failure had it not failed due to the cyclic test. Figures 5 and 6 show the setup of the cyclic test, for the longitudinal, and transverse configurations. In terms of half-depth joints previously studied, Graybeal (2014) conducted research on UHPC connections between deck panels and steel girders. The conclusions were that the composite structure possessed adequate structural performance under fatigue, service, and strength loadings through laboratory testing.

Figure 5: Cyclic test setup for longitudinal UHPC connection (Graybeal 2010)

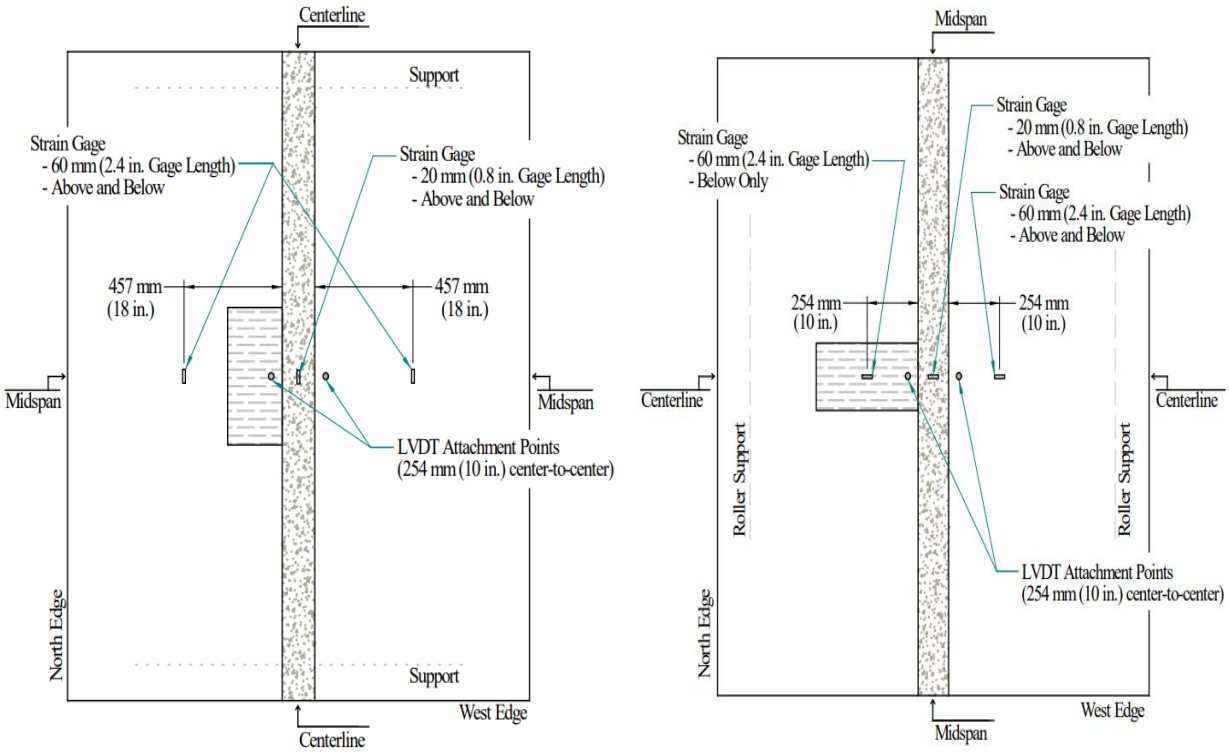

Figure 6: Transverse joint (left) and longitudinal joint (right) configurations tested by Graybeal (2010)

The conclusions from this study were valuable in applications of cyclic tests in future studies. This study indicated that a UHPC joint bonded well with the precast concrete and illustrated favorable cracking behavior without de-bonding at the interface. Both transverse and longitudinal connections exhibited adequate performance relative to bonding UHPC to conventional concrete. Lastly, the cracking behavior of the specimens would not necessarily be affected by the cyclic load slightly less or slightly above the cracking load (Graybeal 2010).

2.7) Coleman, and Funderburg (2018)

In 2018, Coleman (2018) and Funderburg (2018) conducted studies on full-depth proprietary and non-proprietary UHPC deck slab joints as a repair for bridges in Oklahoma. The goals of those studies were to determine the practicality of using UHPC instead of conventional

concrete due to its advanced mechanical properties and to determine if non-proprietary UHPC can be substituted for the more expensive proprietary UHPC. Aging bridges in Oklahoma are a significant problem and UHPC could be a highly effective and low-cost solution. Coleman's study focused on a non-proprietary UHPC mix design developed at the University of Oklahoma by Looney et al. (2019). Funderburg's study focused on proprietary UHPC, which was the LafargeHolcim product Ductal®. Three slab specimens were fabricated in each study to evaluate flexural capacity and the effects of static and cyclic loading on joint interfaces. All three slab specimens in each study possessed a flexural load that exceeded the calculated failure load for a monolithic conventional concrete when statically tested. This was potentially caused by the additional strength provided by the UHPC joint.

2.8) Summary

UHPC applications have been implemented in precast structures and new construction. Due to its availability in the US market for 20 years, its mechanical properties and casting and placement techniques are becoming more familiar to DOTs and contractors and have been studied and tested extensively. However, evaluations and assessments of the application of UHPC as a joint repair material are limited. The limited information about UHPC usage as a repair material was the main source of motivation for this research study. There are few studies that focus on the application of static and cyclic loading in flexure to determine the behavior of non-proprietary UHPC joints. Studies on half-depth UHPC joint are even fewer. These voids in information serve as a starting point for the research conducted in the current study.

3) Approach, Methodology, and Testing

The purpose of this section is to outline the approach and methodology used to conduct the research for this project. All of the specimen construction and testing took place at Donald G. Fears Structural Engineering Laboratory on the University of Oklahoma campus. Firstly, there is discussion of the fabrication of the formwork and the rebar orientation. Next, the discussion focuses on the casting and curing of slab specimens for both proprietary and non-proprietary UHPC. Lastly, the discussion shifts its focus towards instrumentation and testing.

3.1) Formwork Construction and Rebar Orientation

Before casting the slab specimens, six wooden forms were fabricated with interior dimensions of 4 ft x 4 ft x 8 in. However, the forms allow the specimens to have a cut-off section dimension at one end of 4 ft x 8 in. x 4 in. for joint connections as shown in Figures 7 and 8. The cut-off section allowed for exposure of the top reinforcement that would be used to connect the two slabs with UHPC with a half-depth joint.

Figure 7: Slab formwork and steel reinforcement

Figure 8: Formwork prepared for concrete casting

Three slab joint specimens in total were constructed for each UHPC material and each was fabricated from two normal strength concrete panels with dimensions of 4 ft x 4 ft x 8 in. and a cut-off dimension of 4 ft x 8 in. x 4 in. The normal strength concrete slabs were spaced 2 in. apart and the UHPC joints cast between the normal strength concrete slabs formed a T-shape from elevation view (see Figure 10). Slab reinforcement was spaced to match the deck reinforcement in an existing bridge in Oklahoma. Number 5 steel reinforcing steel bars were used for all slab reinforcement and the formwork design allowed the reinforcing bars to protrude 7 in. from one end in the cut-off portion to allow for bar splices between the slabs, as shown in Figures 9 and 10. Lifting hooks were tied to the steel reinforcement in each slab to allow for the movement of the heavy slabs.

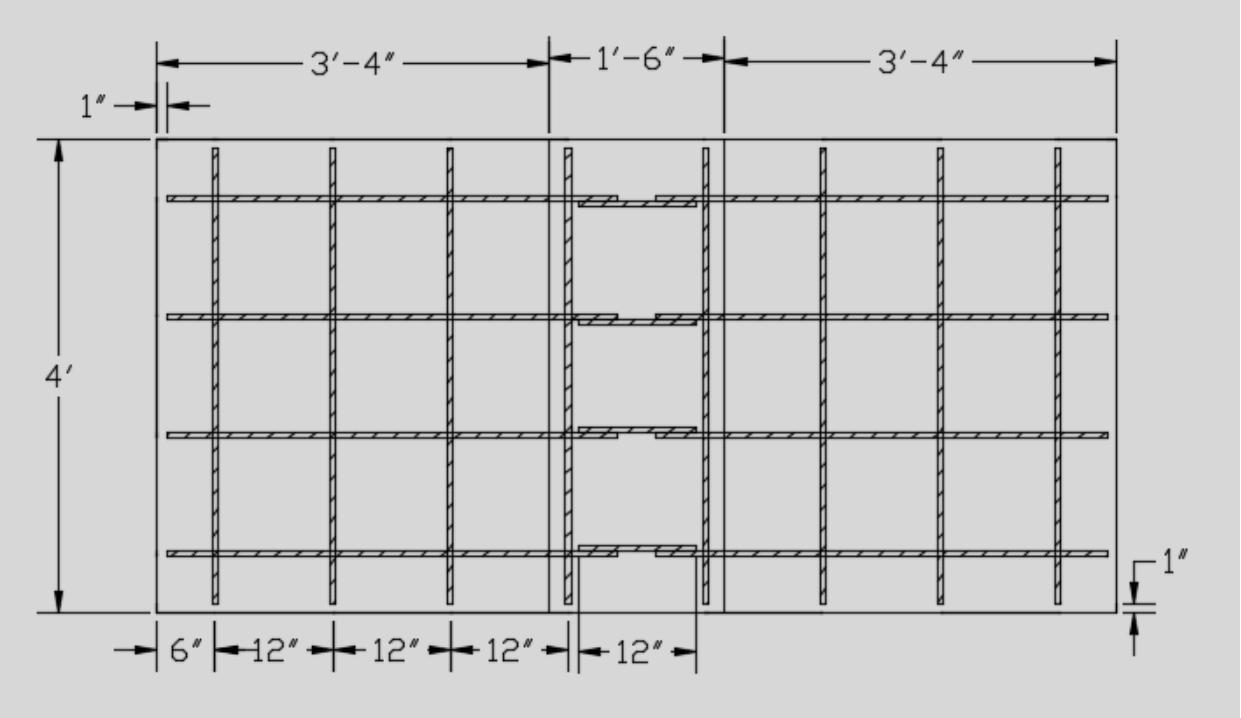

Figure 9: Plan view of reinforcement of slab specimens

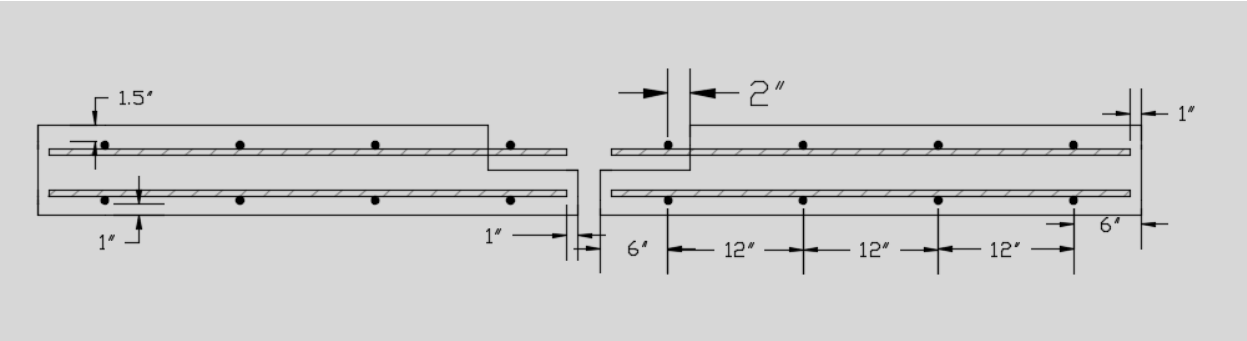

Figure 10: Elevation view of reinforcement excluding splice bar between slab specimens

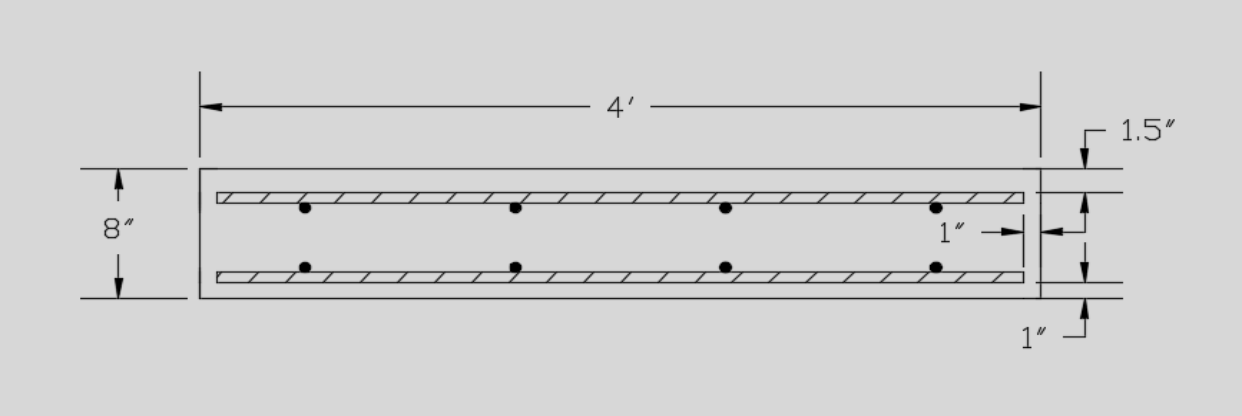

Figure 11: Cross-sectional view of reinforcement for slab specimens

3.2) Construction of Slab Specimens

3.2.1) Casting Conventional Concrete

A total of 6 slab joint specimens were constructed to examine the behavior of proprietary and non-proprietary UHPC joint connections. Before the UHPC joints were cast, twelve conventional concrete slab sections were cast first and allowed to reach adequate strength (taken as 28 days of age with a target of 4000 psi). The conventional concrete was an ODOT Class AA concrete mixture designed, mixed, and transported by Dolese Bros. Co. due to the large volume required for this study. The concrete arrived at Donald G. Fears Structural Engineering Laboratory already mixed and ready to be poured into the slab formwork. Finishing work was required at the top surface as shown in Figure 12 before a final broom finish was applied. Completeted slabs are shown in Figure 13.

Figure 12: Finishing application on the top surface of the slab

Figure 13: Side-by-side slabs after finishing applied

Next, the concrete slabs were covered with wet burlap and a plastic tarp to allow for moisture retention when the concrete was curing. A total of 24 cylinders were also cast from the same conventional concrete mixture. 12 cylinders were used for testing compressive strength of conventional concrete for non- proprietary UHPC joint connections. The other 12 cylinders were used for testing compressive strength of conventional concrete for proprietary UHPC joint

connections. These cylinders were 4 in. in diameter by 8 in. in height. Figures 14 and 15 show the slabs covered in burlap and a plastic tarp.

Figure 14: Concrete panels curing covered by wet burlap

Figure 15: Plastic tarp covering curing concrete panels

3.2.2) Joint Formwork and Strain Gauge Installation

After the conventional concrete reached adequate strength (taken as 28 days of age), the conventional concrete panels were positioned 2 in. apart so that splice bars could be placed across the exposed bars on each slab to connect the two panels as shown in Figure 16. The formwork was constructed spanning across the two panels to create the 18 in. wide joint and allow for UHPC to be poured in. Next, foil strain gauges were installed on the protruding bars and splice bars to observe the changes in reinforcing bar strain during testing as shown in Figure 16. Before the strain gauges were installed, the protruding and splice bars were smoothened using an angle grinder and sandpaper. Figures 18 and 19 show the smoothed splice bars and the location of the strain gauges installed.

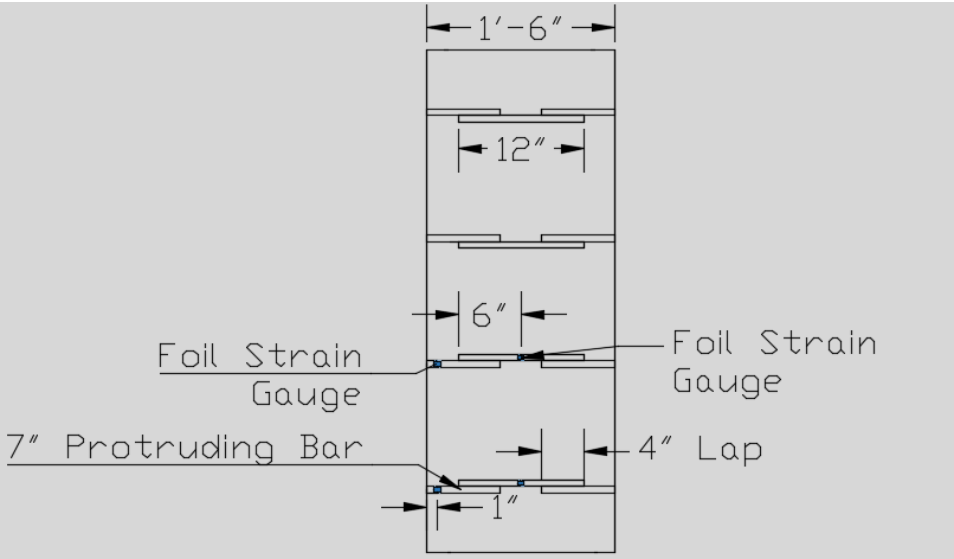

Figure 16: Plan view of UHPC joints with foil strain gauge

Figure 17: Smoothing splice bar with an angle grinder

Figure 18: Splice bars ready for strain gauge installation

Figure 19: Two slab panels with formwork in place and strain gauges installed

3.2.3) UHPC Mixing and Casting

The UHPC was mixed using a large horizontal axis high-shear mixer available at Donald G. Fears Structural Engineering Laboratory. The non-proprietary UHPC mix design was based on the study by Looney et al. (2019). This mix design was given the name, J3, and the mix proportion could be seen in Table 1. The proprietary UHPC was the LafargeHolcim product Ductal®. UHPC was transported from the mixer to the joint formwork using a concrete transfer bucket and overhead crane. UHPC was poured into the forms and allowed to self-level, as shown in Figures 20 and 21. No consolidation was applied to the UHPC material. The width of the top half of the UHPC joint (the half-depth portion) was 18 in. and UHPC was allowed to fill the 2 in. between the bottom halves of the slabs. No reinforcement was placed to connect the bottom halves of the slab. The slab joints were slightly over-poured (approximately 0.25 in.) so air bubble formation on the top of the joints occurred in the over-poured surface and not in the main part of the joints. Two sets of 12 cylinders were cast for testing compressive strength of UHPC.

A total of 12 cylinders were cast from the same J3 non-proprietary UHPC mixture, and the other 12 cylinders were cast from the same Ductal® proprietary UHPC mixture. These cylinders were 3 in. in diameter by 6 in. in height.

Figure 20: Placement of UHPC connecting two slab panels

Figure 21: Self-consolidating UHPC filling the joints

3.2.4) Heat Curing

Copper tubing was embedded in the UHPC joints and thermocouples were installed to monitor the temperature of the joints during heat curing.

The non-proprietary UHPC joints were heat-cured for 36 hours with heat lamps installed at 16 in. above the top surface of the joints to ensure constant heat was provided throughout the joints as determined by Coleman (2018) and the internal temperature was approximately 200°F. The proprietary UHPC joints were cured using the same setup but for a duration of 12 hours and the internal temperature was approximately 180°F. Heat resistant plastic sheeting was placed over the UHPC joints to retain moisture during. Companion cylinder specimens were placed alongside the joints to be subjected to heat curing as well. At the end of the 36 or 12 hour curing period, the heat lamps were removed, and the joints were allowed to cure under ambient laboratory conditions for at least 28 days before testing. Figure 22 shows the setup of the heat lamps and the UHPC joints being cured.

Figure 22: Heat lamp setup to cure UHPC

3.3) Slab Testing

Once the joints reached 28 days of curing, the slab joints were ready to be tested. Each slab was flipped with its orientation for testing as shown in Figure 23 to represent negative moment occurring over a bridge pier. Each slab was positioned within a steel portal frame supported by concrete beams and 6 in. wide rubber pads at each end. Each specimen was tested using a hydraulic ram and pump. Deflection was measured on both sides of the joint and at the rubber pad supports using 7 linear variable differential transformers (LVDTs) or using a combination of LVDTs and wire potentiometers (pots). These LVDTs were placed underneath the slab in different positions as shown in Figure 24, except for LVDT 1 which was included inside the MTS hydraulic cylinder. The strain gauges described in Section 3.2.2 were also used to measure strain in the reinforcing bars within the joint during the test. These gauges were installed on two of the splice bars and two of the protruding bars on the load side of the joint as shown in Figure 15. The difference in overhang on each end of the slab as shown in Figure 24 is due to the location of the support pads and LVDT 1. The support pads' location was based on the slabs tested by Coleman (2018) and Funderburg (2018), which were 10 in. longer.

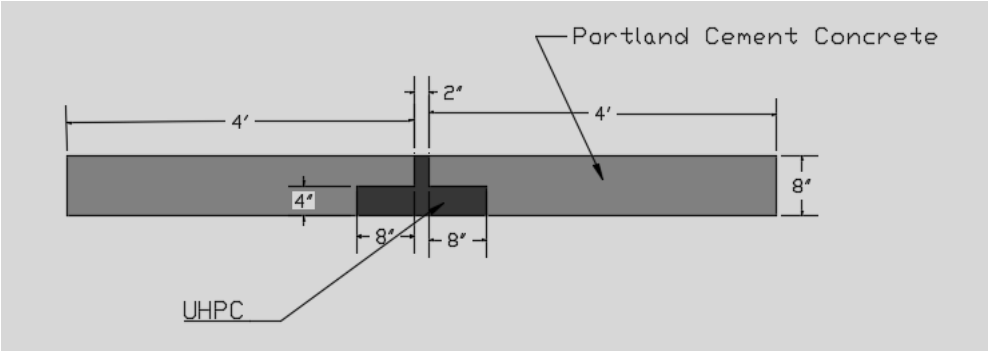

Figure 23: Elevation view of slab orientation during testing

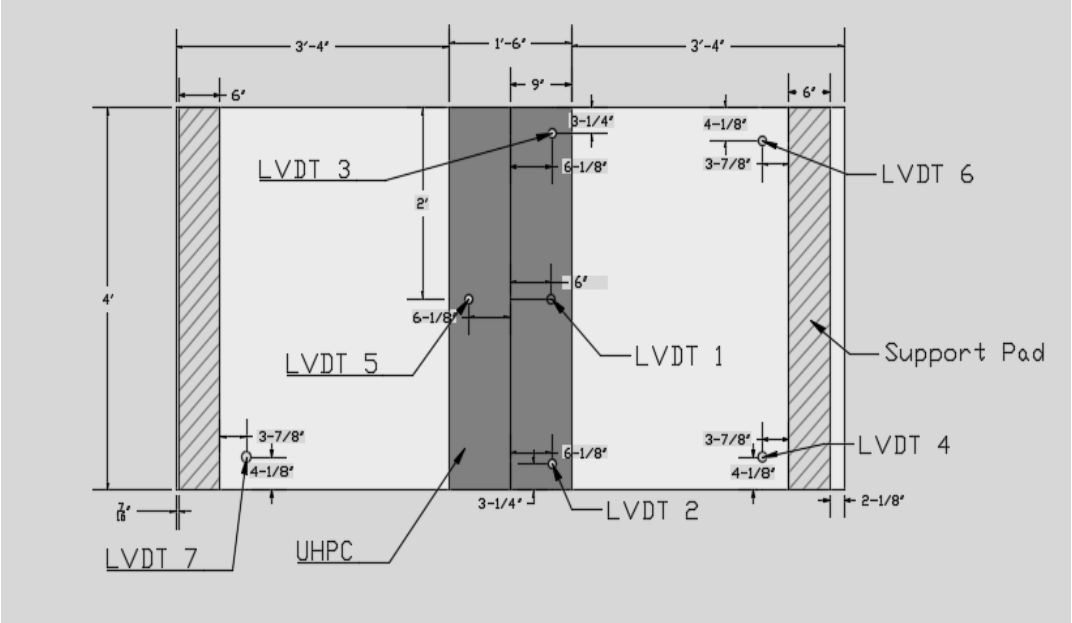

Figure 24: LVDT layout for slab testing

Slabs 1 and 2 with non-proprietary UHPC joints were tested using an MTS hydraulic ram with a maximum capacity of 22 kips. A load cell was used to measure the load, and the load was applied through a 10 in. by 20 in. metal plate on top of a rubber pad. Both slabs were loaded in 1-kip increments up to the maximum capacity of the MTS. Once the MTS capacity was reached, the slab was unloaded and the MTS was replaced with a manually controlled hydraulic cylinder and pump with a capacity of 50 kips. The slabs were then reloaded again to failure. In addition, the three LVDTs around the joint were replaced with wire pots to provide more deflection measurement capacity and prevent damage to the LVDTs. The slabs were then loaded until flexural failure using 1-kip load increments. The results of the tests of slab 1 and 2 were used to plan the loading used for slab 3.

Figure 25: Test setup for slabs using the MTS hydraulic ram

Figure 26: Test setup for slabs using the manually controlled hydraulic cylinder and pump

Slab 3 with the non-proprietary UHPC joint was cyclically loaded using the MTS hydraulic ram. The 7 LVDTs were installed in the same positions as used for slabs 1 and 2. A total of 3 million cycles were applied to this slab with minimum cyclic load of 500 lb and maximum cyclic load of 90% of the cracking load (which was 5.3 kips) observed during the slab 1 and 2 tests. After 3 million cycles were completed, the maximum cyclic load was increased to 110% of the cracking load (which was 6.5 kips) observed during the Slab 1 and 2 tests. This test was run for 850,950 cycles and the slab did not deflect enough to fail. The decision was to increase the maximum cyclic load to 8.7 kips. This value was loosely based on the maximum load for cyclic test performed by Funderburg (2018) and Coleman (2018). The test was then run for another 473,425 cycles without failure.

The same set of slab tests was repeated for the proprietary UHPC slab joints and the results were compared for the half-depth joints and to the previous tests of full-depth joints (Funderburg 2018 and Coleman 2018). Slabs 1 and 2 for proprietary UHPC joints were tested using a manual hydraulic pump to failure without the initial loading done for the non-proprietary joint specimens because the MTS system broke down during the campus closure resulting from the coronavirus pandemic. They were loaded in 1-kip increments up to the deflection capacity of the manual hydraulic pump. For part 2 of testing, the slabs were loaded with 3-kip increments instead of 1-kip increment until the slabs failed. Part 2 of testing was necessary because part 1 loading exceeded the extension capacity of the hydraulic ram.

Slab 3 with proprietary UHPC joint was cyclically loaded using the MTS hydraulic ram. The cyclic test was performed the same way as slab 3 with non-proprietary UHPC joints. However, the cyclic test could not be completed due to the unavailability of MTS hydraulic ram

until late October 2020. The slab was tested cyclically for 3 million cycles, and the results were analyzed over a representative period of time to compare stiffness between the slab joints.

4) Test Results and Discussion

4.1) Compressive Strength Results

4.1.1) Conventional Concrete of Slab Panels for J3 Joint Specimens

The six slab panels for each series of joints were poured at the same time using the same mix that was batched and delivered to Fears Lab by Dolese Bros. Co. The compressive strength of each cylinder and the average of the three specimens exceeded the desired 4000 psi at 28 days (Table 2). The cylinders were 4 in. in diameter by 8 in. in height. Test day is defined as the day that the cyclic test began for this study, which applies to other compressive strength results in the following tables.

Table 2: Compressive Strength (psi) for Conventional Concrete of Slab Panels for J3 Joints

Age	Specimen 1	Specimen 2	Specimen 3	Average
1-Day	923	1796	1424	1380
7-Day	3545	3367	3062	3330
28-Day	4974	4618	4486	4690
Test Day	4258	4266	4129	4220

4.1.2) J3 Non-proprietary UHPC Mixture

When the conventional concrete slab panels intended for the J3 joints gained sufficient strength (taken as 28 days or more), J3 non-proprietary UHPC was cast in the joints. All the UHPC joints were cast and poured at the same time using the same batch. The joints were heat-cured for 36 hours before they cured at ambient temperature for the remainder of the 28 days and until testing. Compressive strength results are presented in Table 3.

Table 3: Compressive Strength (psi) for J3 UHPC Joints

Age	Specimen 1	Specimen 2	Specimen 3	Average
3-Day	14,699	13,826	14,395	14,310
7-Day	14,395	14,145	13,538	14,030
28-Day	15,605	16,745	15,250	15,870
Test Day	16,507	17,163	17,332	17,000

4.1.3) Conventional Concrete of Slab Panels for Ductal® Joint Specimens

The concrete for the six slab panels used for the Ductal® joint specimens was batched and delivered to Fears Lab by Dolese Bros. Co. The compressive strength of each cylinder and the average of the three specimens, however, did not exceed the desired 4000 psi at 28 days and showed reduced values at time of testing (Table 4). This is not from the same batch as the one used for to cast the six slab panels for J3 joint specimens. The lower than desired compressive strength could be caused by high water to cement ratio due to water added during casting or the cylinders were not properly rodded.

Table 4: Compressive Strength (psi) for Conventional Concrete of Slab Panels for Ductal® Joints

Age	Specimen 1	Specimen 2	Specimen 3	Average
1-Day	1924	1929	1993	1950
7-Day	4071	3681	3343	3700
28-Day	3746	4181	3850	3930
Test Day	3356	3317	3427	3370

4.1.4) Ductal® Proprietary UHPC Mixture

The prepackaged Ductal® UHPC was cast in the joints after the conventional concrete aged past 28 days. Measured compressive strength values for the Ductal® UHPC are presented in Table 5.

Table 5: Compressive Strength (psi) for Ductal® UHPC Joints

Age	Specimen 1	Specimen 2	Specimen 3	Average Strength
3-Day	12,633	12,181	14,703	13,170
7-Day	18,065	18,962	18,089	18,370
28-Day	20,948	22,748	19,272	20,990
Test Day	26,765	21,588	25,773	24,710

4.2) J3 Slab Static Test Results

Figures 37-33 show the results from testing the J3 UHPC slab 1, parts 1 and 2. Figures 34-40 show the results from testing the J3 UHPC slab 2, parts 1 and 2. The MTS loading system was used for part 1 of testing the J3 UHPC slabs 1 and 2. Part 1 of testing provides the elastic

range and early post-cracking behavior. A manual hydraulic pump was used for part 2 testing, which provides behavior at failure.

4.2.1) J3 UHPC Slab 1 Static Test Results

The maximum load applied to slab 1 in part 1 was approximately 20 kips. Due to the limitations of the MTS system loading capacity, the test was stopped at this point before switching to the manual hydraulic pump for part 2. The first cracks appeared at the conventional concrete and UHPC interface at an approximate load of 6 kips. This cracking load was determined from when the first crack became visible to the observing eyes. Additional graphical analysis using the change in stiffness at the point of cracking indicates that the first crack appeared at approximately 5.9 kips, which is almost the same as the cracking load observed by naked eye. Figure 27 shows the load vs. deflection curve for J3 slab 1 part 1. The curve showed the crack appears at approximately 5.9 kips. This cracking load was determined graphically by observing the point of the curve where there was an increase in deflection but no increase in load since the MTS loading was load controlled. Once the cracking load was reached, there was a slightly less steep slope which demonstrated a reduction in stiffness. The load corresponding to the cracking moment of a monolithic conventional concrete slab was calculated as 11.1 kips (as shown in Appendix B). This calculation assumed a monolithic normal-strength (4000 psi) concrete slab and was determined based on the span and loading configuration of the specimen set up. The graphically calculated cracking load of this slab specimen was considerably less than

that of a monolithic normal-strength concrete slab, which was potentially due to a cold joint between the conventional concrete and the UHPC.

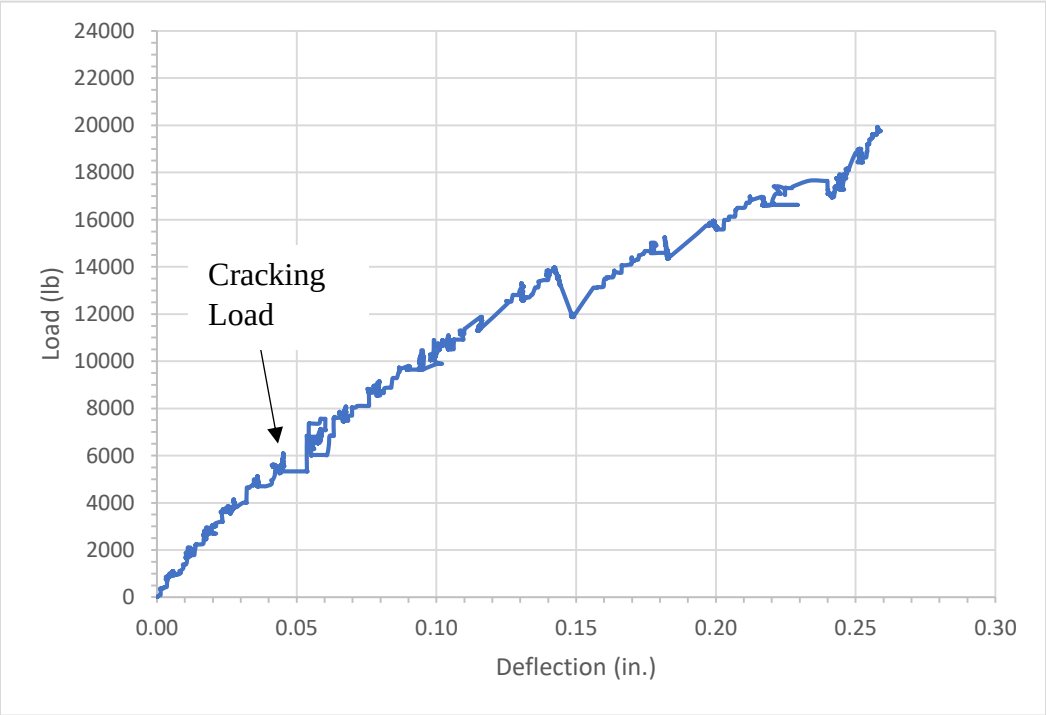

Figure 27: Load vs. deflection curve for J3 slab 1, part 1

Figure 28 shows the load vs. deflection curve for part 2 of slab 1 testing. This testing was performed using a manual hydraulic pump, which caused more variability in the load application that the digital MTS system. Load increments of 1 kip were applied, and the slab was observed for cracks using a flashlight and marker to highlight and label where and when each crack appeared. The load dropped slightly within that timeframe due to fluid being pushed back through the pump; this drop in load can be observed from the trend of the curve. The ultimate load achieved for slab 1 was approximately 35 kips. The calculated failure load for a monolithic normal-strength concrete slab with the same reinforcement and dimensions was calculated to be 27.3 kips (as shown in Appendix B). The actual failure load of the specimen exceeded the

calculated failure load by 28%. Failure was defined as the point when the specimen could not sustain any additional load, produced yielding behavior, and concrete crushing was observed at the top of the slab specimen in the conventional concrete. The load vs. deflection curve plateaued and there was concrete crushing at the top of the slab. This suggested that the slab had failed.

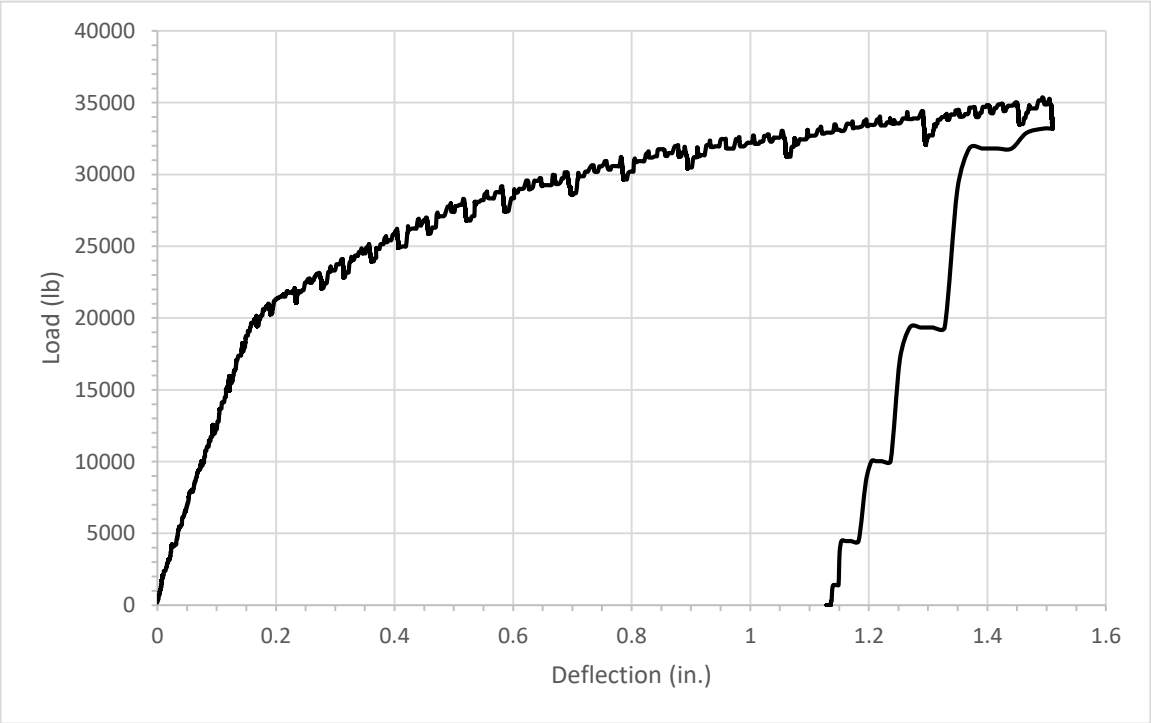

Figure 28: Load vs. deflection curve for J3 slab 1, part 2

Figure 29 shows a comparison for slab 1 part 1 and part 2 load vs. deflection curves. The part 2 curve started at the residual deflection of part 1 curve. Because there was not enough data for residual deflection in part 1 curve, the starting point of part 2 curve is based on slope and pattern of both curves. Based on this figure, the total deflection at failure was 1.6 in. and total residual deflection was 1.22 in. after failure. The slope of each curve is similar up until the cracking load after which the slope of the part 1 curve decreases. This result is unexpected as the

part 2 curve was expected to have a lower slope than part 1 since the slab had already been cracked.

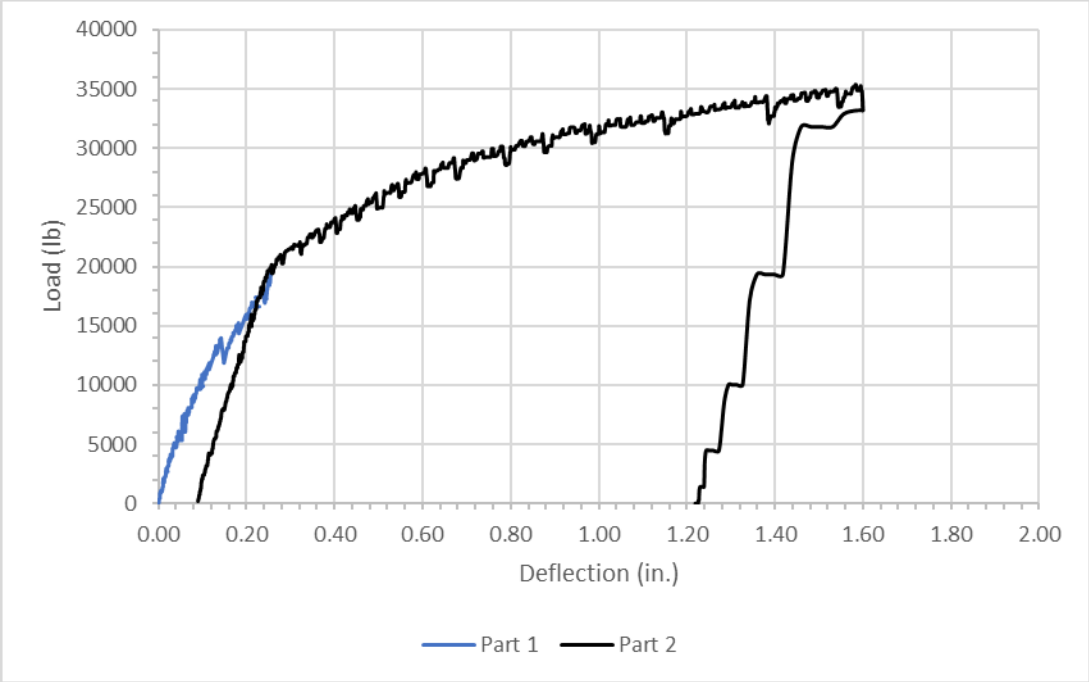

Figure 29: Load vs. deflection curve for J3 slab 1, part 1 and 2

At failure, the cracks were mainly at the interface between the conventional concrete and UHPC, with some cracks in the conventional concrete. Figure 30 and 31 show cracks on the slab after failure. The majority of the cracks at failure appeared to be evenly distributed on both sides of the joint. Significant cracks appeared at the interface between the UHPC and conventional concrete. Additional cracks can be found approximately 3, 4, and 5 in. away from the interface. There was also substantial separation at the conventional concrete to UHPC interface at the as-tested bottom of the slab, which was visible while loading, but could not be seen once the load was removed from the slab. Figures 32 and 33 show images of cracks and deformation of the slab after failure.

Figure 30: Cracks formed at interface between UHPC and conventional concrete and underneath the load point on the south side

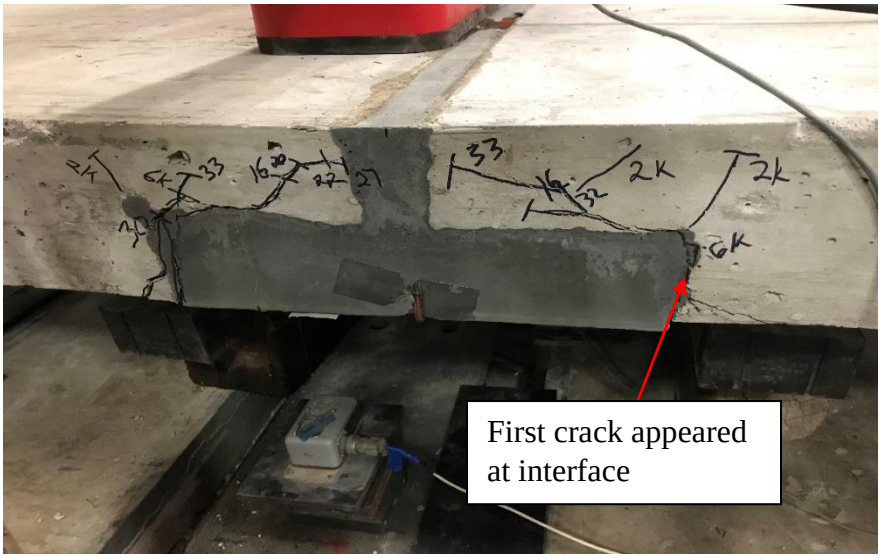

Figure 31: Cracks propagating from the bottom of the slab to the top at failure on the north side

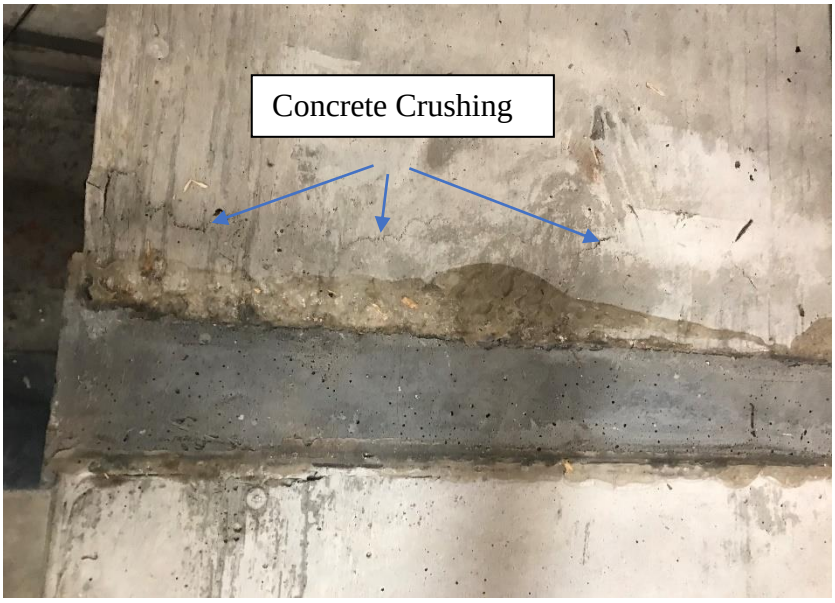

Figure 32: Concrete crushing at the top surface indicating failure

Figure 33: Slab curvature after failure

4.2.2) J3 UHPC Slab 2 Static Test Results

The initial plan was to test J3 slab 2 cyclically and test slab 3 statically. Slab 2 was loaded cyclically with loads ranging from 0.5 kips to 7.8 kips for 397 cycles. Realizing that the slab showed cracks, the test was stopped and switched to a static test instead. The maximum load applied to J3 slab 2 during the subsequent part 1 of static testing was approximately 20 kips as shown in Figure 35. The slope did not change much because the slab may have already cracked. The first visible crack was observed at approximately 8 kips using the naked eye with the help of

flashlight. Graphical analysis revealed the crack could potentially happened at a load of approximately 4 kips. This is a smaller load compared to slab 1, which could be caused by cracks that took place during the cyclic load cycles. Hence, this may not accurately represent the actual cracking load. Once the cracking load was reached, there was a slightly less steep slope which demonstrated a slight reduction in stiffness. Similar to slab 1, the cracking load of a monolithic conventional concrete was calculated as 11.1 kips. Again, the lower cracking load observed graphically is considerably less than that of a monolithic normal-strength concrete slab is potentially due to a cold joint between the conventional concrete and the UHPC. For part 1, there are enough data to show the returned deflection value of 0.055 in. when the slab specimen was unloaded.

The load vs. deflection curves for the part 1 tests of slabs 1 and 2 are shown together in Figure 36. Slab 1 has a shallower loading slope than slab 2. This may have been caused by different interaction between conventional concrete and the UHPC for the two slab specimens. There was not enough data to show the unloading slope for slab 1 for comparison of the residual deflections. The different slope could be attributed to the impact of cyclic loads on slab 2 before switching to static loads.

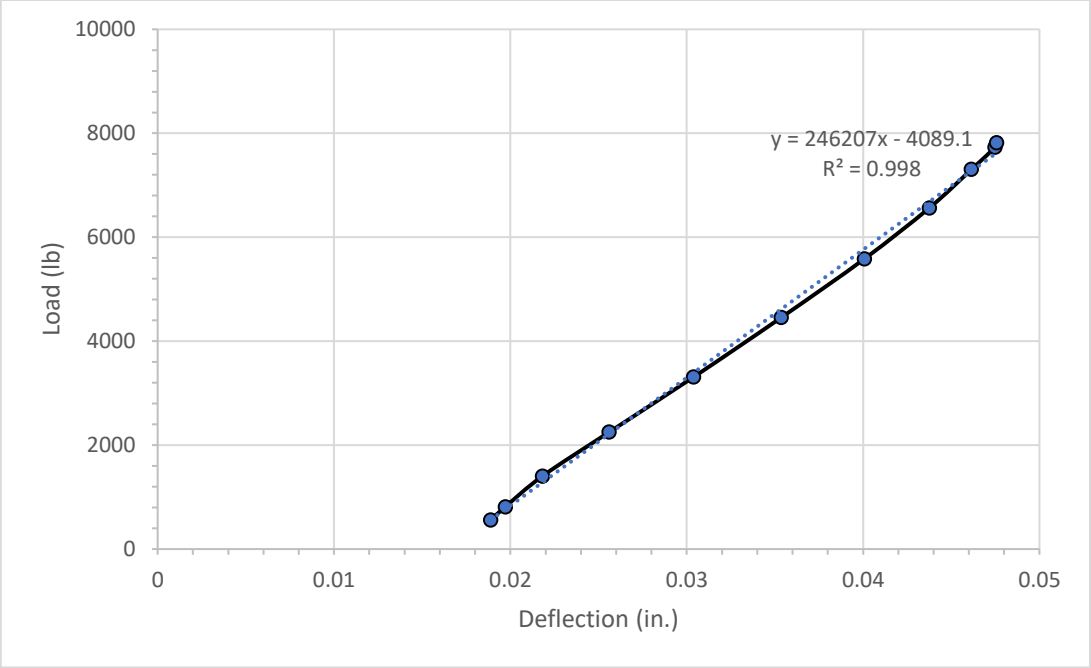

Figure 34: Load vs. deflection curve for J3 slab 2, single load cycle

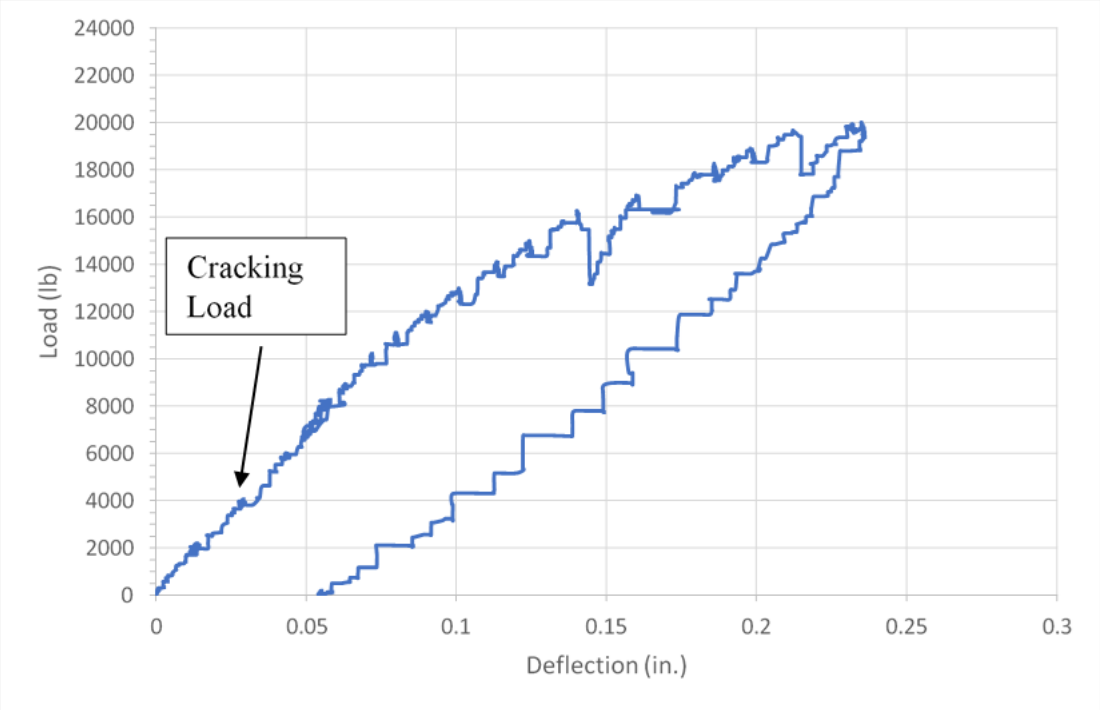

Figure 35: Load vs. deflection curve for J3 slab 2, part 1

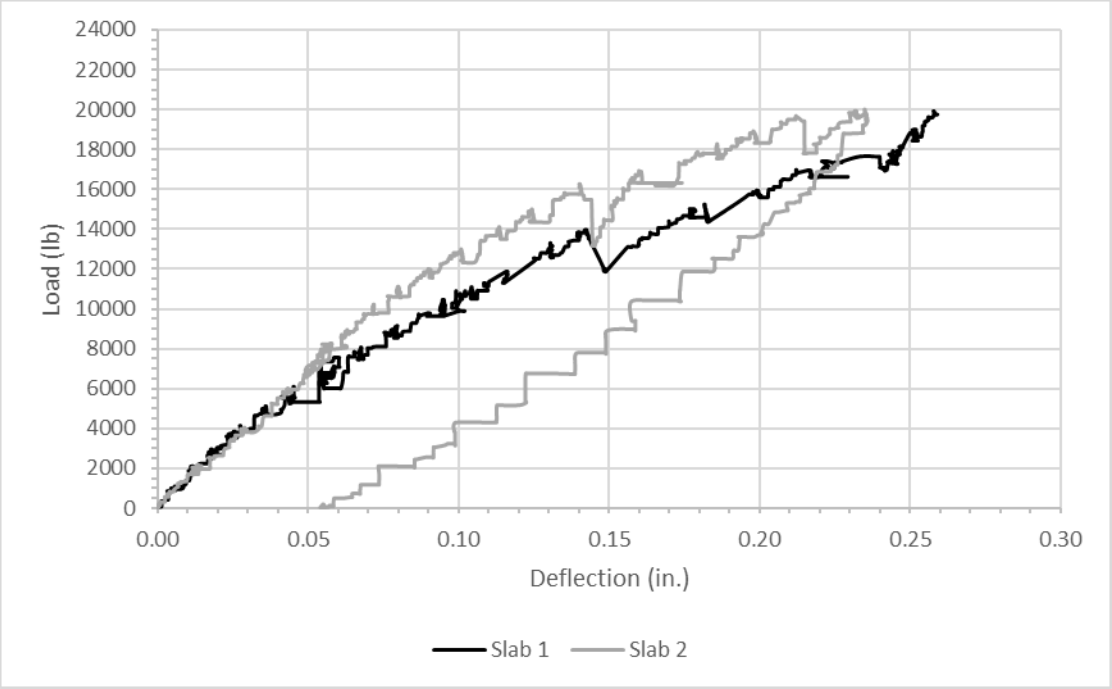

Figure 36: Load vs. deflection curve for J3 slab 1 and 2, part 1

Figure 37 shows the load vs. deflection for J3 slab 2 part 2. Like J3 slab 1 part 2, the load was applied using a manual hydraulic pump instead of the MTS system. The load dropped slightly with every 1 kip of load increase. The calculated failure load for a monolithic normal-strength concrete slab is 27.3 kips, the same as for J3 slab 1. The ultimate load achieved for J3 slab 2 was approximately 32.5 kips. The actual failure load of J3 slab 2 exceeded the calculated failure load by 19%. The plateau visible on the load vs. deflection curve indicates that the steel reinforcement yielded. The maximum deflection at failure is approximately 1.0 in. After failure, the specimen was unloaded and had a residual deflection of 0.68 in. Concrete crushing at the top of the slab indicated that the slab had failed.

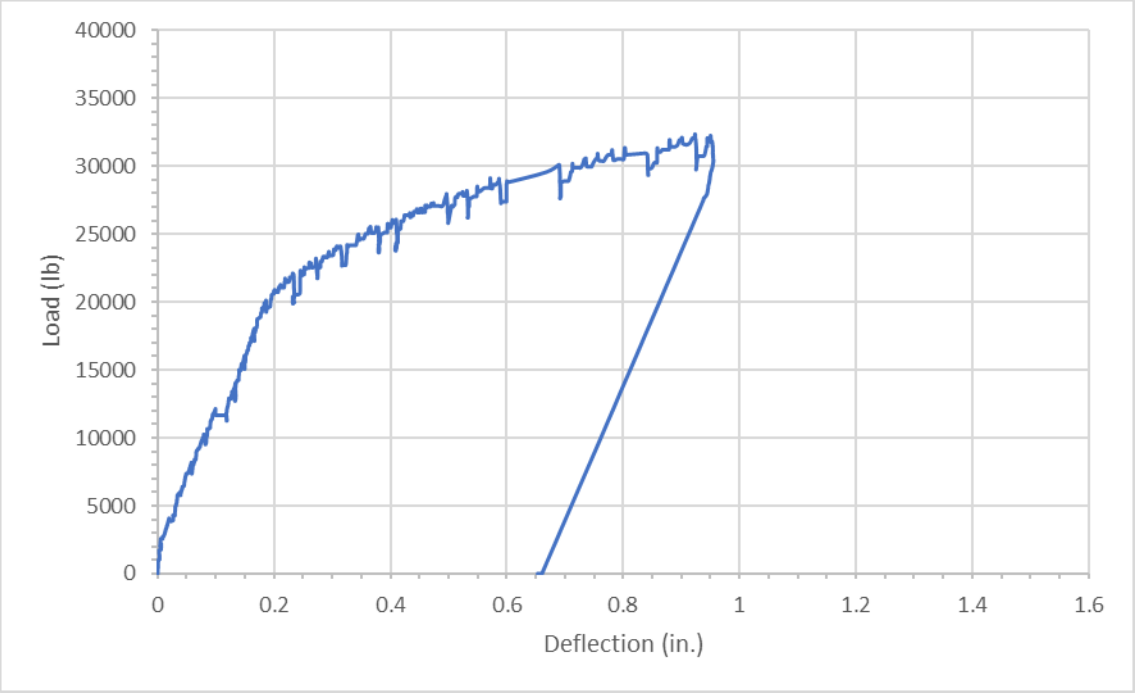

Figure 37: Load vs. deflection curve for J3 slab 2, part 2

Figure 38 shows a comparison of part 1 and part 2 of the load vs. deflection curves for J3 slab 2. The part 2 curve started at the residual deflection of the part 1 curve. Based on this figure, the total deflection at failure was 1.01 in. and total residual deflection was 0.72 in. The part 2 curve has a lower slope than part 1, which was the expected result since the slab was already cracked in part 1.

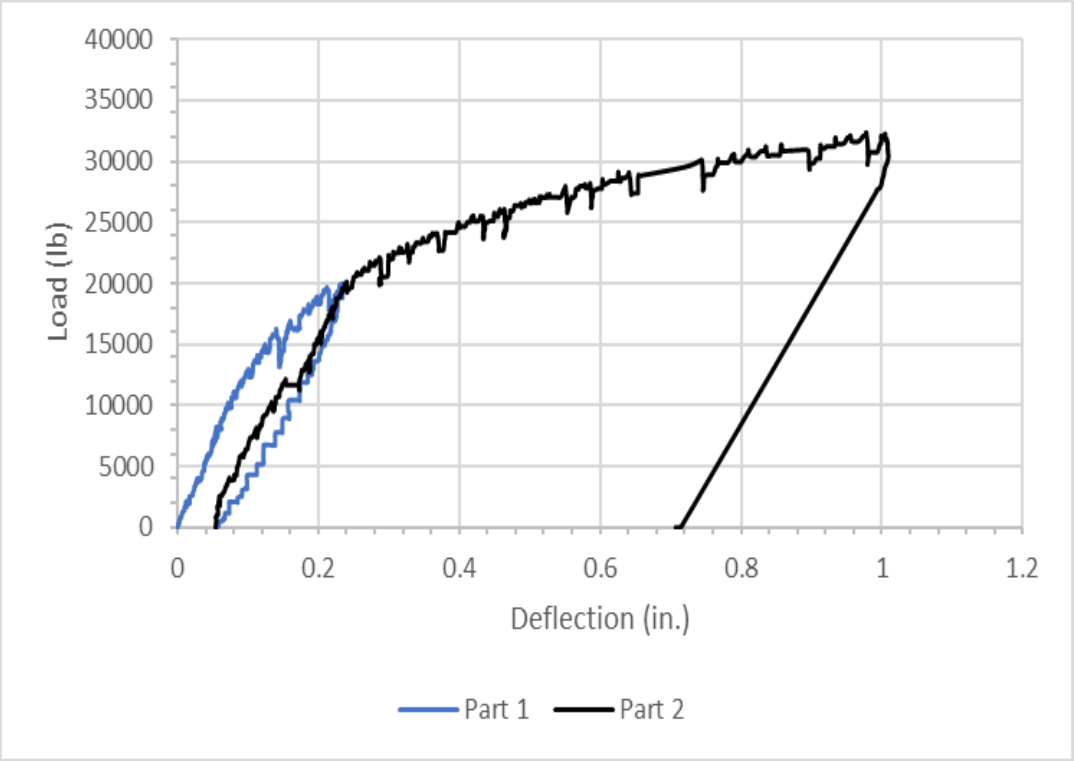

Figure 38: Load vs. deflection curves for J3 slab 2, parts 1 and 2

Similar to slab 1, multiple cracks appeared at the interface between the conventional concrete and UHPC. Some cracks also appeared in the conventional concrete. Figures 39 and 40 show cracks in the slab after failure for the north and south sides of the slabs. The majority of the cracks at failure appeared below the load point and there was a large separation between the conventional concrete and UHPC. A gap of approximately 0.25 in. was visible. Figure 42 shows concrete crushing at the top of the slab indicating failure.

Figure 39: Cracks formed at the conventional concrete to UHPC interface on the north side of J3 slab 2

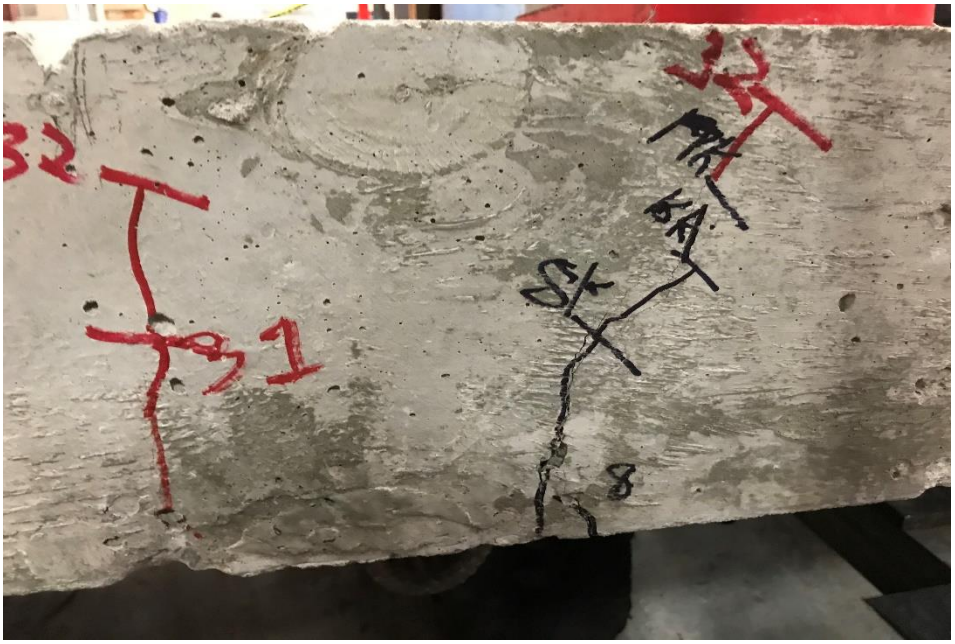

Figure 40: Cracks formed further away from the interface on the north side of J3 slab 2

Figure 41: Cracks formed at the conventional concrete to UHPC interface and propagating upward on the south side

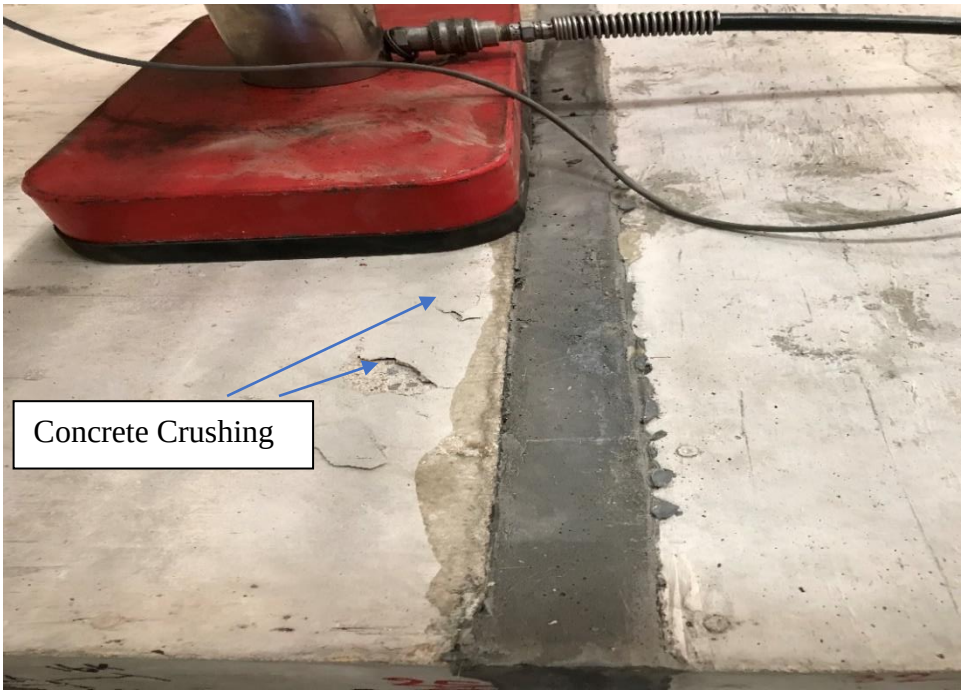

Figure 42: Concrete crushing at the top of the slab for J3 slab 2 at failure

4.3) Ductal® Slab Static Test Results

Figures 43-50 show the results from testing Ductal® UHPC slab 1, parts 1 and 2. Figures 51-59 show the results from testing slab 2, parts 1 and 2. Due to the issue with the MTS system, both parts 1 and 2 were tested using manual hydraulic pump. Part 1 of testing provided elastic range and early post cracking behavior. Part 2 slab testing provided behavior at failure.

4.3.1) Ductal® UHPC Slab 1 Static Test Results

Due to the unavailability of MTS system, the test was performed using the manual hydraulic pump for parts 1 and 2. Part 1 of testing was completed when the hydraulic cylinder reached its maximum extended length. Before part 2 of testing was conducted, the hydraulic cylinder was adjusted to provide additional extended length. The first crack observed with the naked eye appeared at the intersection between the conventional concrete and UHPC at 6 kips. The graphical analysis of the load vs. deflection curve did not provide enough indication of where the crack appeared if the deflection range was set to 0 in. to 1.6 in., as in Figure 43. However, if the range of the load and deflection is set to the same as the J3 UHPC slab 1, part 1 curve, as shown in Figure 44, the cracking load appeared to be at 7.5 kips. Figure 43 shows the load vs. deflection for slab 1 part 1. As the 1-kip load increments were applied, the slab was examined for cracks using a flashlight and marker to label when and where the crack appeared. The load dropped slightly within the timeframe between load increments; this can be observed from the trend of the curve. Once the cracking load was reached, the slope became slightly less steep indicating a slight reduction in stiffness. The load corresponding to the cracking moment of a monolithic conventional concrete slab was calculated as 11.1 kips. This calculation assumed for a monolithic normal-strength (4000 psi) concrete slab and was determined based on the span and loading configuration of the test specimen set up. The graphically calculated cracking load

for this slab specimen is considerably less than that of a monolithic normal-strength concrete slab, which is potentially due to the presence of a cold joint between the conventional concrete and UHPC.

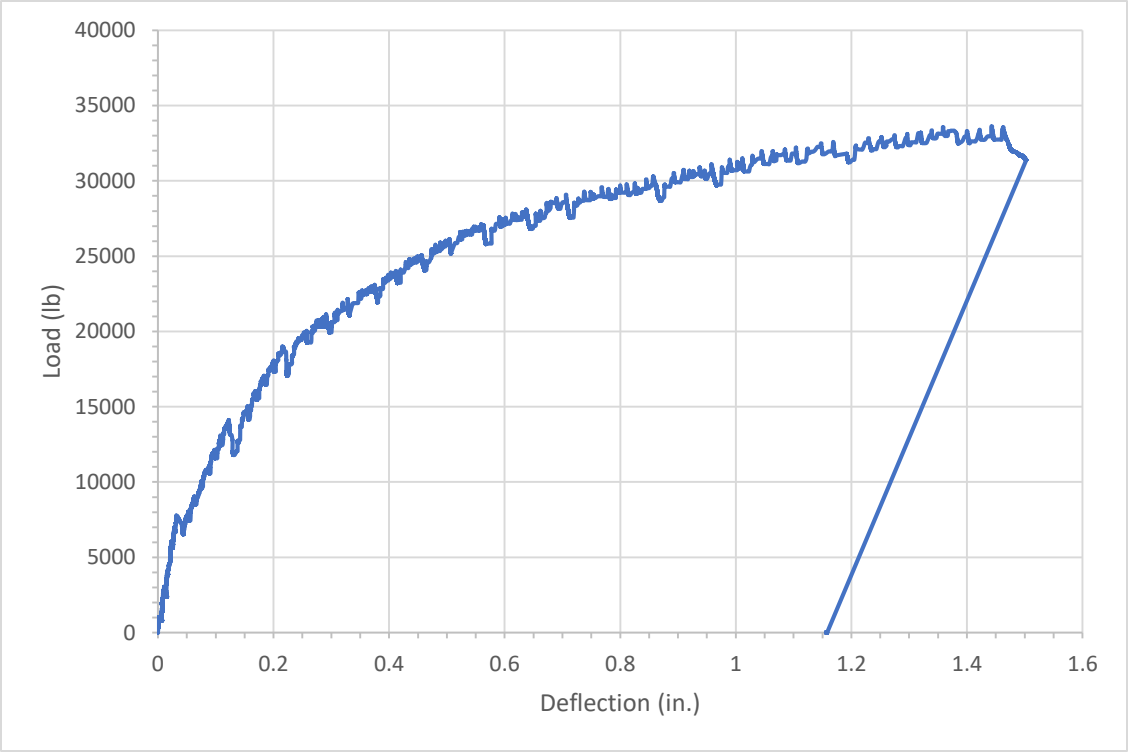

Figure 43: Load vs. deflection curve for Ductal® slab 1, part 1

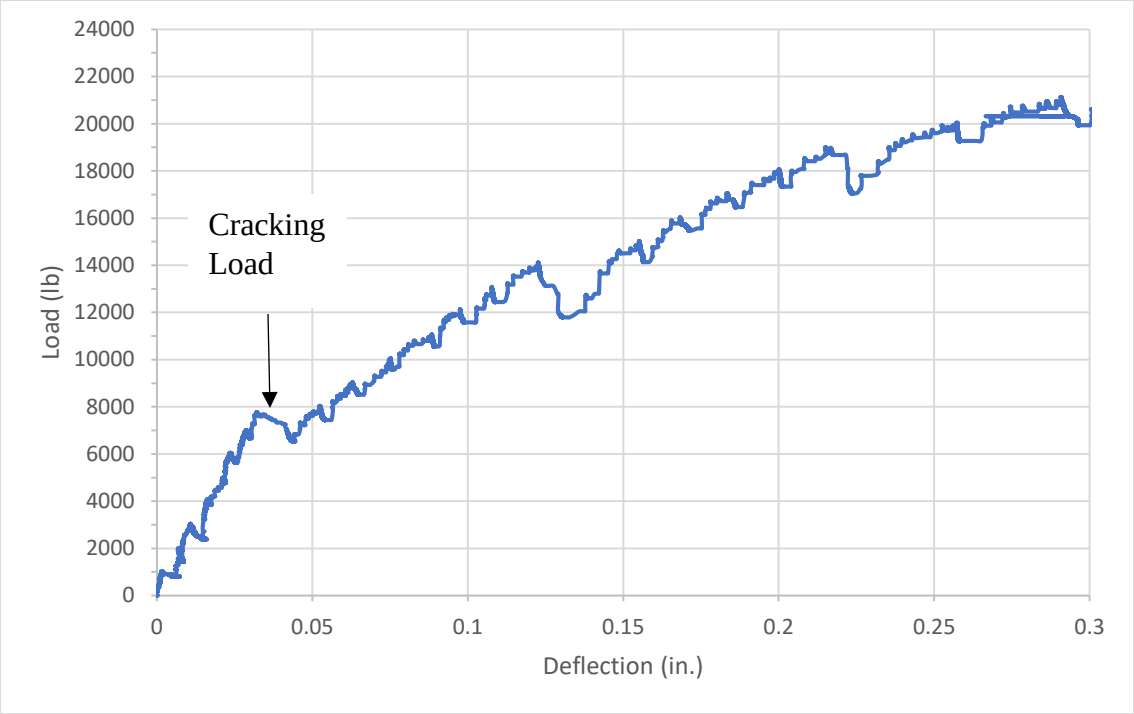

Figure 44: Load vs. deflection curve for Ductal® slab 1, part 1 after adjusting load and deflection range to the anticipated elastic portion

Figure 45 shows cracks after part 1 of testing where the maximum load was 33.3 kips. The primary cracks occurred at the interface between the conventional concrete and UHPC. The gap grew larger as higher loads were applied. Cracks started at the bottom of the slab and propagated toward the top of the slab. In addition, cracks appeared at 2.25 in. away from the interface.

Figure 45: Large cracks at the conventional concrete to UHPC interface after part 1 of testing

Figure 46 shows the load vs. deflection curve for part 2 of the Ductal® slab 1 testing. Similar to part 1, this testing was performed using a manual hydraulic pump. However, 3-kip load increments were applied instead of 1-kip load increments until the maximum load from part 1 was applied, and the slab was inspected for cracks between load increments using a flashlight and marker to label when and where the cracks appeared. The ultimate load for Ductal® slab 1, part 2 was approximately 35.8 kips. The maximum load from part 2 was 8% greater than the maximum load of part 1. For comparison, the calculated failure load for a monolithic normal-strength concrete slab was 27.3 kips. The actual failure load of the specimen exceeded the calculated failure load by 31%. The curve plateaued, which suggests yielding of the steel reinforcement within the joint. Failure was evident due to the concrete crushing at the top surface.

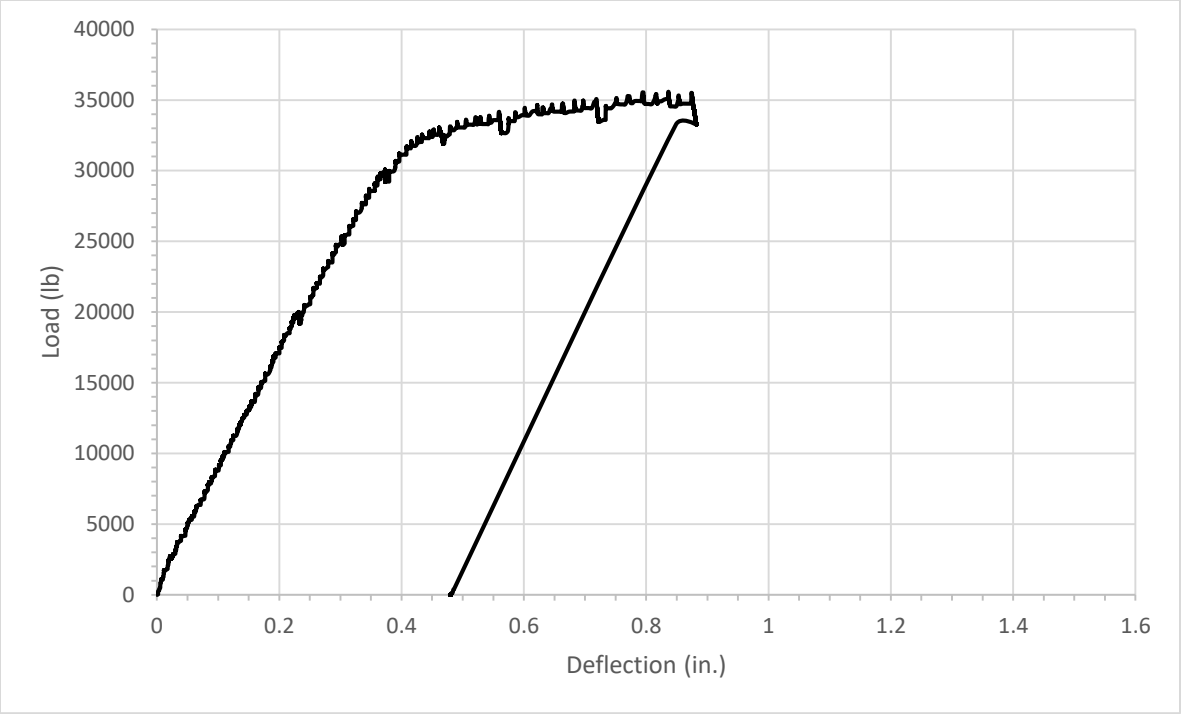

Figure 46: Load vs. deflection curve for Ductal® slab 1, part 2

Figure 47 shows a comparison of the part 1 and part 2 load vs. deflection curves for Ductal® slab 1. The part 2 curve started at the residual deflection of the part 1 curve. Based on this figure, the total deflection aft failure was 2.05 in. and total residual deflection was 1.64 in. The part 2 curve has a lower slope than part 1 up until 20 kips. This was expected as the slab already cracked in part 1. From about 20 kips to 32 kips, it shows a much higher slope.

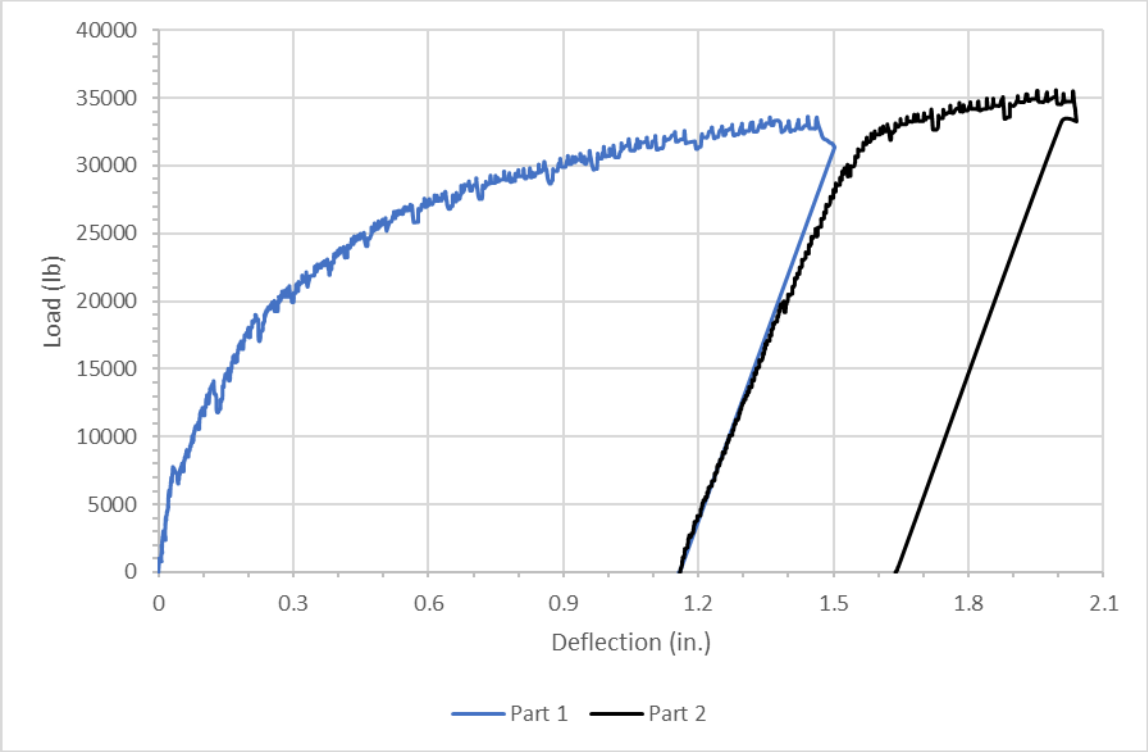

Figure 47: Load vs. deflection curve for Ductal® slab 1, part 1 and part 2

After the completion of part 2 of testing, more cracks were observed at the interface between the conventional concrete and UHPC. Additional cracks also appeared in the conventional concrete. Figures 48-50 show cracks on the north side of the slab after failure, on the as-tested underside of the slab, and concrete crushing on the as-tested top of the slab. The majority of the cracks at failure appeared below the load point. From the bottom surface of the slab, it was evident that cracks extended across the entire width of the slab at the interface and approximately 3 in. away from the interface as shown in Figure 49. Large separation between the conventional concrete and the UHPC joint was visible. Figure 50 shows concrete crushing at the top of the slab indicating failure.

Figure 48: Ductal® slab 1 after part 2 of testing

Figure 49: Cracks extending across the entire width of the slab at the joint and in the conventional concrete

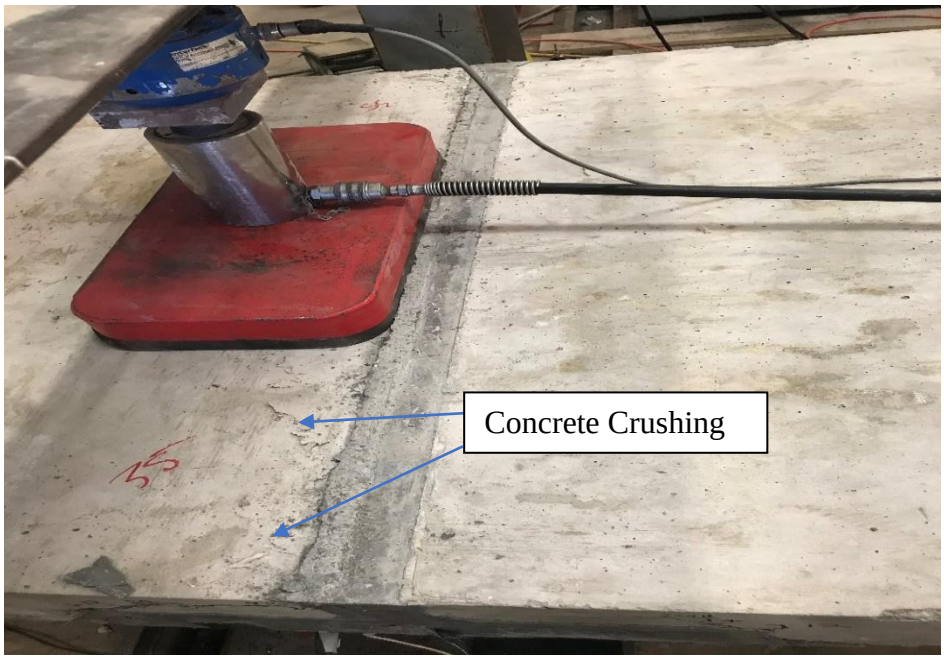

Figure 50: Concrete crushing at the top of Ductal® slab 1 indicating failure

4.3.2) Ductal® UHPC Slab 2 Static Test Results

Part 1 of Ductal® slab 2 testing was completed when the hydraulic cylinder reached its maximum extended length. The part 2 test was performed using the manual hydraulic pump used for part 1. Load was applied in 1-kip increments and between increments a flashlight was used to observe cracks and a marker was used to mark out where cracks occurred and how they propagated. The first crack observed by the naked eye appeared at the intersection between the conventional concrete and UHPC at a load of 9 kips. The load vs. deflection curve was plotted to determine the cracking load. During testing, one wire pot fell off the slab at approximately 1.6 inches deflection causing error in measurement deflection. Hence, the data were neglected for deflection greater than 1.6 inches. By adjusting the range of the load and deflection, the cracking load appeared to be at 7 kips. Figures 51 and 52 show the load vs. deflection curve for Ductal® slab 2 part 1 before and after adjustment of the deflection range. The slope of the curve became

less steep as more load was applied. This indicated that the stiffness of the slab had been reduced. The cracking load of a monolithic conventional concrete slab was determined to be 11.1 kips. The graphically calculated cracking load is 37% less than the calculated value.

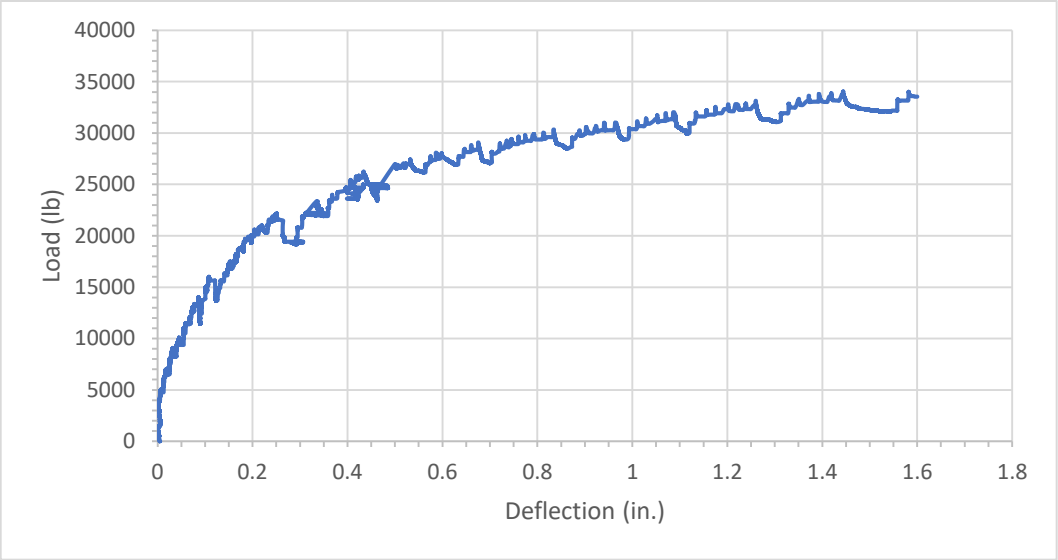

Figure 51: Load vs. deflection curve for Ductal® slab 2, part 1

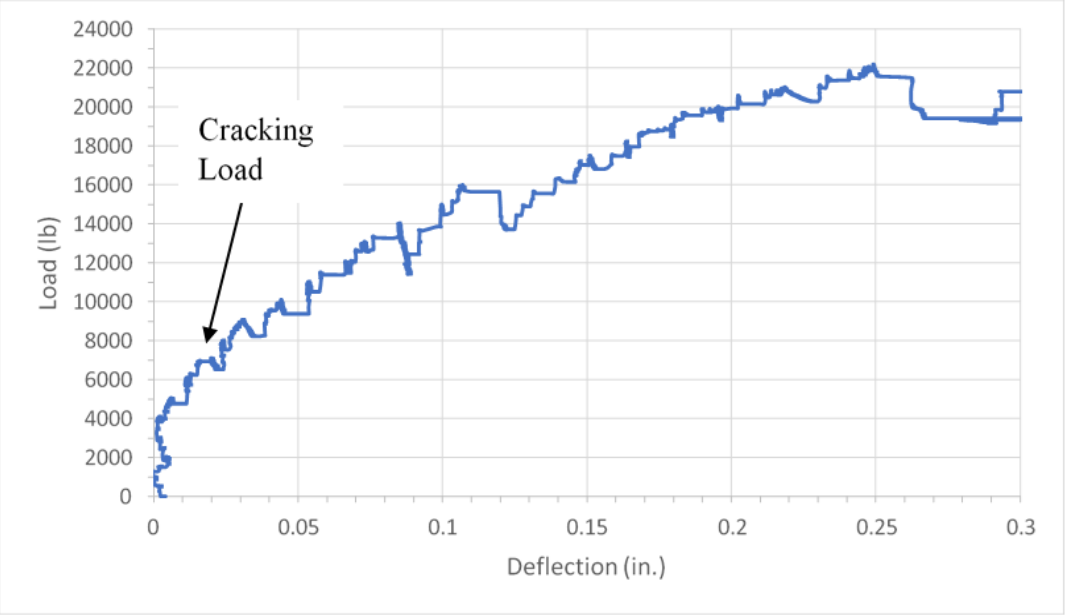

Figure 52: Load vs. deflection curve for Ductal® slab 2, part 1 after adjusting load and deflection range

Figures 53 and 54 show cracks after part 1 of testing on the north and south sides of the slab. Cracks occurred at the interface between the conventional concrete and UHPC and within the conventional concrete away from the joint. The gap between the UHPC and conventional concrete grew larger as higher loads were applied. All cracks started at the bottom of the slab and propagated toward the top of the slab while curving toward the load point.

Figure 53: Cracks on the north side of Ductal® slab 2 after part 1 testing

Figure 54: Cracks on the south side of Ductal® slab 2 after part 1 testing

Figure 55 shows the load vs. deflection curve for part 2 of slab 2 testing. Part 1 of testing was completed when the hydraulic cylinder reached its maximum extended length. Before part 2 of testing was conducted, the hydraulic cylinder was adjusted to provide additional extended length. Similar to part 1, this testing was performed using a manual hydraulic pump. However, larger load increments of approximately 3 kips were applied instead of 1-kip load increments because the slab was loaded almost to failure in part 1 and to substantially reduce testing time. The slab was inspected for cracks using a flashlight between load increments and a marker was used to label when and where the crack appeared. The ultimate load for Ductal® slab 2, part 2 was approximately 36 kips. In comparison, the calculated failure load for a monolithic normal-strength concrete slab was 27.3 kips. The actual failure load of the specimen exceeded the calculated failure load by 32%. The curve plateaued near the ultimate load and concrete crushing on the top surface indicated failure. There were not enough data to plot the unloading curve.

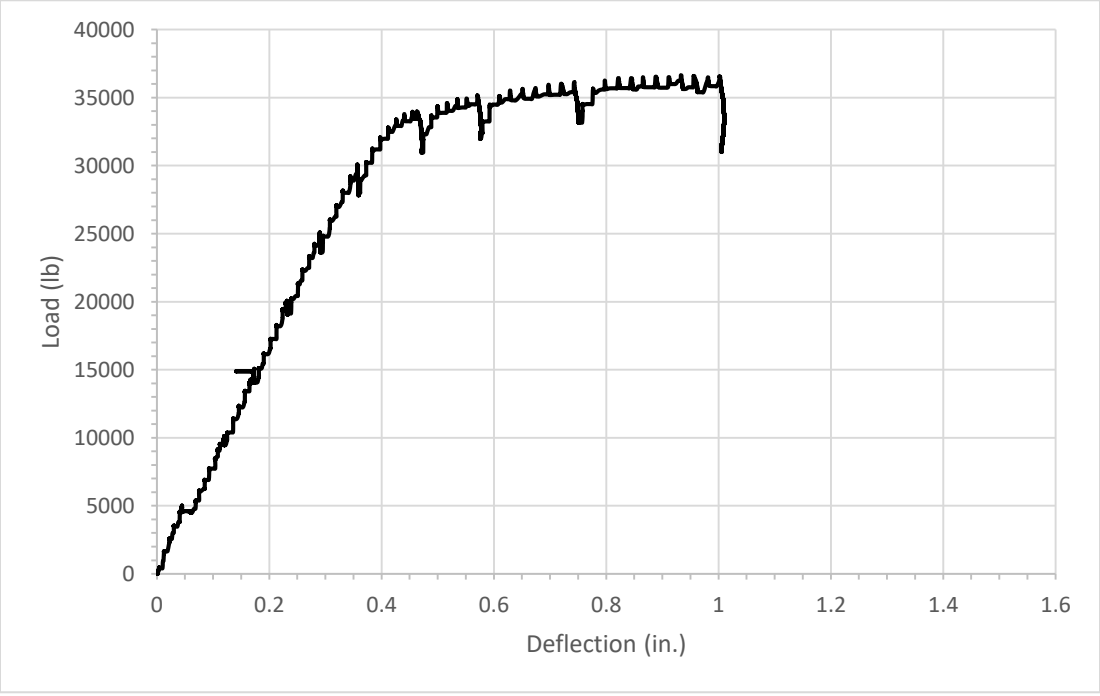

Figure 55: Load vs. deflection curve for Ductal® slab 2, part 2

Figure 56 shows a comparison for slab 2 by plotting the part 1 and part 2 load vs. deflection curves on the same graph. The part 2 curve started at the residual deflection of the part 1 curve. Because there was not enough data from the part 1 test to determine residual deflection, the starting point of the part 2 curve is based on the slope and pattern of both curves. Based on this figure, the total deflection at failure was 2.14 in. There was not enough data to determine the total residual deflection. The part 2 curve has a lower slope than part 1. This was expected as the slab already cracked in part 1.

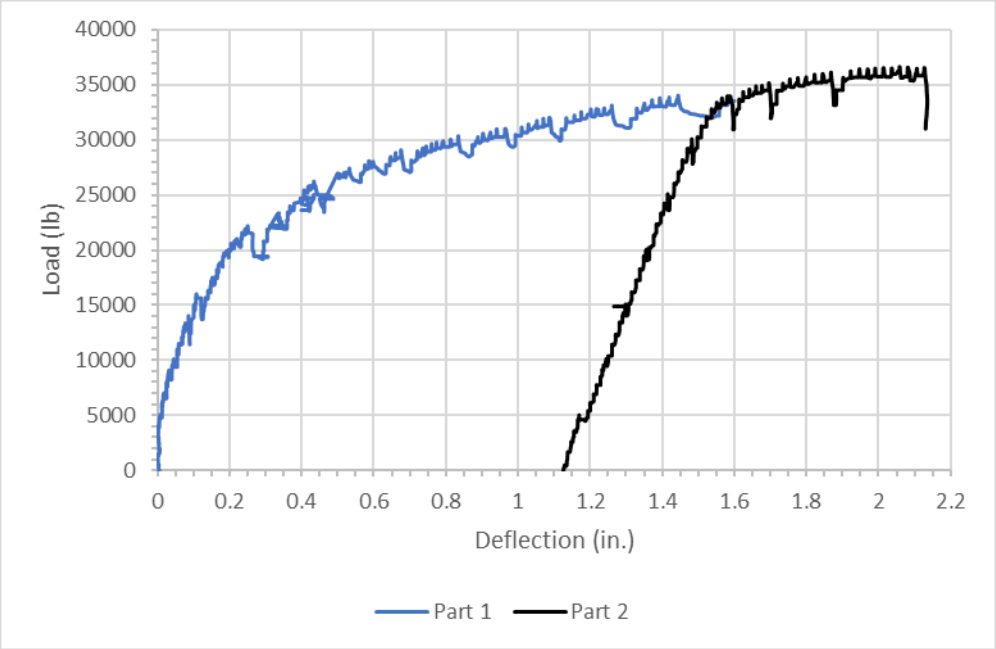

Figure 56: Load vs. deflection curve for Ductal® slab 2, part 1 and part 2

Additional cracks were observed at the conventional concrete to UHPC interface during part 2 of testing. These cracks also propagated from the bottom of the slab to the top and curved toward the load point. Figures 57-59 show cracks on the slab after failure on the north side of the slab, cracks on the as-tested underside the slab, and concrete crushing on the as-tested top of the slab. The majority of the cracks occurred below the load point. There was significant separation

between the conventional concrete and UHPC at the interface, which Figure 57 illustrates. Similar to previous static tests, concrete crushing at the top of the slab indicated that the slab failed.

Figure 57: Cracks on the north side of Ductal® slab 2 after part 2 testing

Figure 58: Cracks on the as-tested underside of Ductal® slab 2 after testing

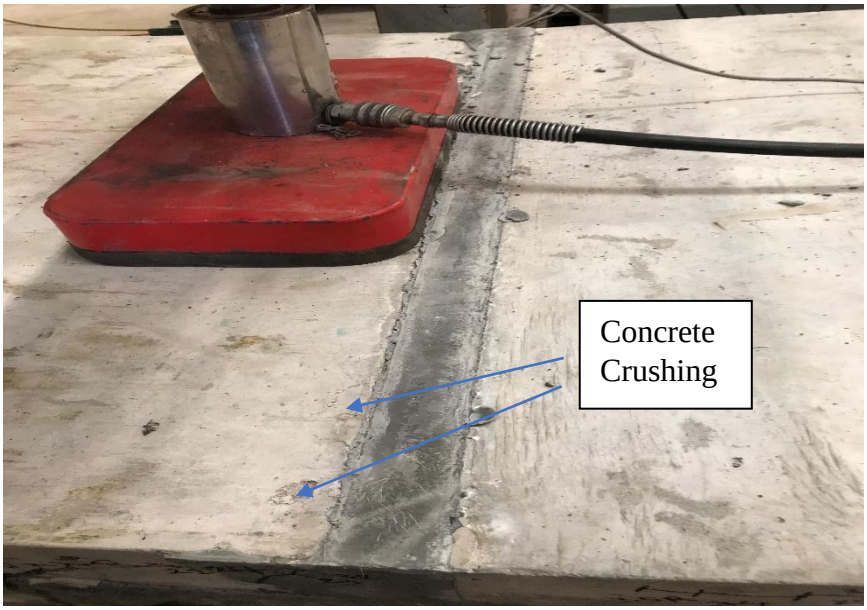

Figure 59: Concrete crushing at the top of the slab indicating failure

4.4) Comparison of J3 and Ductal® UHPC Slab Static Test Results

This section provides analysis and comparison between the J3 and Ductal® UHPC static test results. The focus will be on the comparison between part 1 of the slab 1 test for both UHPC's, and part 1 of the slab 2 test for both UHPCs. The same also applies for part 2 comparisons. Finally, part 1 curves of all slabs are plotted on the same graph, and the same procedure is applied to part 2.

Figure 60 shows the J3 UHPC and Ductal® UHPC slab 1, part 1 curves together on the same graph. Both curves had similar patterns, the main difference was the cracking load. The Ductal® slab had a higher stiffness and a cracking load of 7.5 kips, whereas the J3 slab had a cracking of load of 5.9 kips.

Figure 61 shows the J3 UHPC and Ductal® UHPC slab 2, part 1 curves together on the same graph. Both curves possessed some similarity in pattern, but substantial difference in cracking load was apparent. This is primarily because the J3 slab 2 was tested cyclically with 397 cycles of load that caused cracking before the static load test was performed. The cracking load for the J3 slab 2 was approximately 4 kips. However, this may not have represented actual cracking load as the slab cracked during the cyclic testing. The cracking load for the Ductal® slab 2 was approximately 7 kips. The plot for J3 slab 2 did not include the unloading part to help compare behavior of the two slabs.

Figure 62 shows part 1 curves for all four slabs plotted on the same graph. All the curves displayed similar patterns and excluded the unloading parts for comparison.

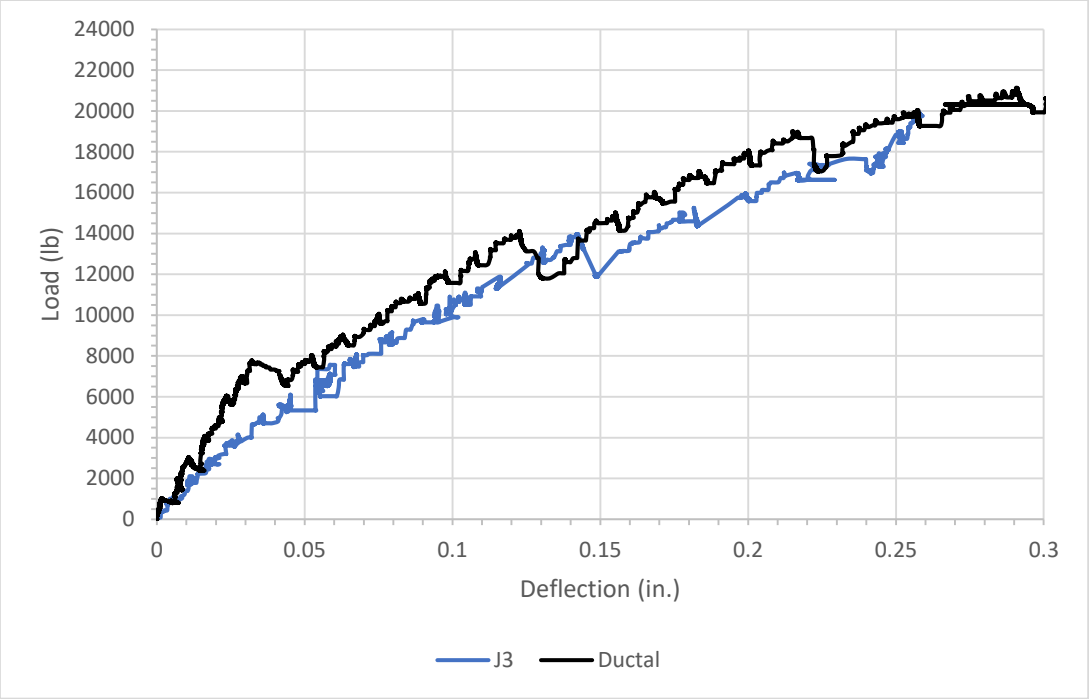

Figure 60: Load vs. deflection curves for J3 and Ductal® slab 1, part 1

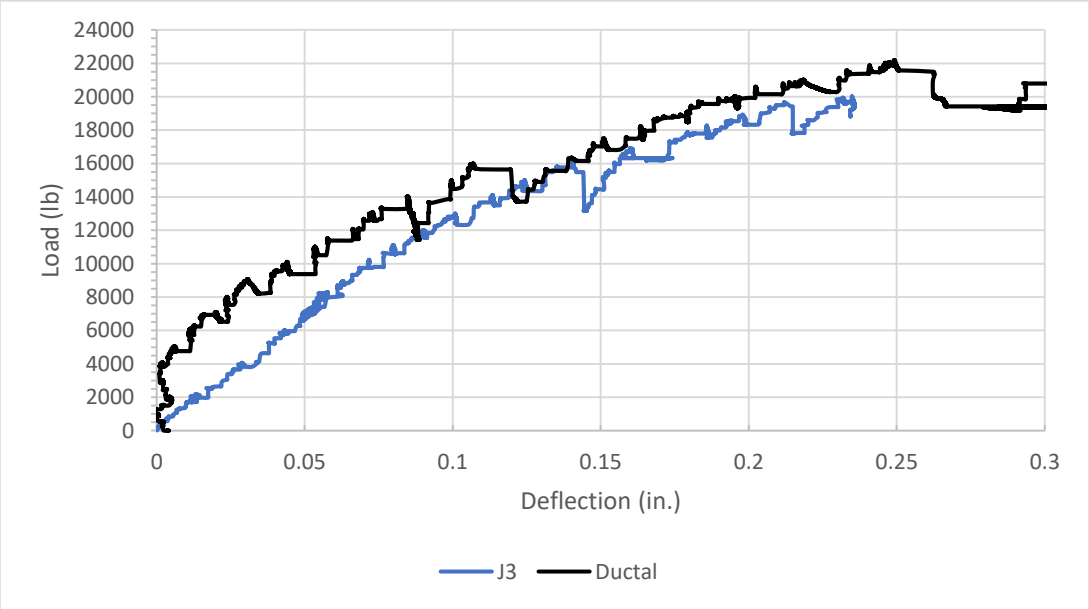

Figure 61: Load vs. deflection curves for J3 and Ductal® slab 2, part 1

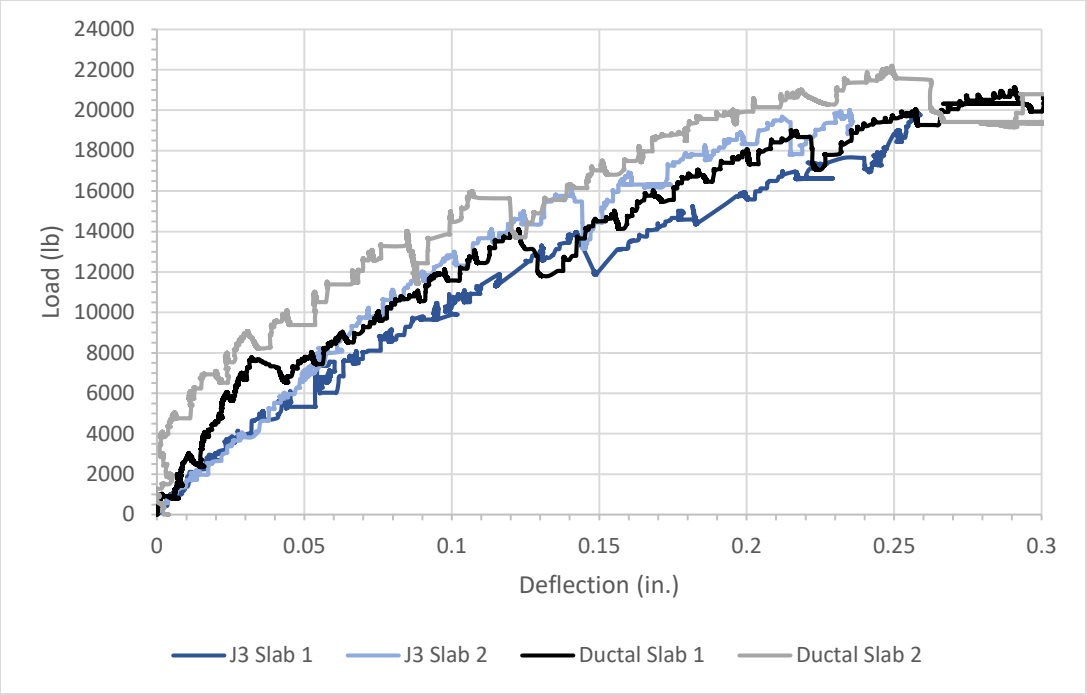

Figure 62: Load vs. deflection curves for J3 and Ductal® part 1 static tests

Figure 63 shows the J3 UHPC and Ductal® UHPC slab 1, part 2 curves together on the same graph. The J3 slab had a higher stiffness compared to the Ductal® slab, but the Ductal® slab displayed a more linear behavior before yielding compared to J3. At the same deflection of approximately 0.9 in., the Ductal® slab had reached the ultimate load of approximately 35 kips compared to approximately 32 kips for the J3 slab.

Figure 64 shows the J3 UHPC and Ductal® UHPC slab 2, part 2 curves together on the same graph. Both curves possess some similarity in pattern. The ultimate load for the Ductal® slab was approximately 36 kips, whereas the J3 slab had approximately 33 kips ultimate load. The plot for the Ductal® slab 2 did not include the unloading curve as there was not enough data to be analyzed.

The overall stiffness that the Ductal® slabs reached a higher load at a smaller deflection because of the higher initial stiffness compared to J3 slabs. This is possibly because part 1 for Ductal® slabs went to a significantly higher load. Therefore, the load vs. deflection curves for Ductal® slabs part 1 and J3 part 2 were plotted on the same graph for comparison. Figure 65 shows curves for Ductal® slabs part 1 and J3 part 2. All four curves show very similar patterns.

Figure 66 shows the part 2 curves for all four slabs plotted on the same graph. All the curves displayed similar patterns and excluded the unloaded parts for comparison.

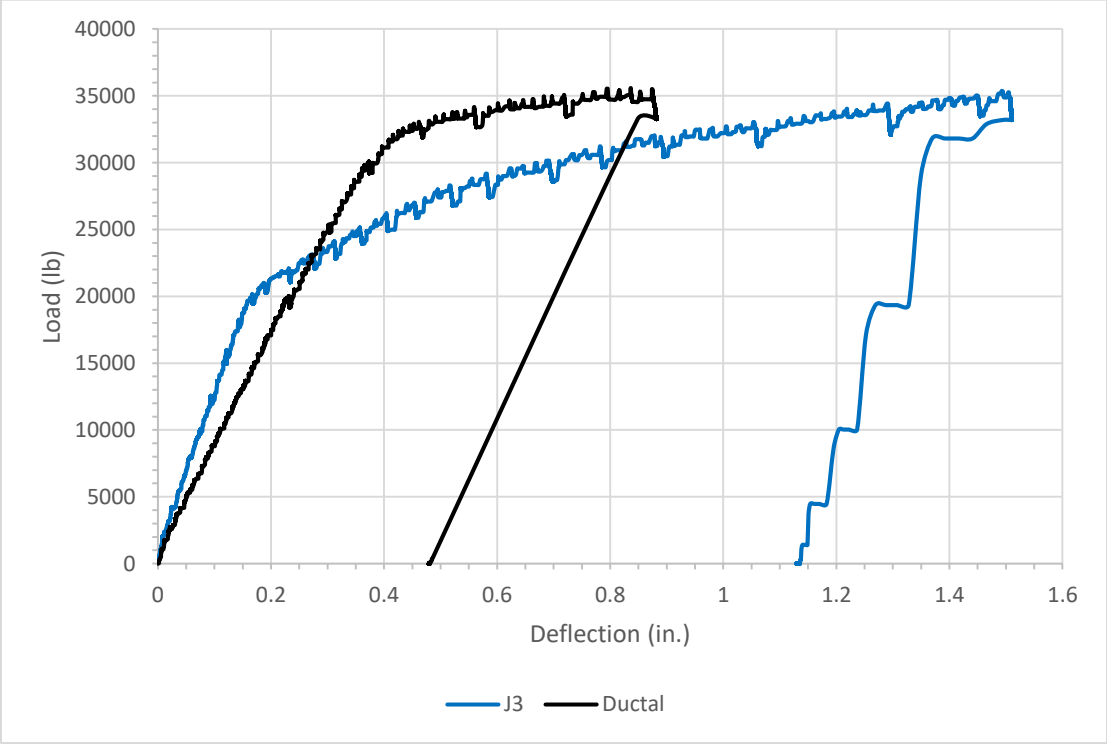

Figure 63: Load vs. deflection curves for J3 and Ductal® slab 1, part 2

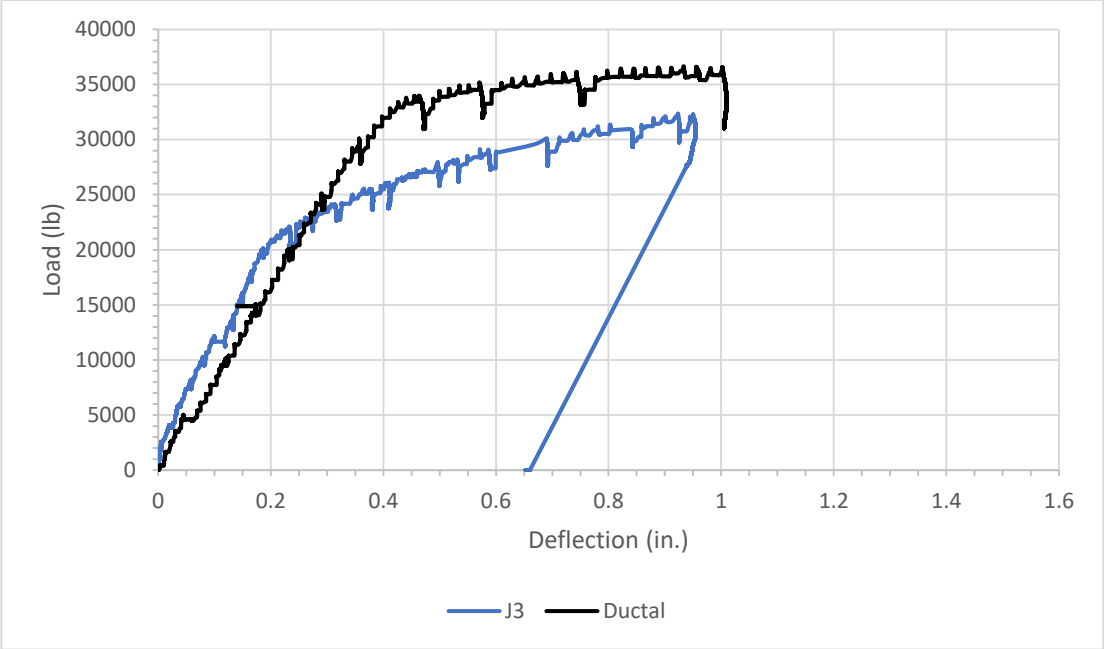

Figure 64: Load vs. deflection curves for J3 and Ductal® slab 2, part 2 of J3 and Ductal®

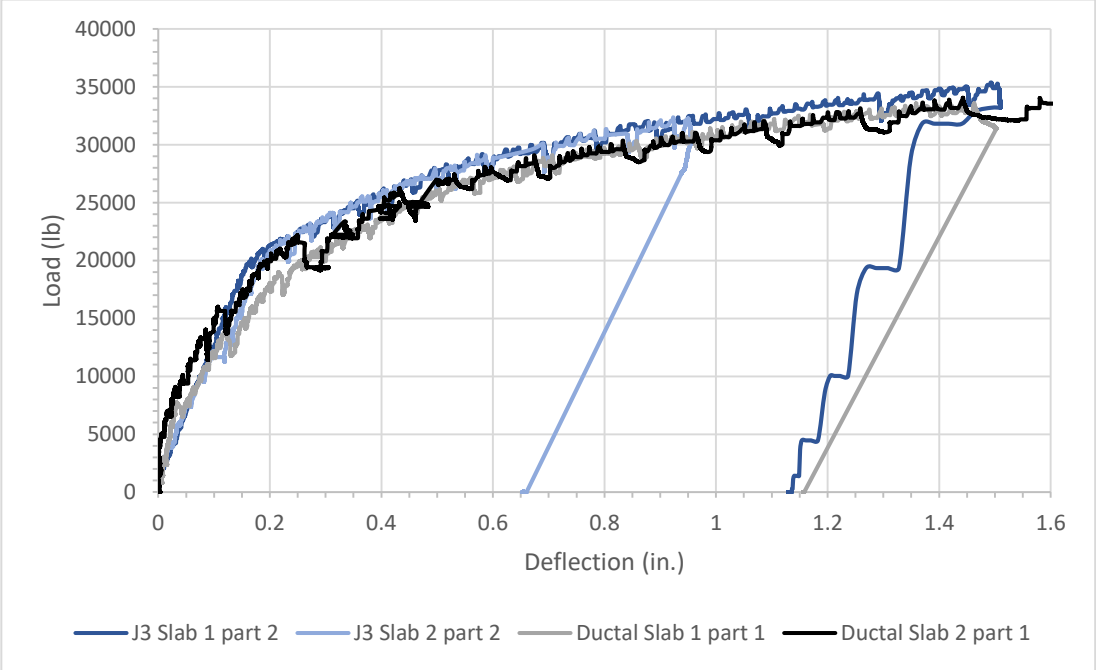

Figure 65: Load vs. deflection curves for J3 part 2 and Ductal® part 1

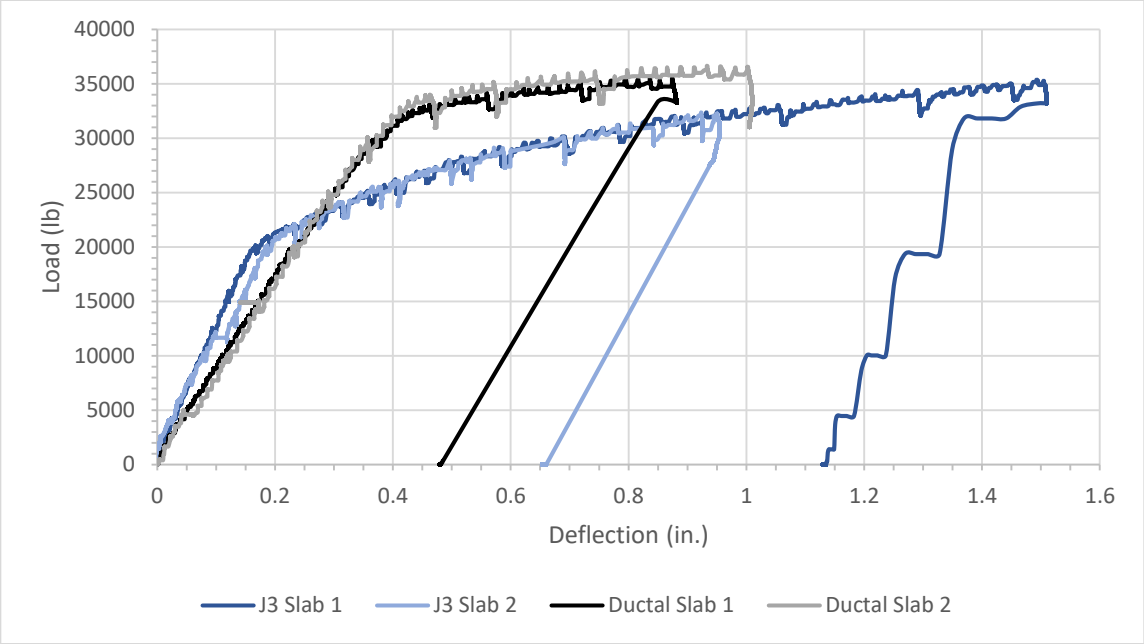

Figure 66: Load vs. deflection curves for J3 and Ductal® static slabs, part 2

4.5) J3 Slab Joint 3 Cyclic Test Results

Slab 3 was tested cyclically under fatigue loading. For the first 3 million cycles, the slab was to be loaded cyclically to a maximum value of 90% of the cracking load. The cracking load for J3 slab 1 was determined to be 5.9 kips. The cracking load for J3 slab 2 was lower due to having been initially tested cyclically. Therefore, the maximum value of the cyclic load for the slab was chosen to be 90% of 5.9 kips. In addition, the cracking loads determined from Ductal® slab 1 and slab 2 were more than the 5.9 kips determined for J3 slab 1. Therefore, a maximum load of 5.3 kips was applied for cyclic loading of the J3 and Ductal® slabs. Using the MTS system, a 1 hertz cyclic load was applied to J3 slab 3 with a maximum value of 5.3 kips. Figure 67 depicts a typical cyclic loading over a period of 10 seconds. Figure 68-85 show the load vs. deflection curves for the loading portion of a single cycle during the first 3 million cycles, analyzed every other day for the duration of initial cyclic loading. Approximately 86,400 cycles were run each day. The unloading portion of the curves are not displayed but were similar to the

loading portion. A 500-pound preload was set to prevent the load from coming up off the slab, so the curves did not begin at zero. This preload is not intended to represent moments of the dead load of the bridge deck. The stiffness of the slab over time was of more interest than the absolute deflection, so a trend line of the entire data for each plotted load cycle is displayed in blue on each graph. The stiffness of the slab could be determined from the slope in the equation shown on the graph. The slope generally decreased throughout the first 3 million cycles. The reason the stiffness gradually decreased over time is due to additional cracking and fatigue. Figure 86 shows load cycles from different days for comparison. On certain days such as days 23 and 25, there were negative deflections. This may have been caused by the correction made with the support deflections. There was possibly more support deflection than slab deflection. For day 7, the load cycles on this day have a different shape from any other days for unknown reasons.

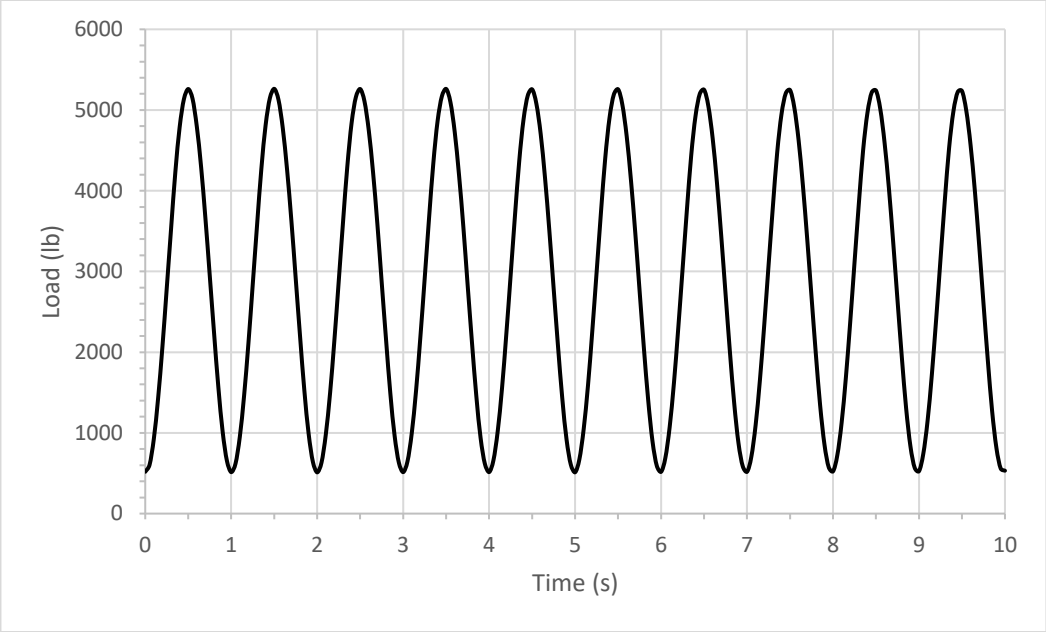

Figure 67: Typical cyclic loading over a period of 10 seconds

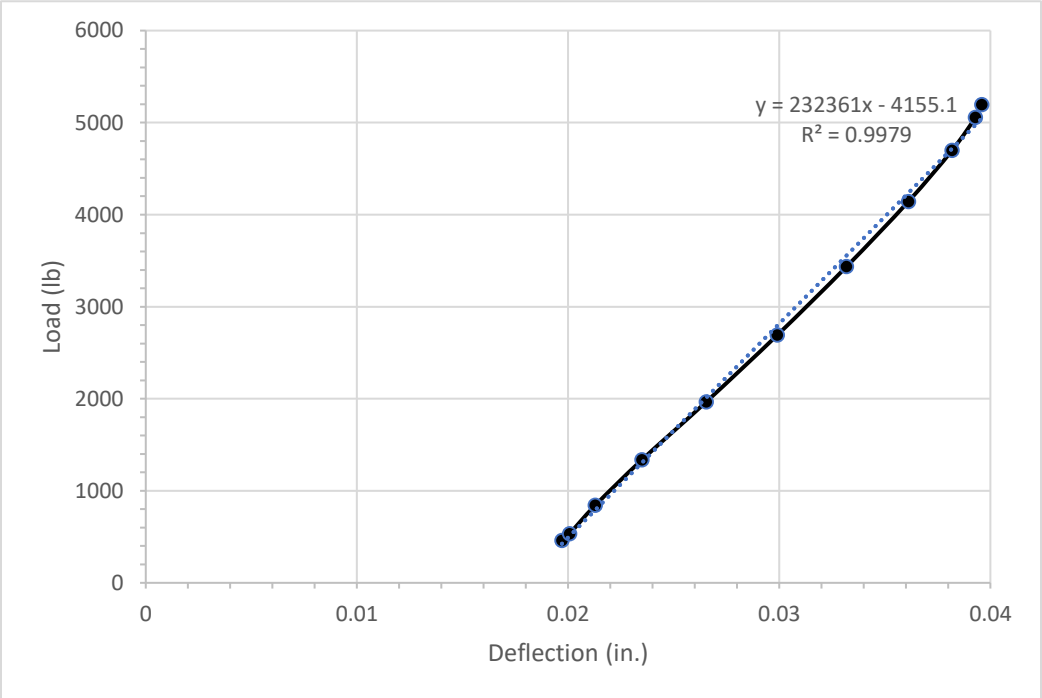

Figure 68: Load vs. deflection for J3 slab 3, single load cycle selected from day 1

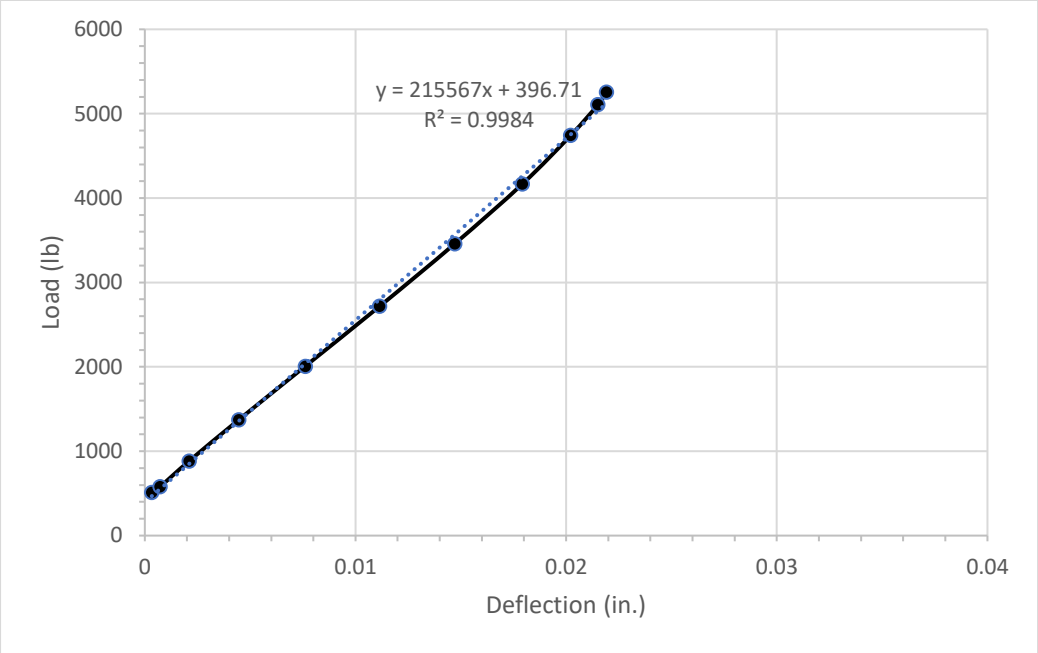

Figure 69: Load vs. deflection for J3 slab 3, single load cycle selected from day 3

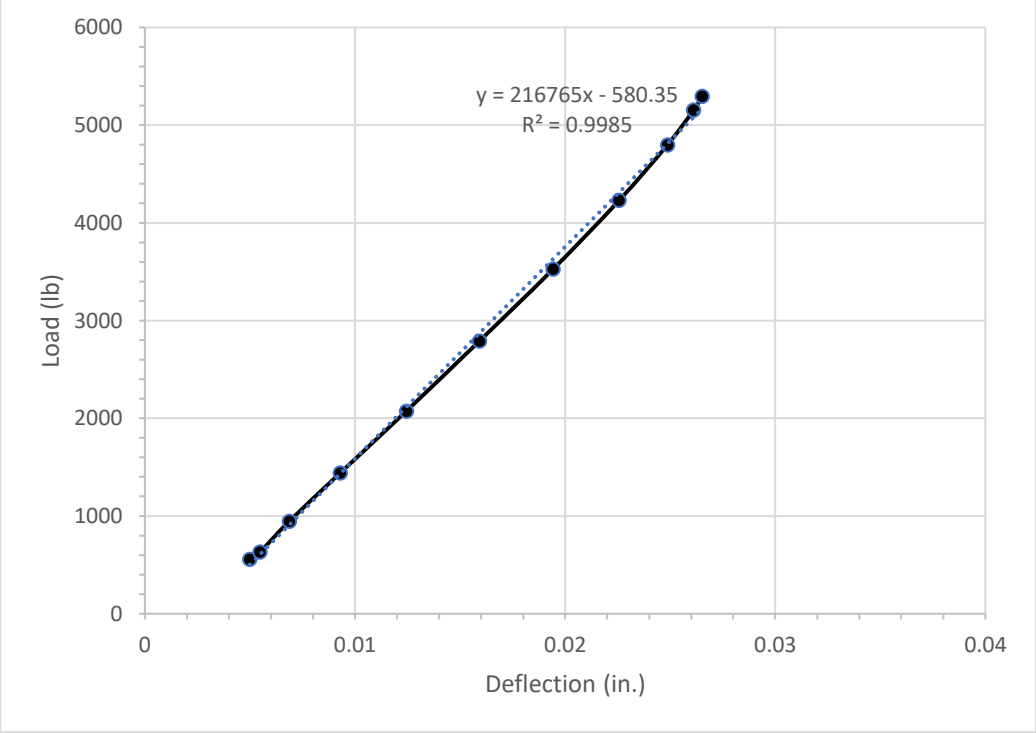

Figure 70: Load vs. deflection for J3 slab 3, single load cycle selected from day 5

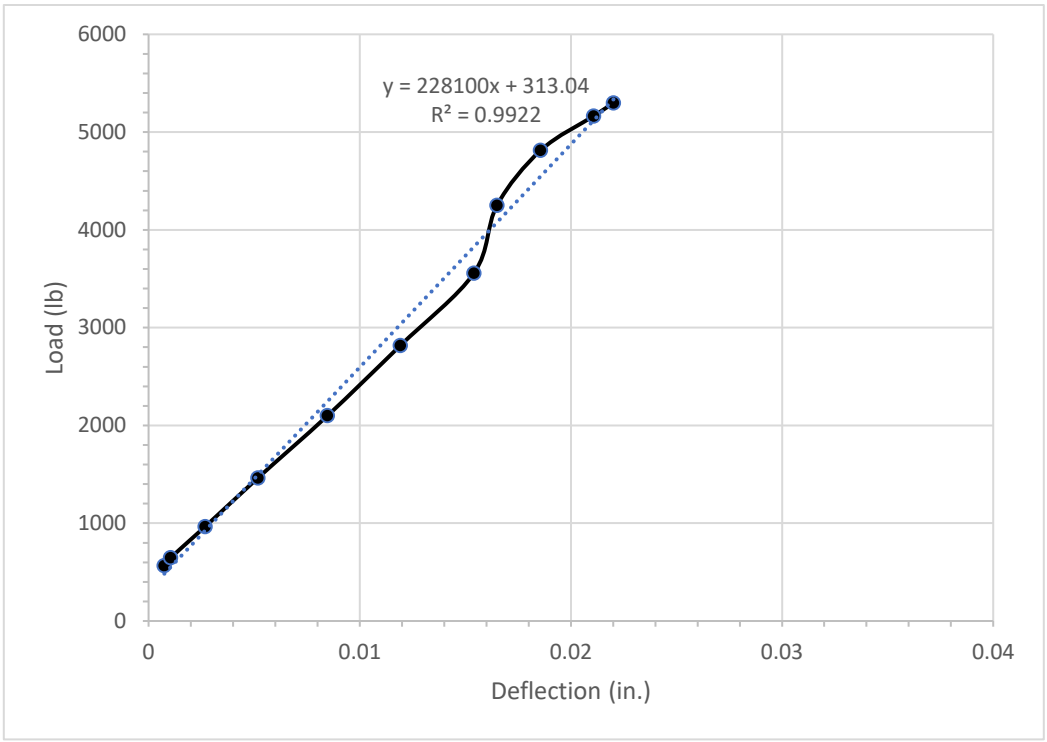

Figure 71: Load vs. deflection for J3 slab 3, single load cycle selected from day 7

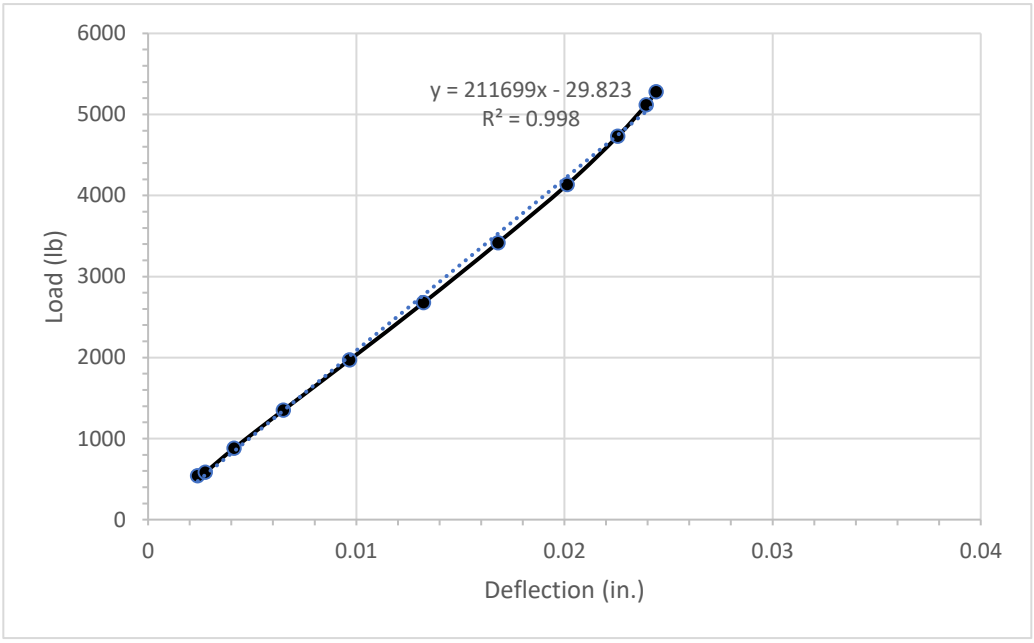

Figure 72: Load vs. deflection for J3 slab 3, single load cycle selected from day 9

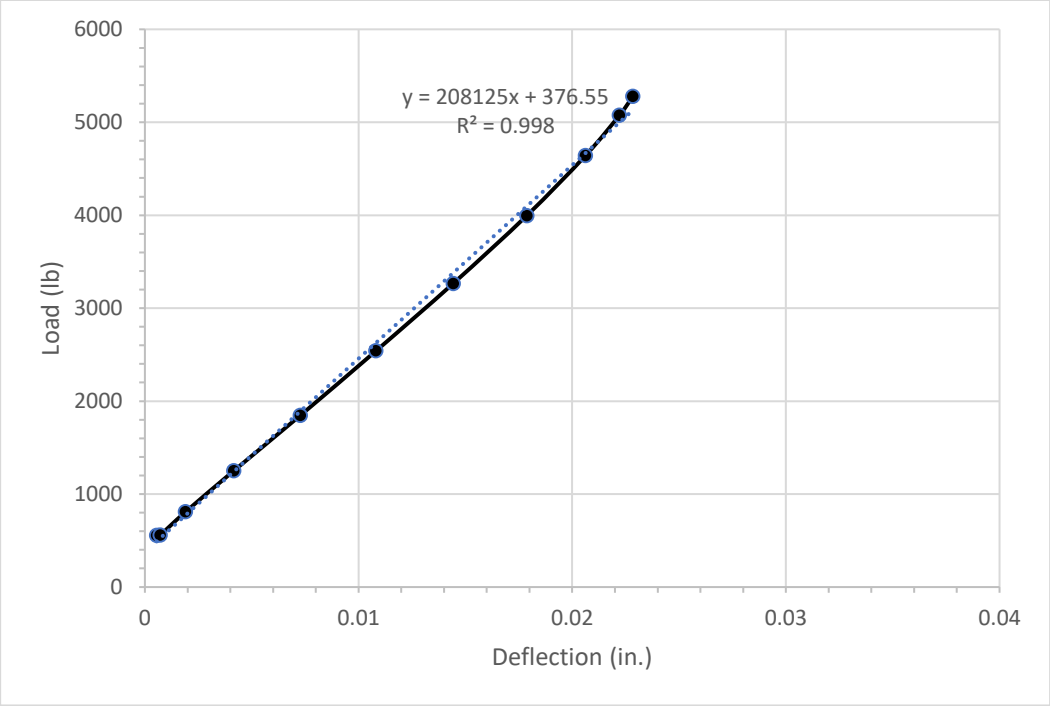

Figure 73: Load vs. deflection for J3 slab 3, single load cycle selected from day 11

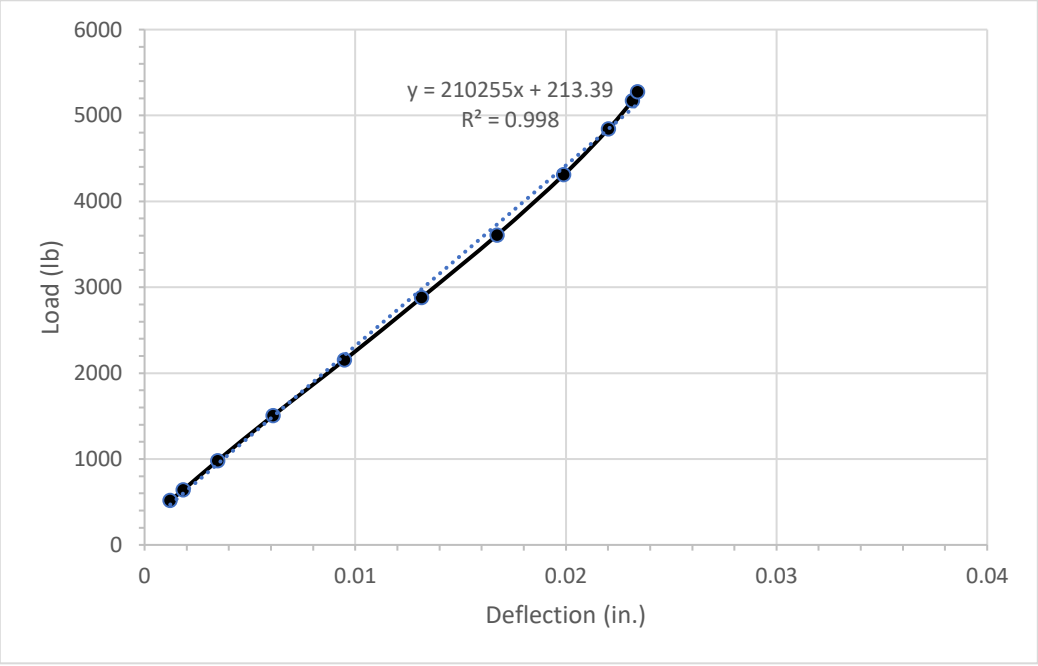

Figure 74: Load vs. deflection for J3 slab 3, single load cycle selected from day 13

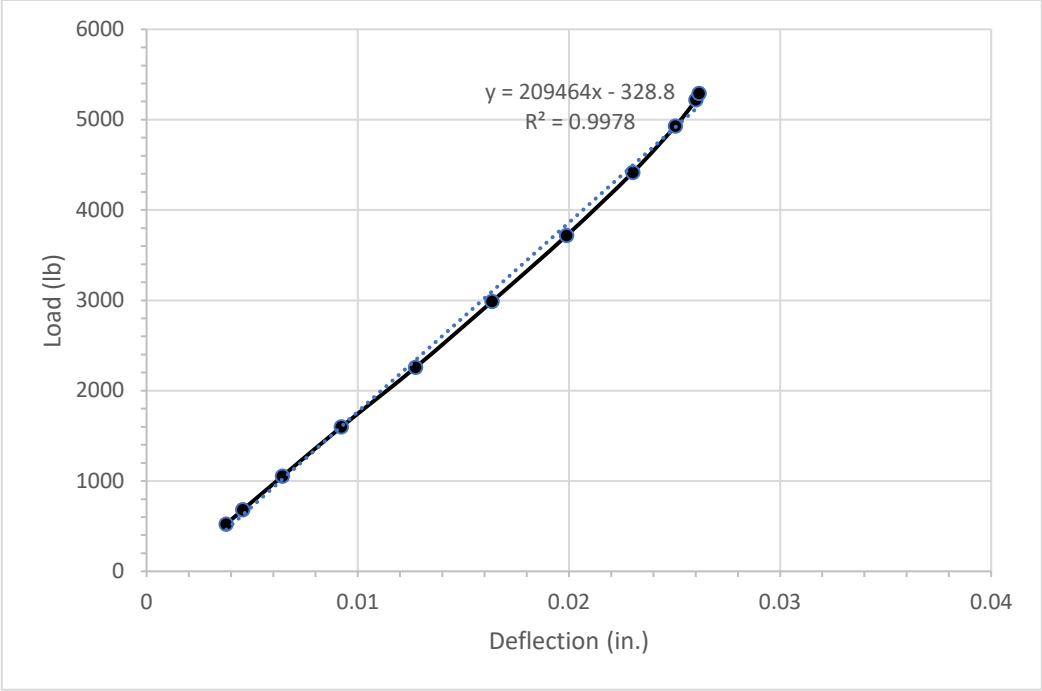

Figure 75: Load vs. deflection for J3 slab 3, single load cycle selected from day 15

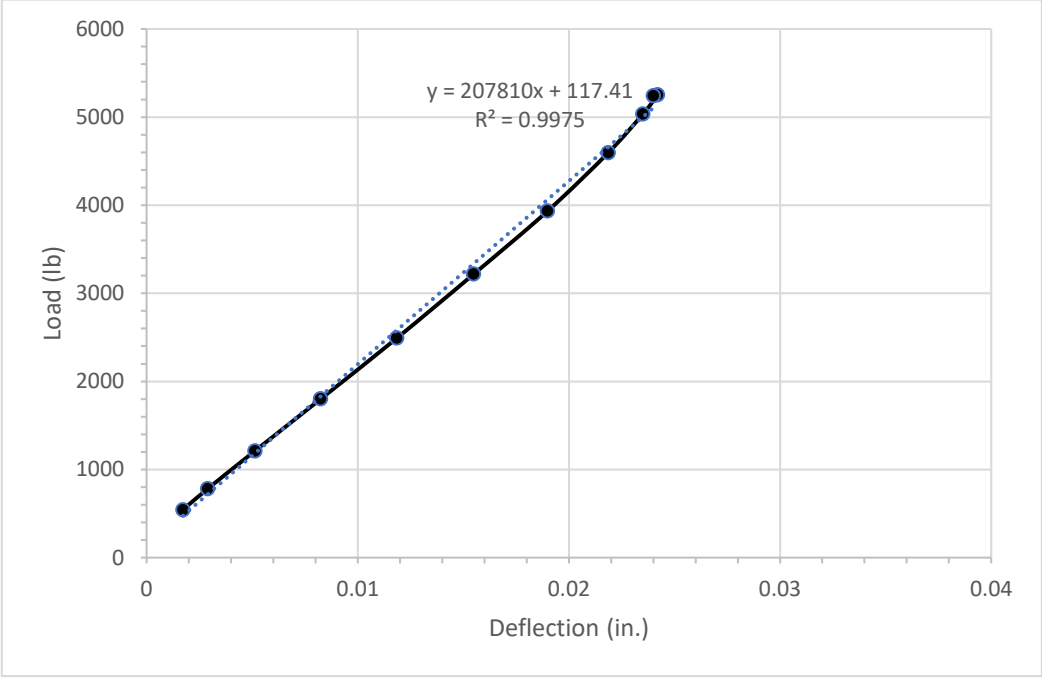

Figure 76: Load vs. deflection for J3 slab 3, single load cycle selected from day 17

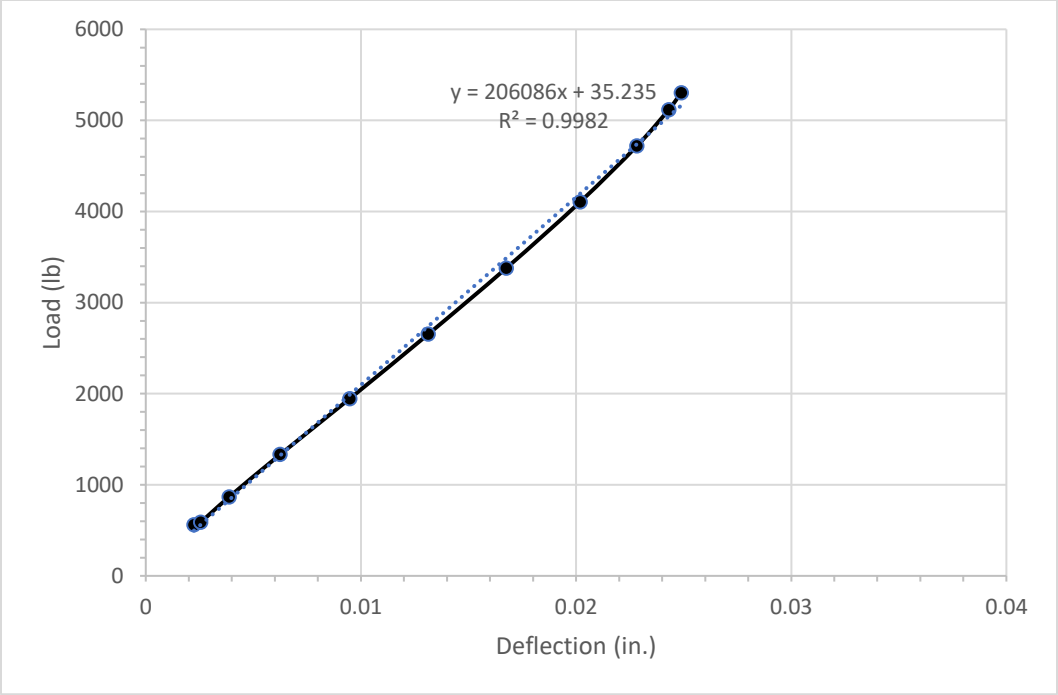

Figure 77: Load vs. deflection for J3 slab 3, single load cycle selected from day 19

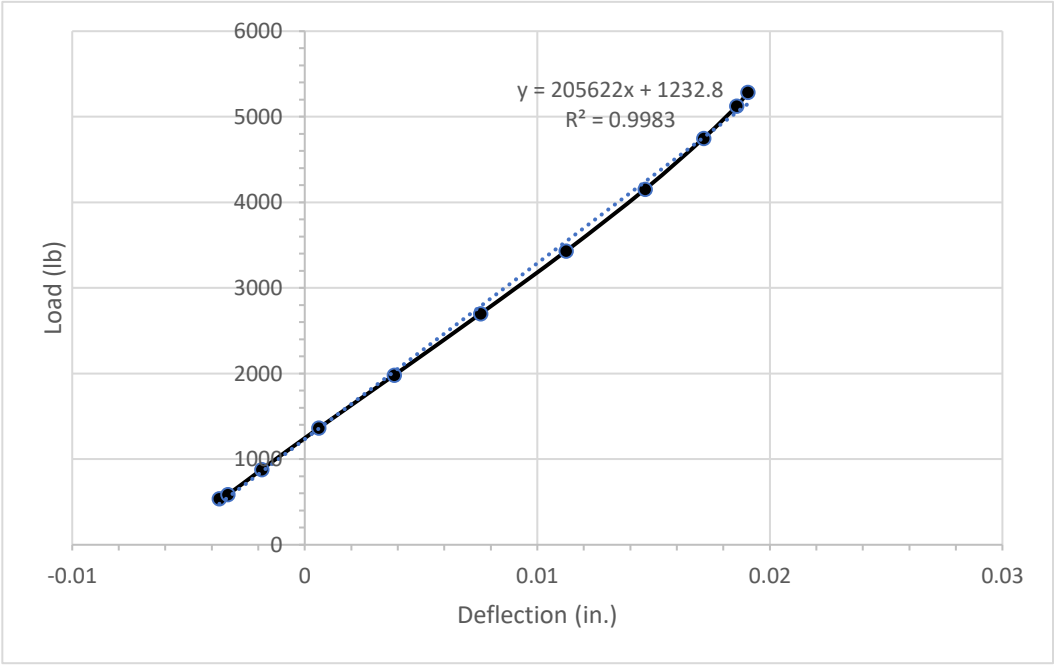

Figure 78: Load vs. deflection for J3 slab 3, single load cycle selected from day 21

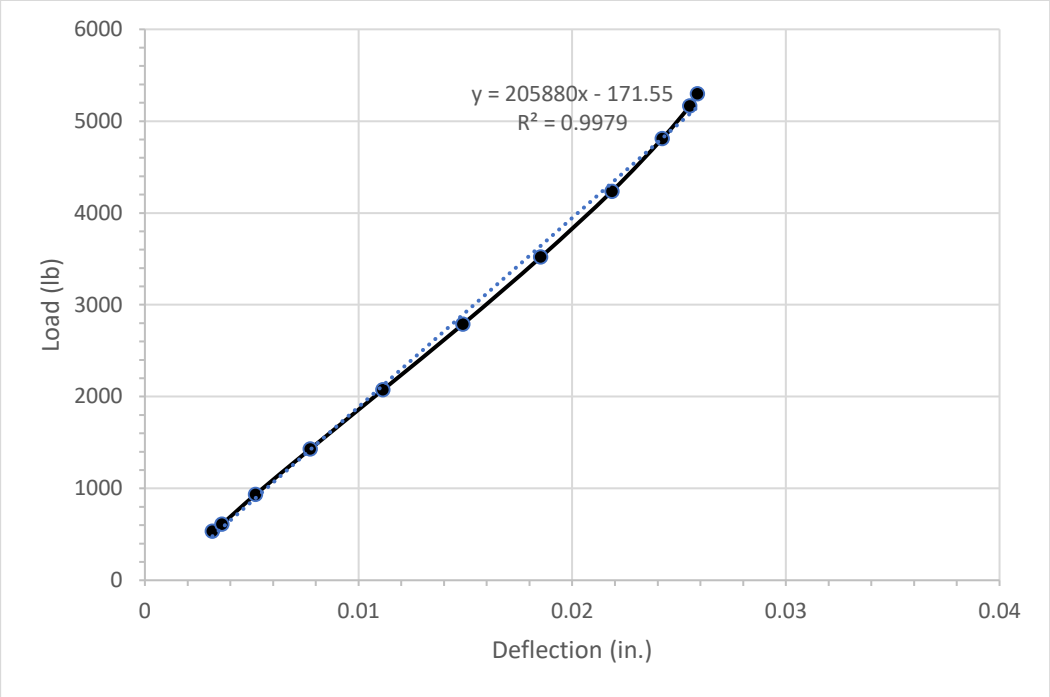

Figure 79: Load vs. deflection for J3 slab 3, single load cycle selected from day 23

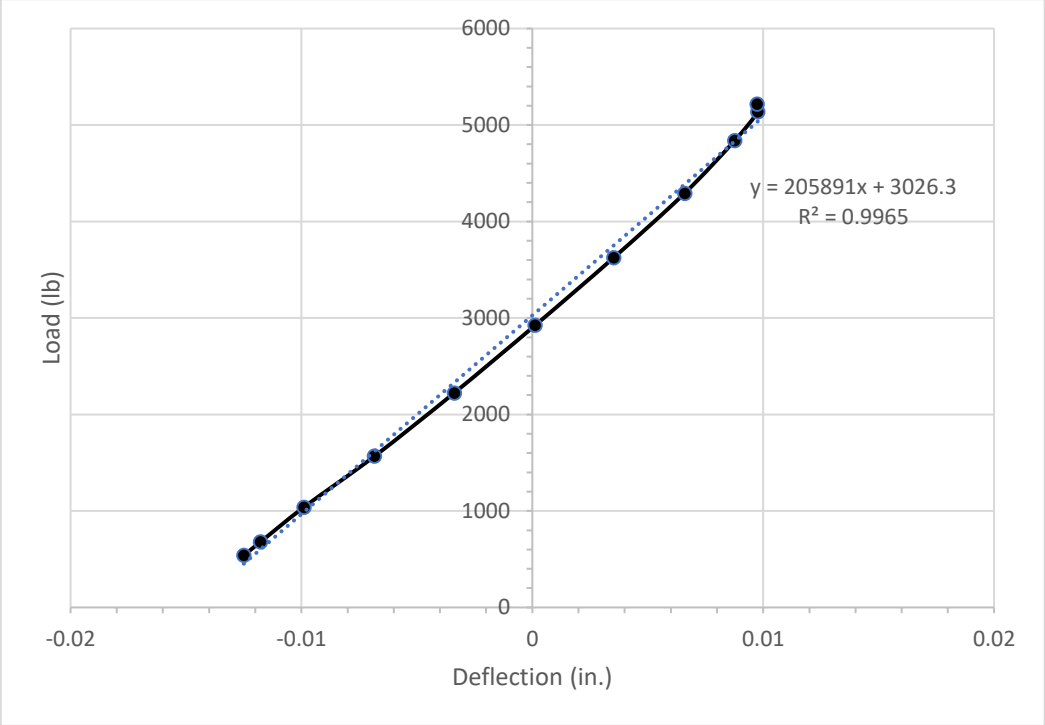

Figure 80: Load vs. deflection for J3 slab 3, single load cycle selected from day 25

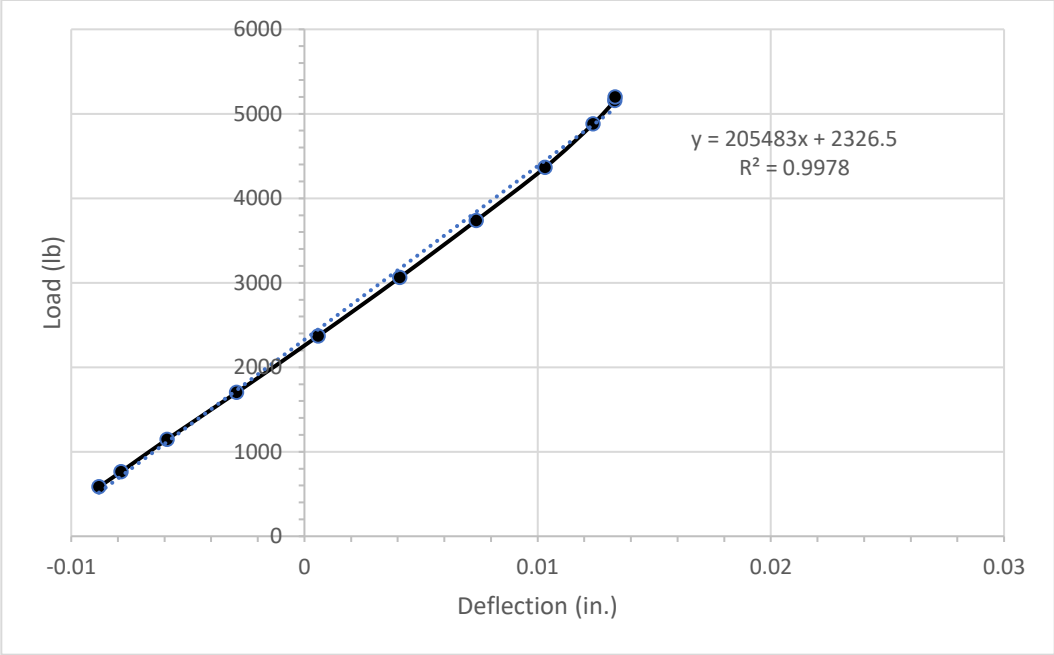

Figure 81: Load vs. deflection for J3 slab 3, single load cycle selected from day 27

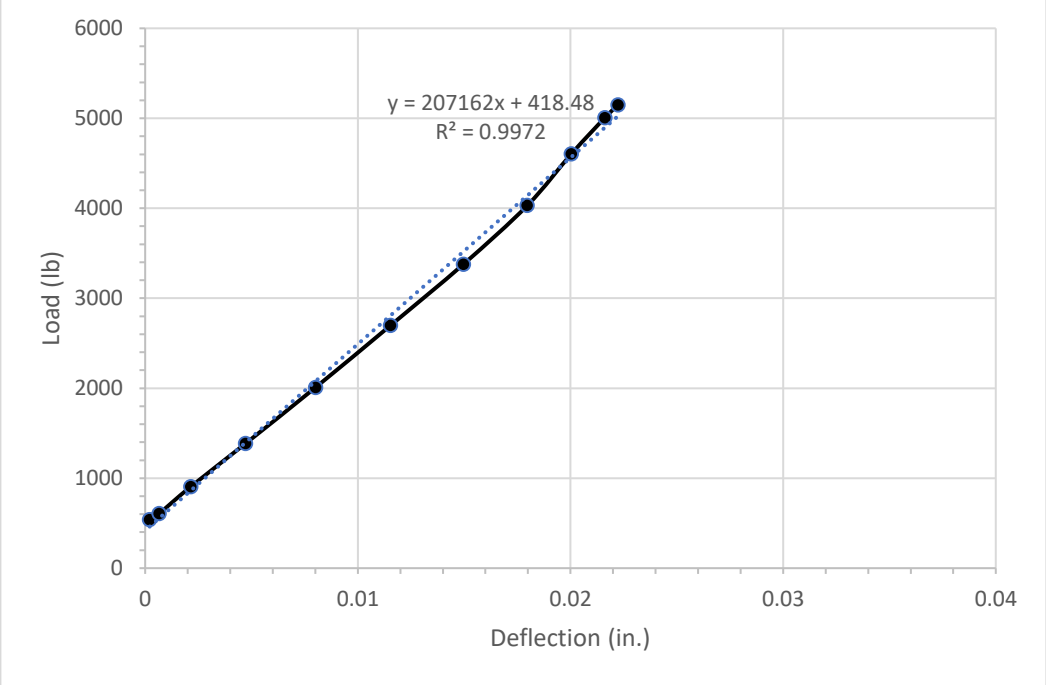

Figure 82: Load vs. deflection for J3 slab 3, single load cycle selected from day 29

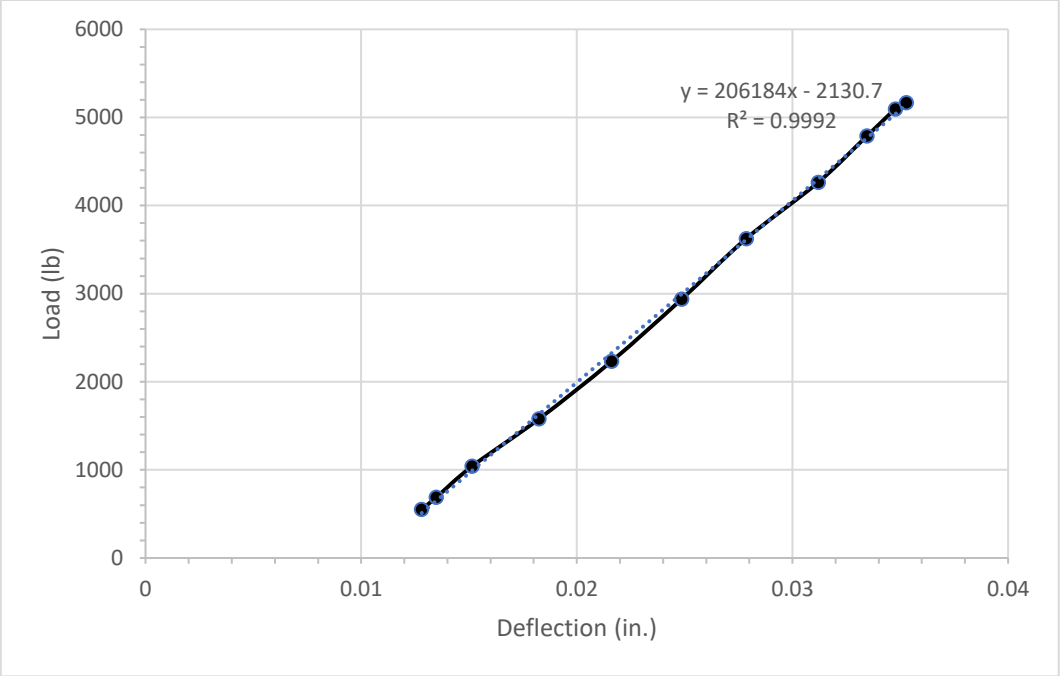

Figure 83: Load vs. deflection for J3 slab 3, single load cycle selected from day 31

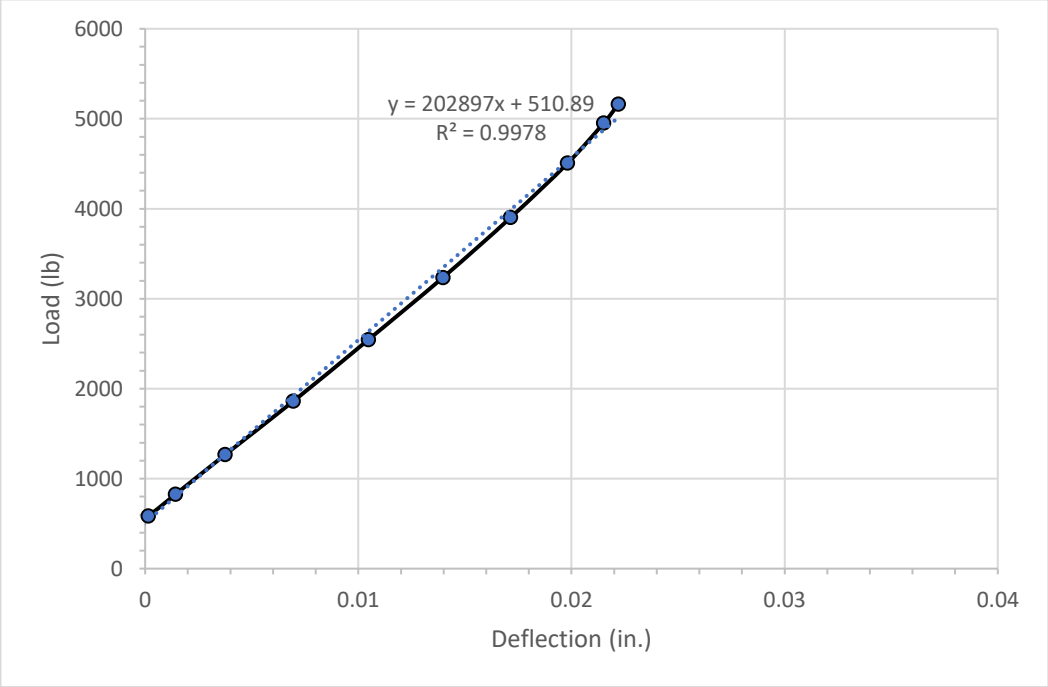

Figure 84: Load vs. deflection for J3 slab 3, single load cycle selected from day 33

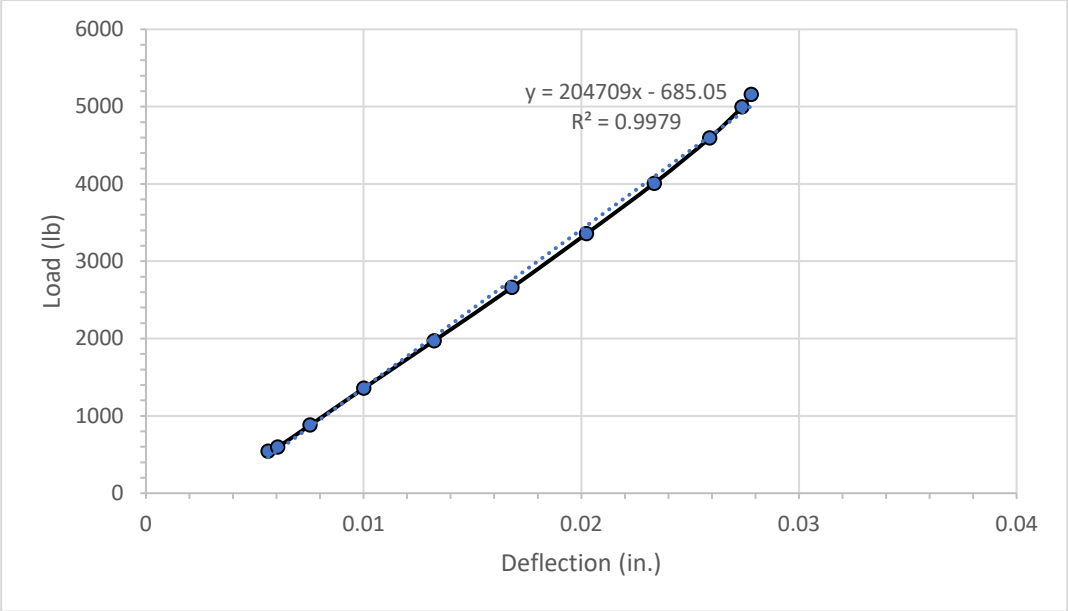

Figure 85: Load vs. Deflection for J3 slab 3, single load cycle selected from day 35

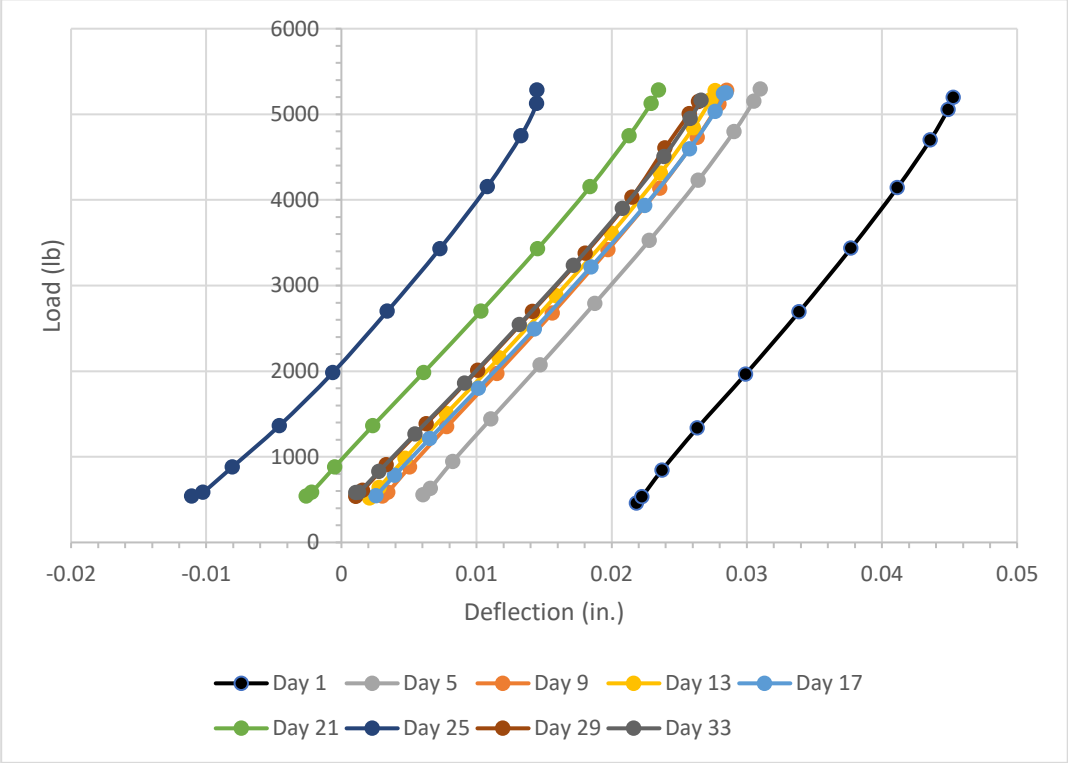

Figure 86: Comparison of load vs. deflection curves of J3 for multiple days

After the specimen had been subjected to 3 million load cycles, the load was increased to 6.5 kips and applied cyclically with a frequency of 1 hertz. This was 10% more than the expected cracking load. The test program demanded for the specimen to be loaded at this rate for 2 million cycles more, or until failure, which is triggered if the slab had excessive deflection (beyond 1.5 in.) or if the reinforcement failed due to fatigue. Figures 87-91 show the load vs. deflection curves for the loading portion of a single cycle analyzed every other day for the 2 million cycles with load above the cracking load. Figure 92 shows multiple cycles from different days after maximum cyclic load was increased to 6.5 kips for comparison. Data did not overlap but they display very similar slopes. The key difference is the y-axis interception. On certain days such as days 36 and 38, there were negative deflections. This may have been caused by the correction made with the support deflections. There was possibly more support deflection than slab deflection.

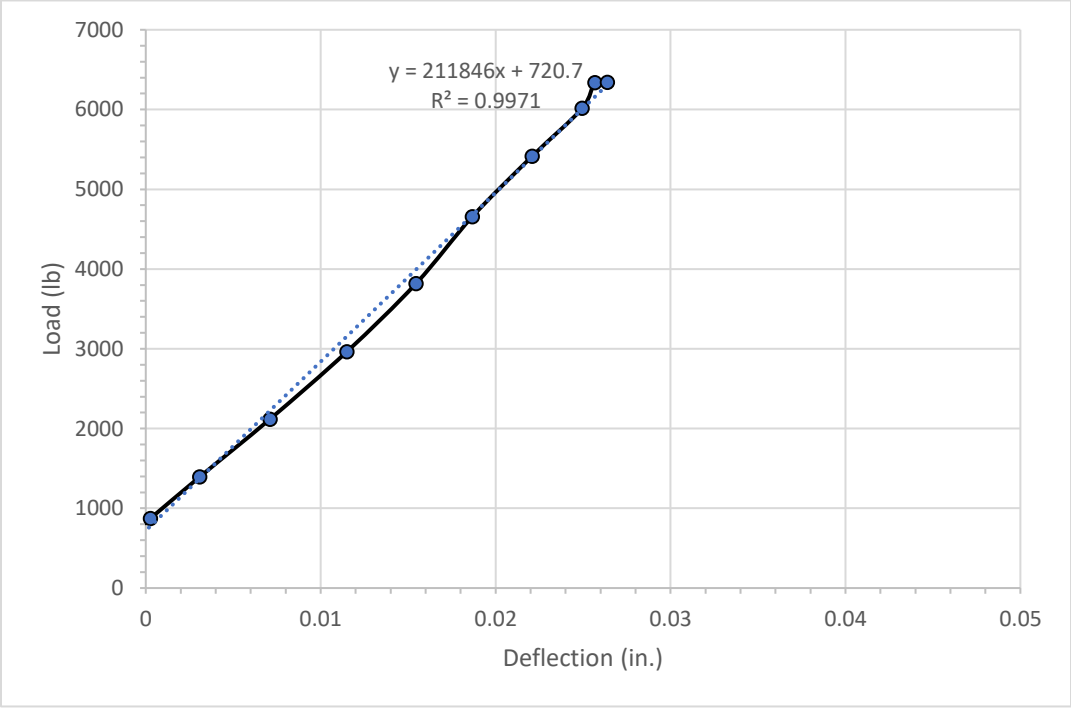

Figure 87: Load vs. deflection for J3 slab 3, single load cycle selected from day 36

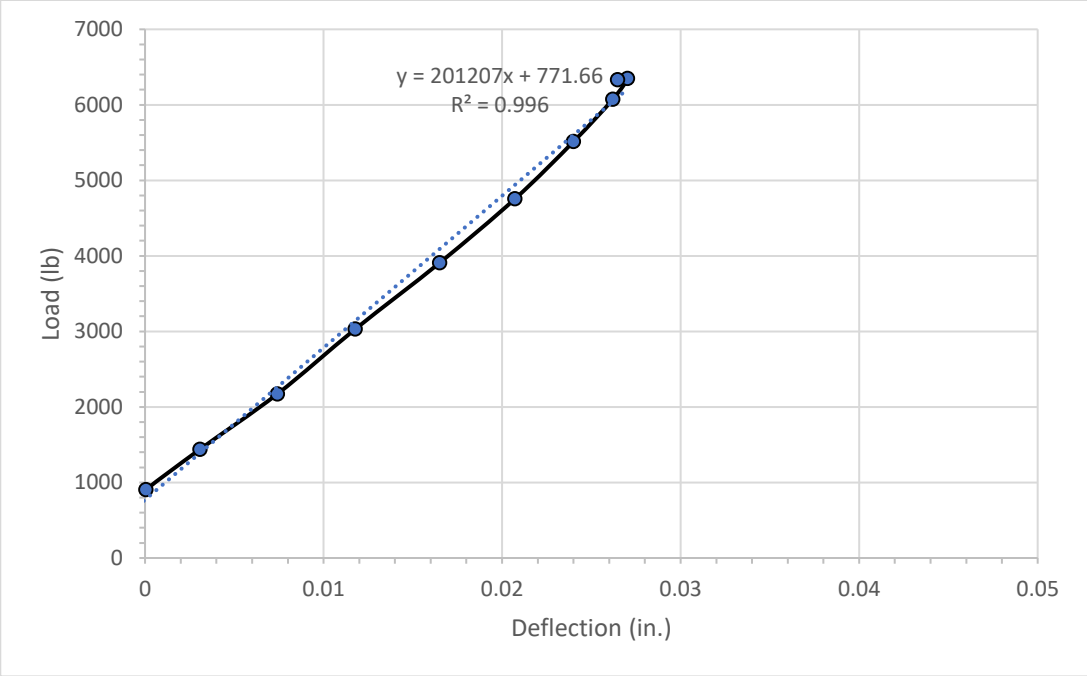

Figure 88: Load vs. deflection for J3 slab 3, single load cycle selected from day 38

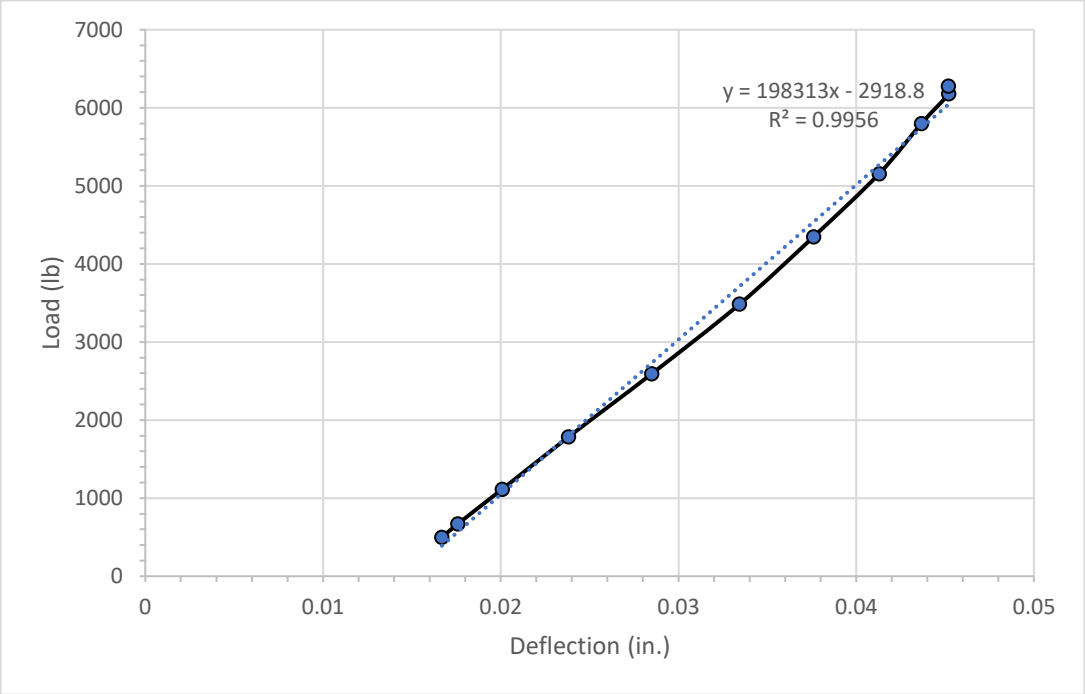

Figure 89: Load vs. deflection for J3 slab 3, single load cycle selected from day 40

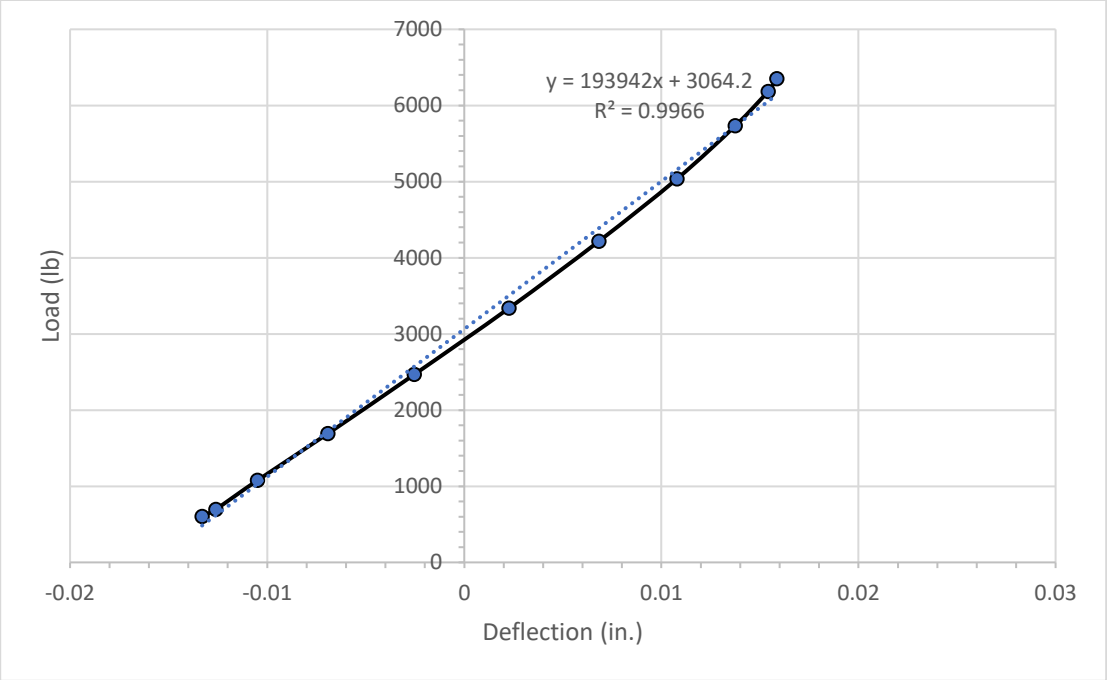

Figure 90: Load vs. deflection for J3 slab 3, single load cycle selected from day 42

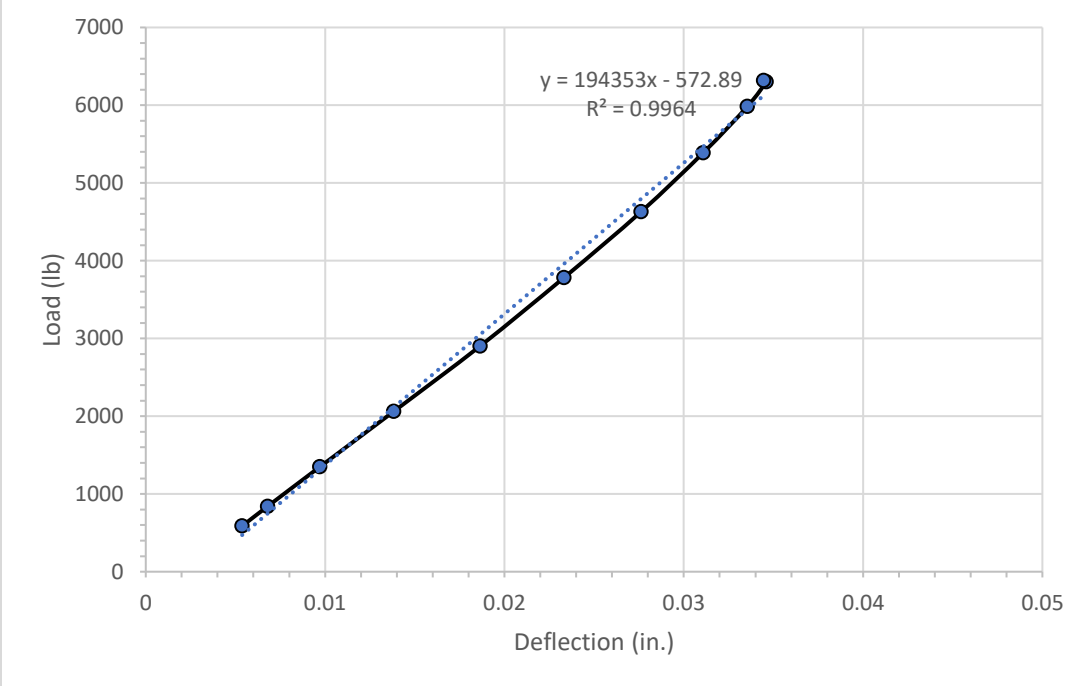

Figure 91: Load vs. deflection for J3 slab 3, single load cycle selected from day 44

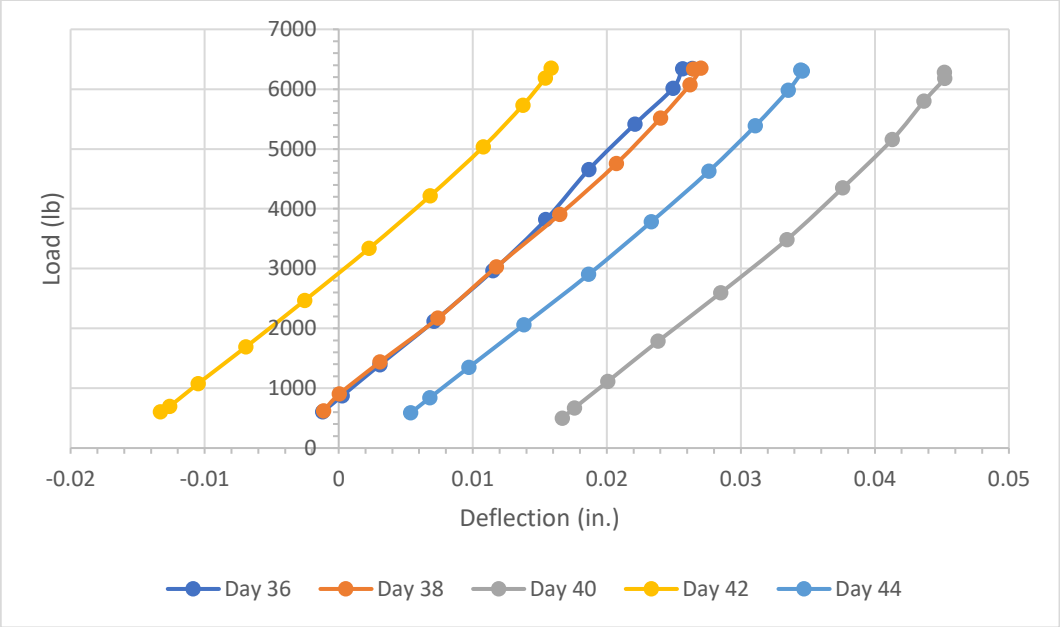

Figure 92: Comparison of load vs. deflection curves of J3 for multiple days after maximum cyclic load was increased to 6.5 kips

The slab was cyclically loaded for 850,950 cycles but it did not deflect enough to consider failure and the reinforcing steel did not fail in fatigue. The decision was made to increase to maximum load to 8.7 kips and cyclically loaded a further 1,149,050 cycles or until failure. The 8.7 kips maximum load was loosely based on the maximum load for the cyclic testing performed by Funderburg (2018) and Coleman (2018) even though it was slightly less than the 9 kip maximum load from that previous research. Unfortunately, the campus closure including research facilities during the coronavirus pandemic in late March 2020 prevented the test from being finished. Nonetheless, the test was run for 473,425 cycles with the 8.7 kips load before the lockdown took place. Figures 93-95 show the load vs. deflection curves for the loading portion of a single cycle analyzed every other day. The graphs also included linear trend lines to show the general slope of the loading curve. Figure 96 shows multiple cycles from different days for comparison. All those data overlap each other indicating that the stiffness did

not decrease much during period. The curves looked non-linear compared to curves plotted in the first 35 days. There were also negative deflections that may have been caused by the correction made with the support deflections. There was possibly more support deflection than slab deflection.

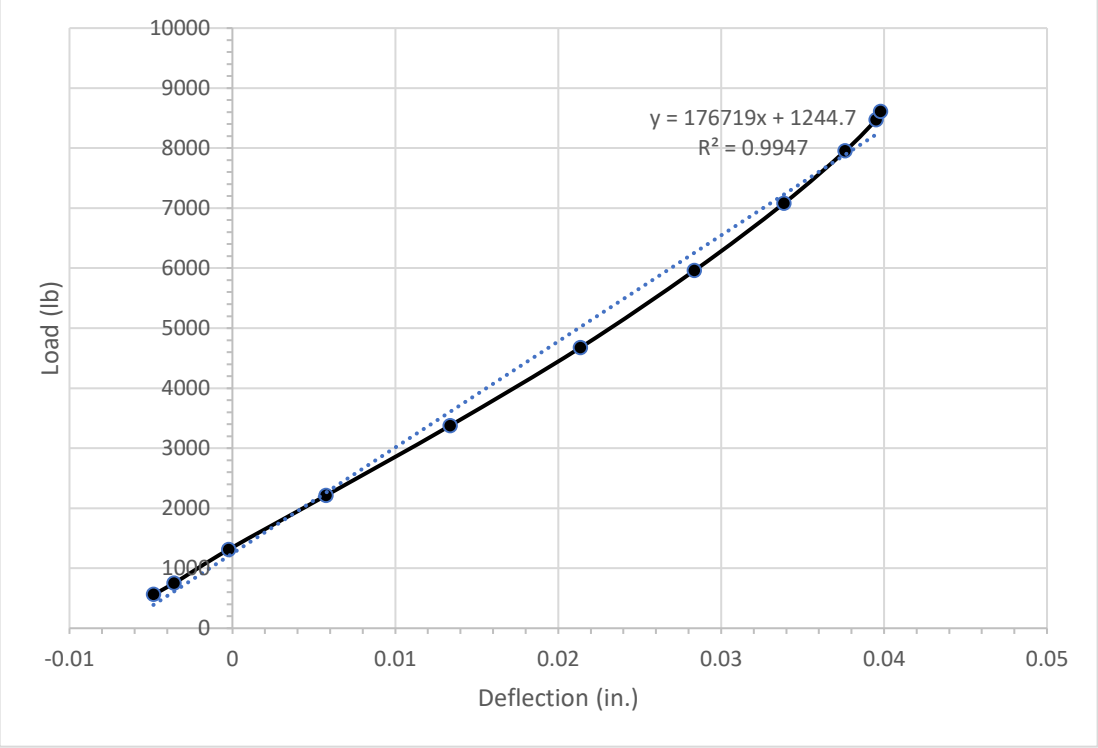

Figure 93: Load vs. deflection for J3 slab 3, single load cycle selected from day 46

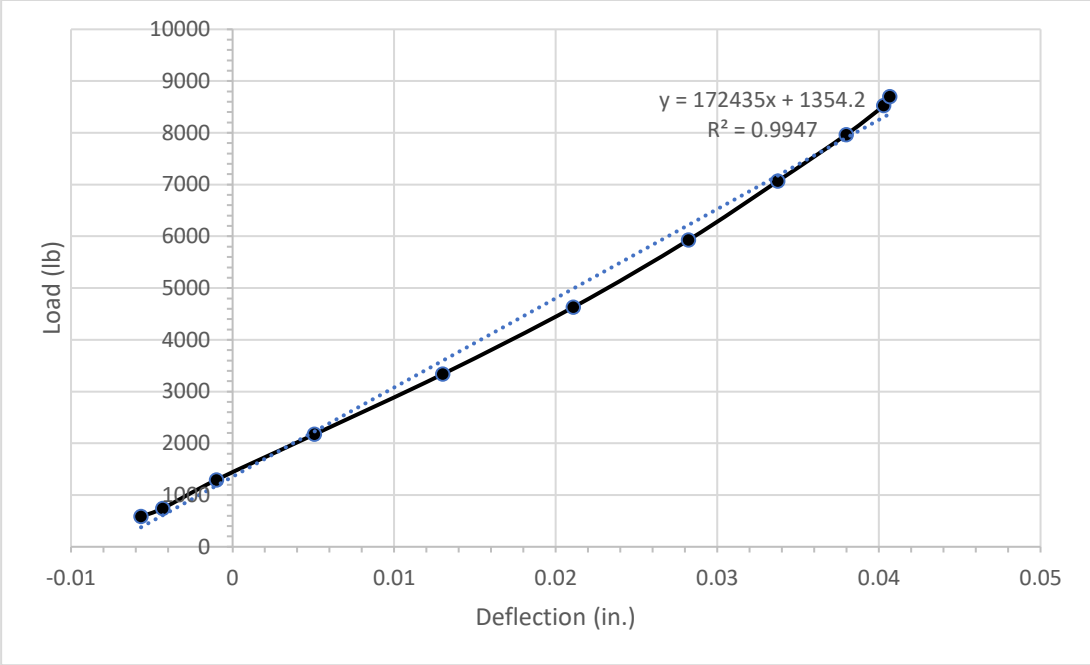

Figure 94: Load vs. deflection for J3 slab 3, single load cycle selected from day 48

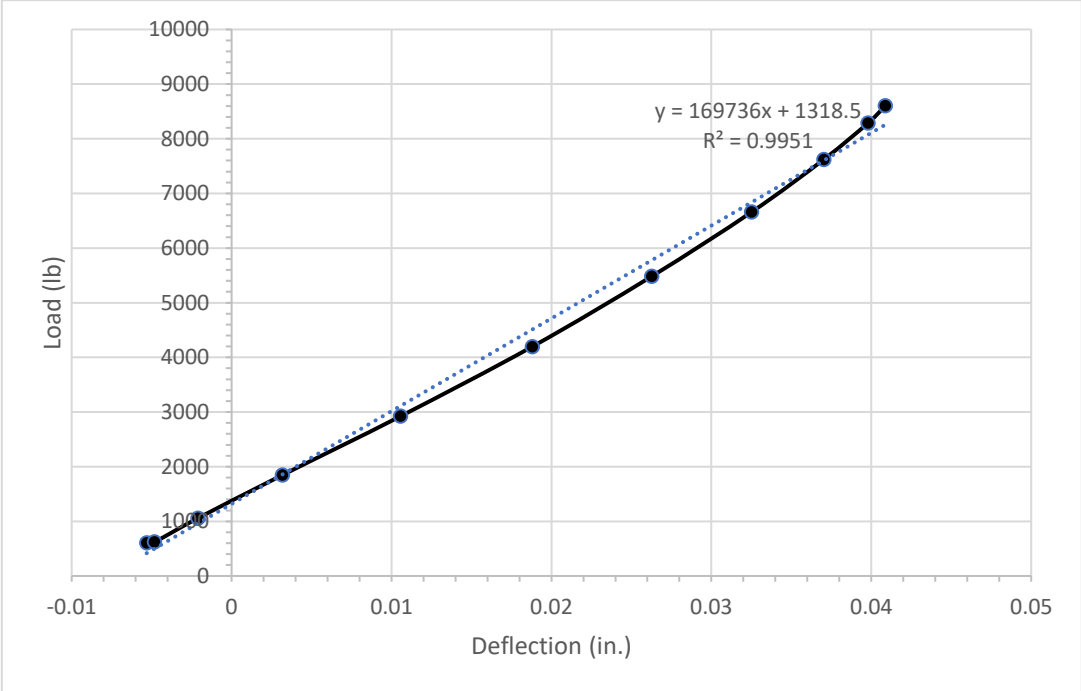

Figure 95: Load vs. deflection for J3 slab 3, single load cycle selected from day 50

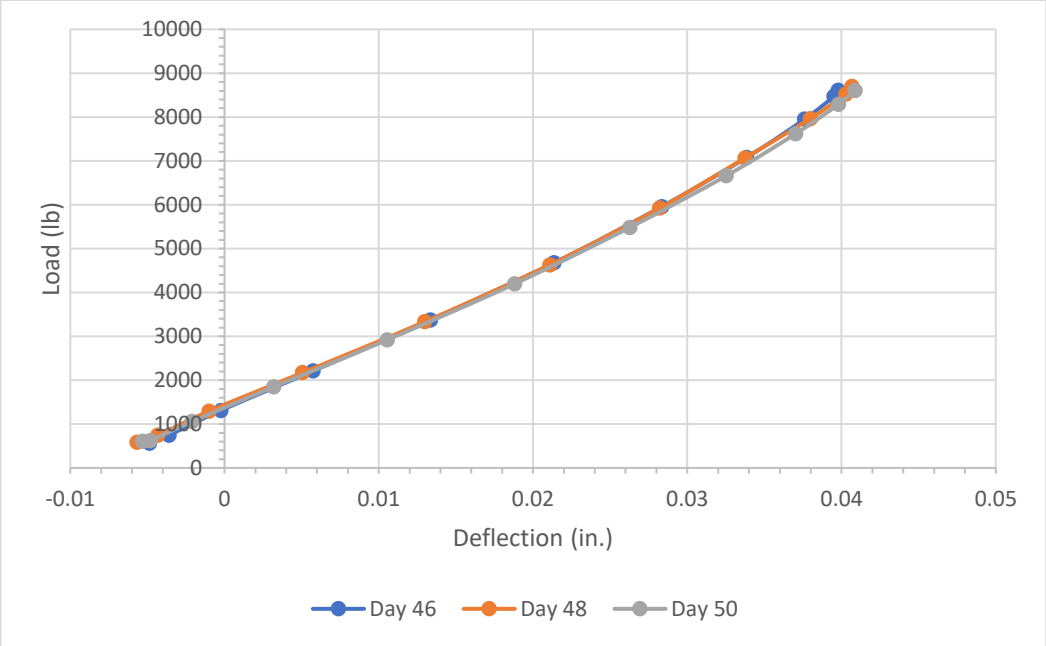

Figure 96: Comparison of load vs. deflection curves of J3 for multiple days after maximum cyclic load was increased to 8.7 kips

Figure 97 shows the slab stiffness vs. time for the 50 day period of cyclic testing. There was a general steady decrease in stiffness over time. From day 2 to day 35, the trend was generally very similar. However, the stiffness decreased by approximately 12.8% between day 35 and 46. The maximum cyclic load was increased on day 36 from 5.3 kips to 6.5 kips. The subsequent days, the trend was similar again starting from day 37-45 and from day 46-50. Day 46 was when the maximum cyclic load was increased from 6.5 kips to 8.7 kips. Figure 98 shows the residual deflection over the 50 day cyclic loading period. Residual deflection is defined as deflection resulting from cyclic load after the removal of the load. Total residual deflection is the cumulative deflections of the 50 days testing period. There were negative deflections that may have been caused by the correction made with the support deflections. For these instances there was possibly more support deflection than slab deflection.

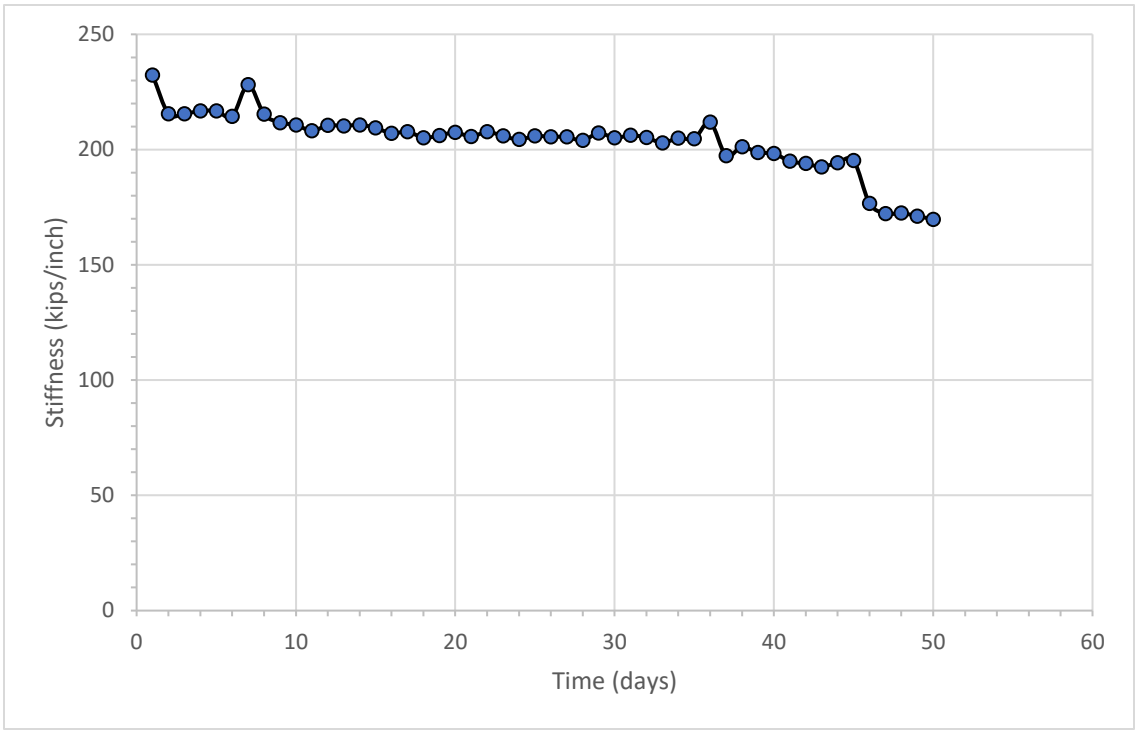

Figure 97: J3 slab stiffness over 50-day loading period

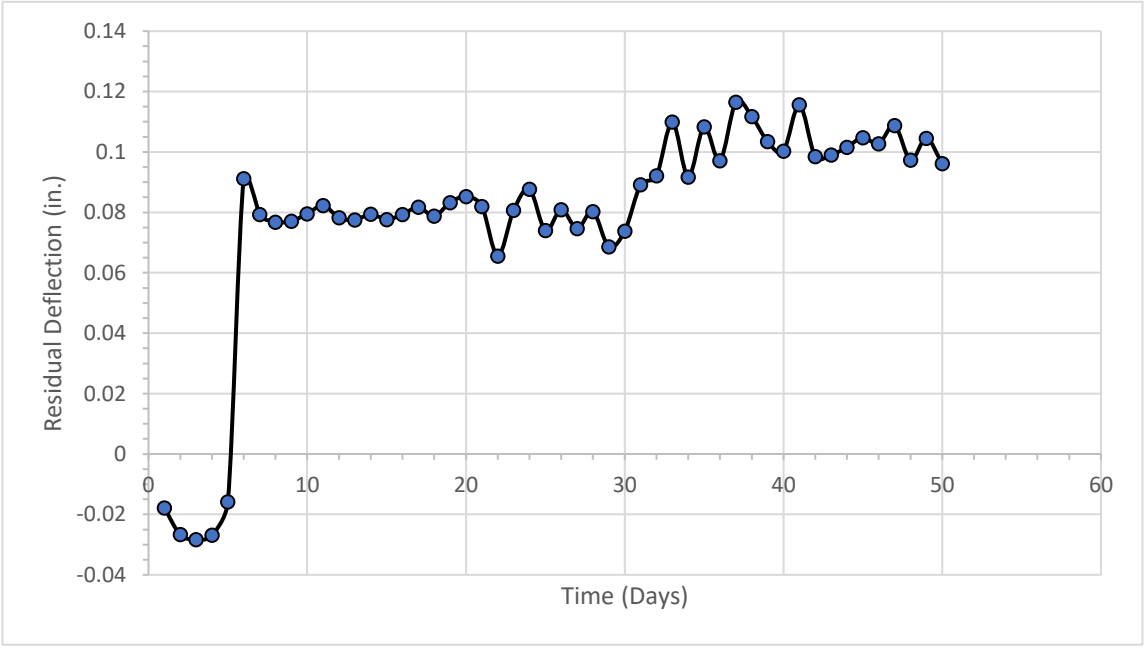

Figure 98: Residual deflection over the course of 50-day cyclic testing period

4.6) Ductal® Slab Joint 3 Cyclic Test Results for

The cyclic test for Ductal® slab 3 essentially followed the same procedure as the cyclic test for J3 slab 3. Ductal® slab 3 was tested cyclically for 3 million cycles with the maximum load of 5.3 kips. Using the MTS system, a 1 hertz cyclic load was applied to Ductal® slab 3 with a maximum load of 5.3 kips. When the campus and research facilities were reopened after the coronavirus lockdown, the MTS machine was not functional and the test could not be conducted until mid-October when the MTS equipment was repaired. The cyclic test ran for 3 million cycles. Figures 99-116 show load vs. deflection curves for the loading portion of a single cycle for the completed 35 days of cyclic testing analyzed every other day. The unloading portion of the curves were not displayed but was similar to the loading portion. A 500-pound preload was set similar to the J3 slab, which resulted in the plots not starting at zero. Since the slab stiffness was of more interest than the absolute deflection, a trend line of the entire data set for each plot is displayed in blue on each graph. The stiffness of the slab is determined from the slope in the equation shown on the graph. Figure 117 shows multiple load cycles from different days for comparison.

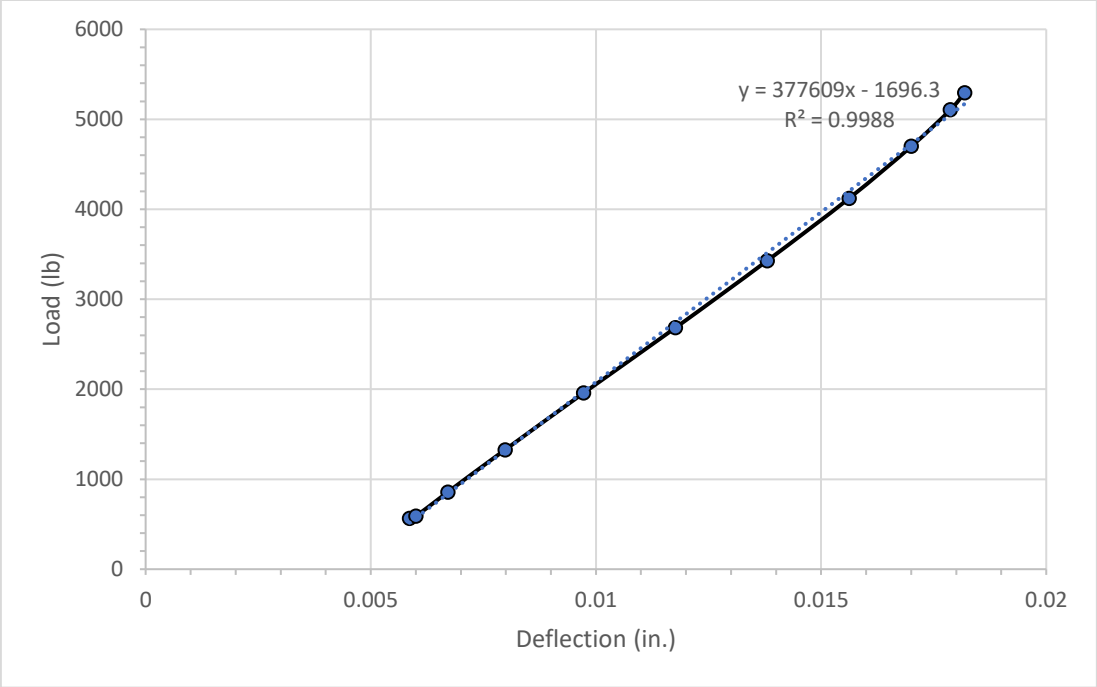

Figure 99: Load vs. deflection for Ductal® slab 3, single load cycle selected from day 1

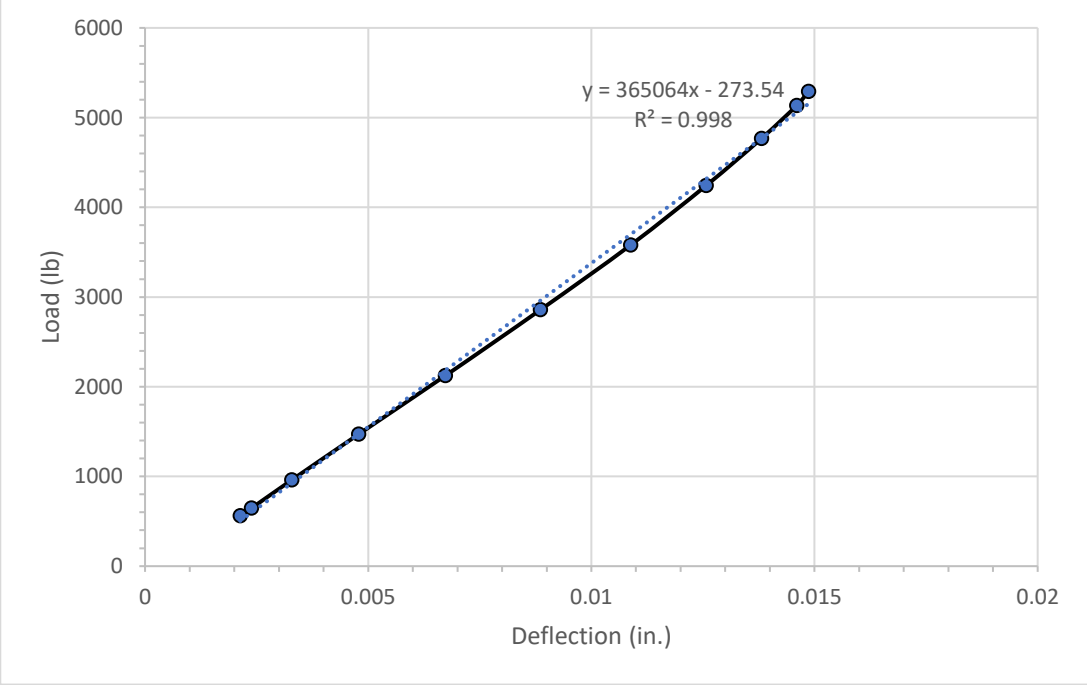

Figure 100: Load vs. deflection for Ductal® slab 3, single load cycle selected from day 3

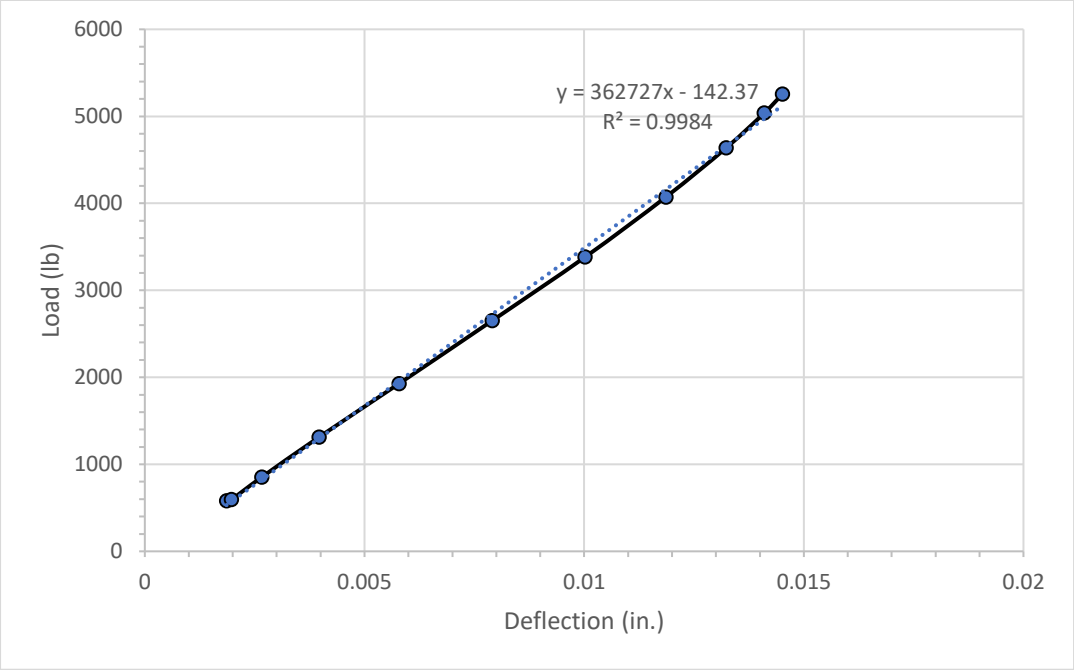

Figure 101: Load vs. deflection for Ductal® slab 3, single load cycle selected from day 5

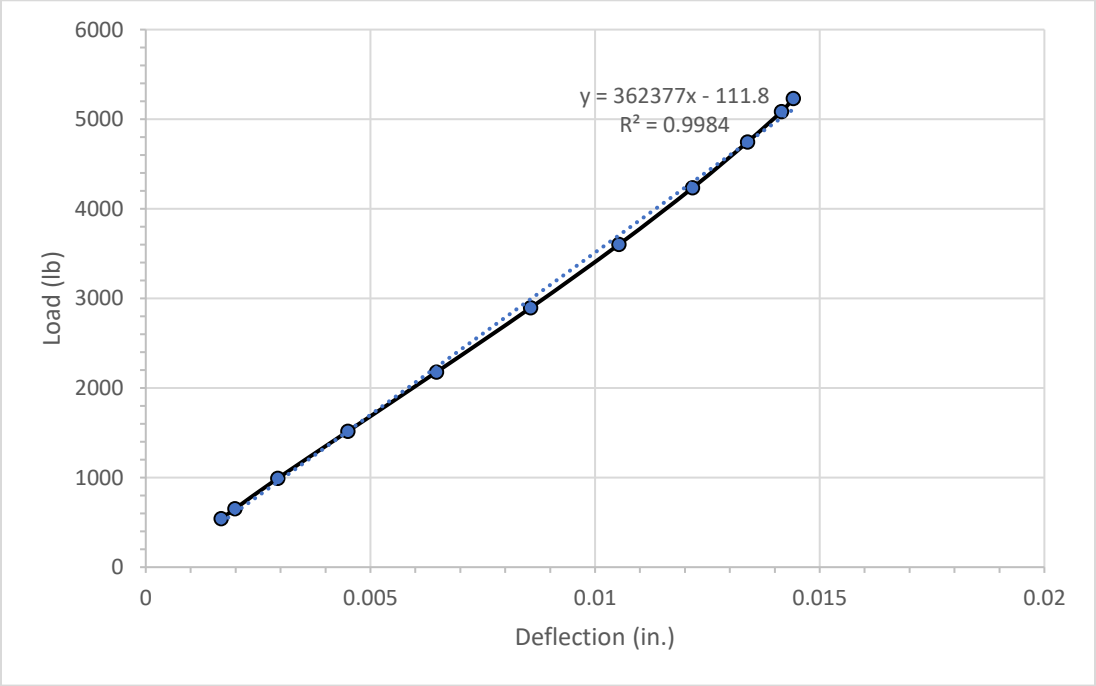

Figure 102: Load vs. deflection for Ductal® slab 3, single load cycle selected from day 7

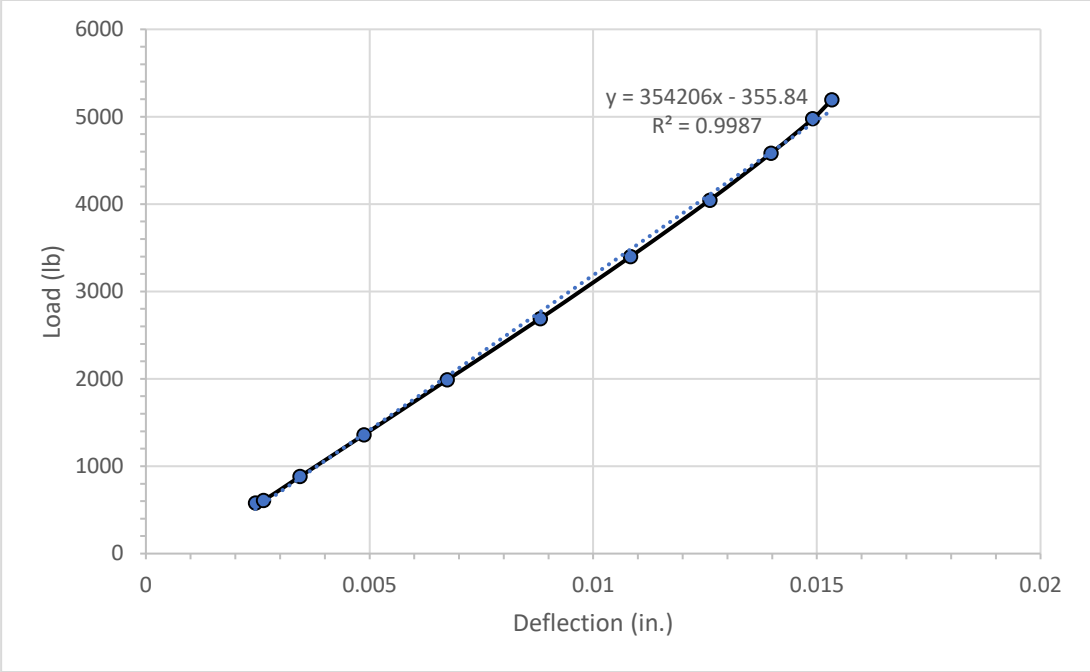

Figure 103: Load vs. deflection for Ductal® slab 3, single load cycle selected from day 9

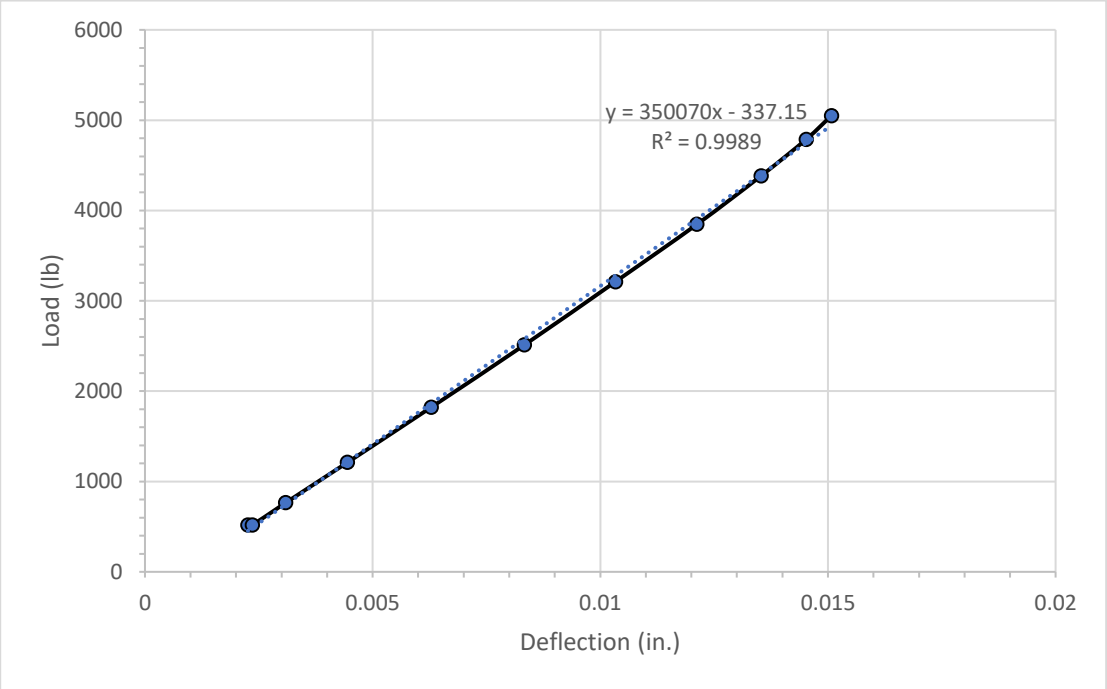

Figure 104: Load vs. deflection for Ductal® slab 3, single load cycle selected from day 11

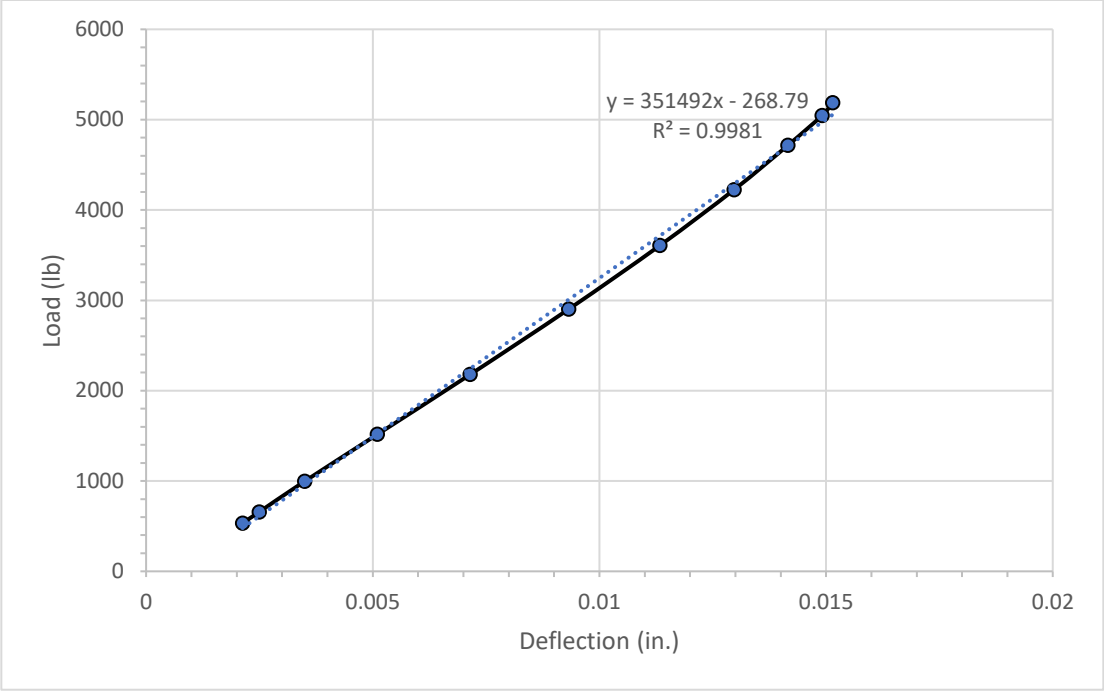

Figure 105: Load vs. deflection for Ductal® slab 3, single load cycle selected from day 13

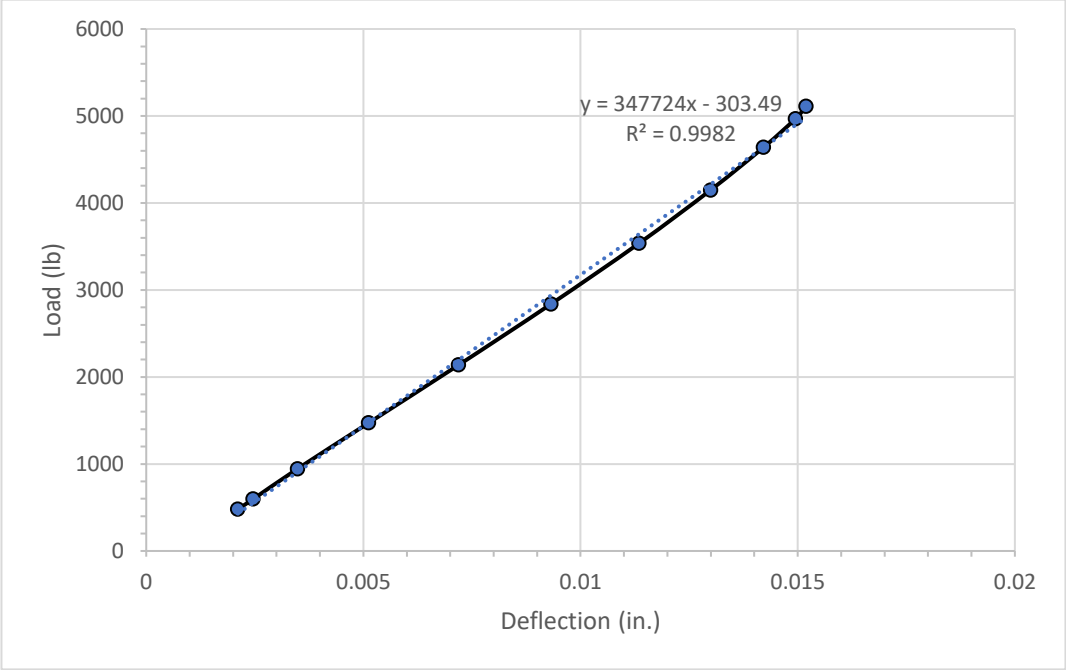

Figure 106: Load vs. deflection for Ductal® slab 3, single load cycle selected from day 15

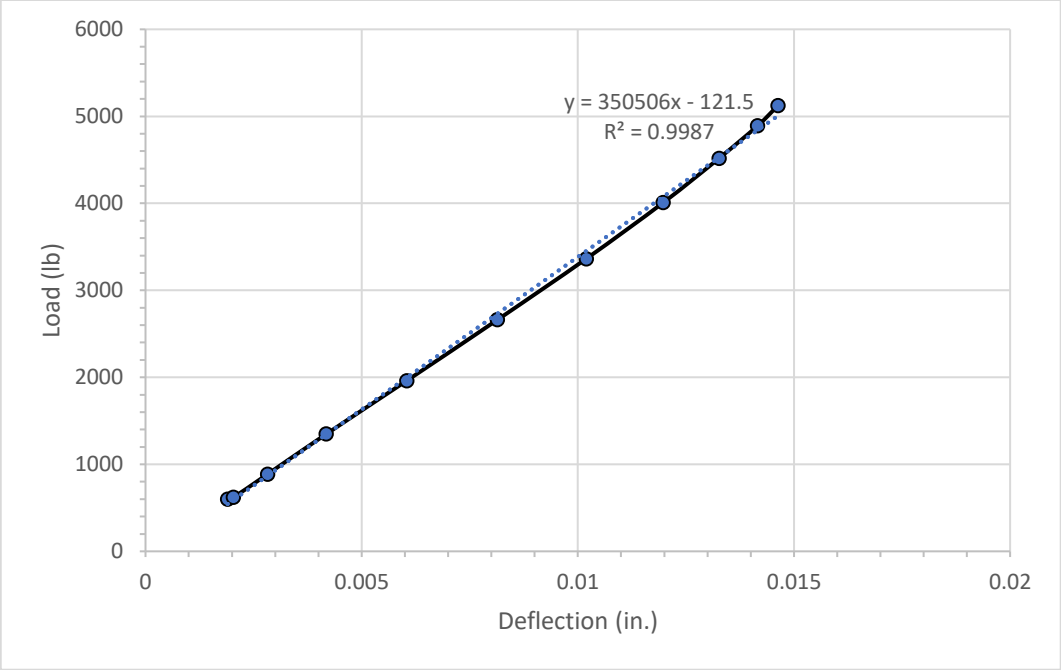

Figure 107: Load vs. deflection for Ductal® slab 3, single load cycle selected from day 17

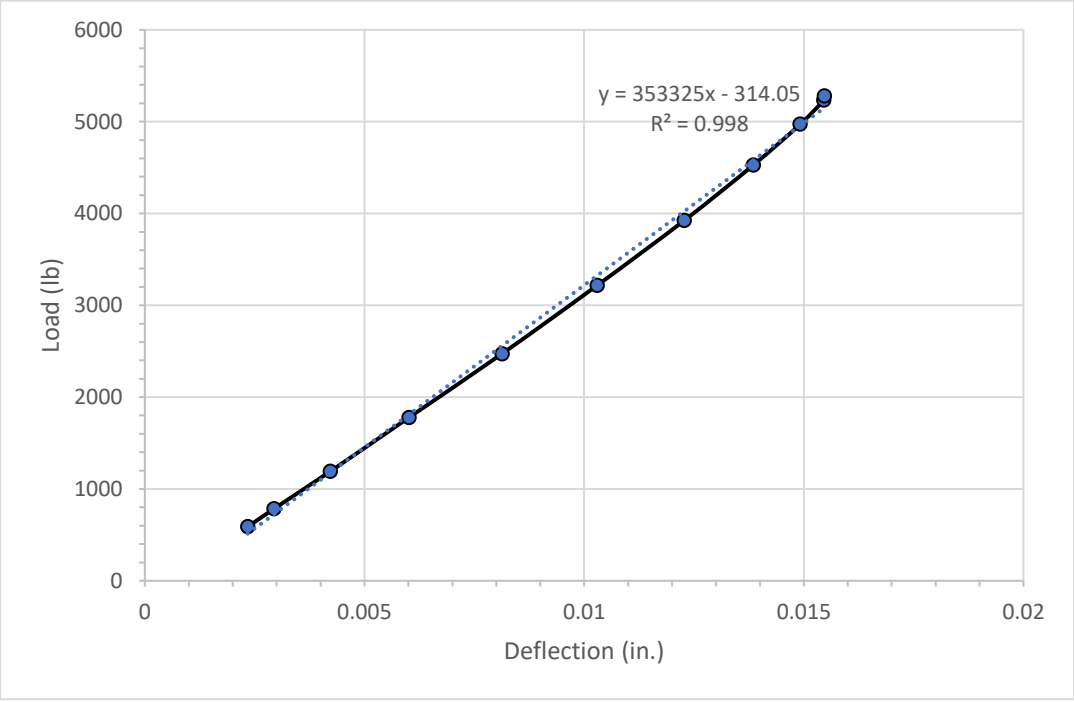

Figure 108: Load vs. deflection for Ductal® slab 3, single load cycle selected from day 19

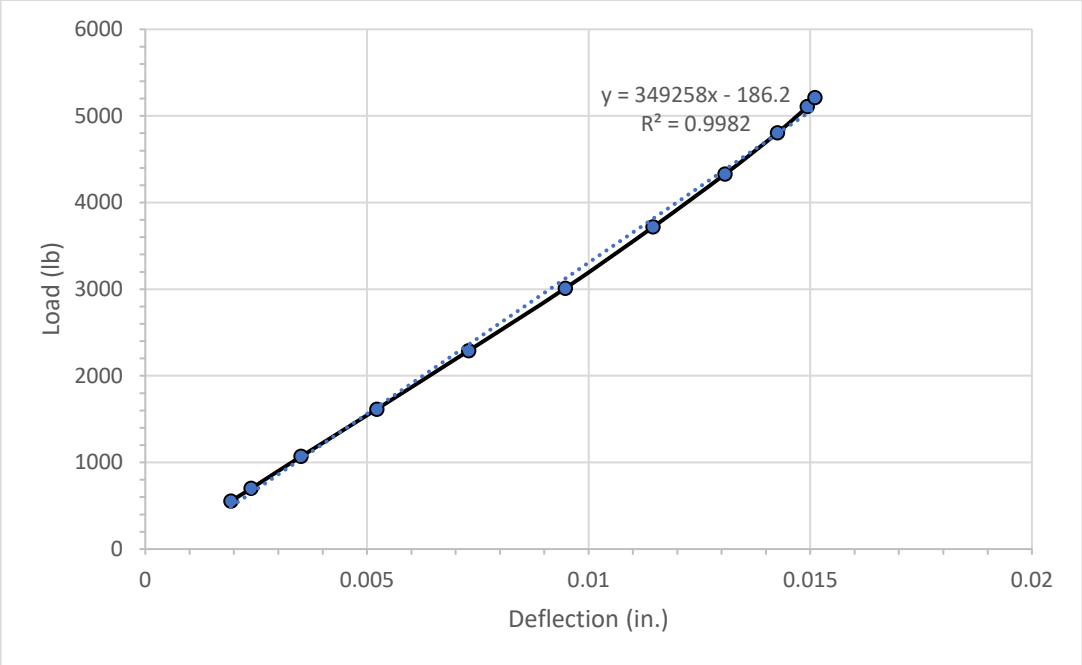

Figure 109: Load vs. deflection for Ductal® slab 3, single load cycle selected from day 21

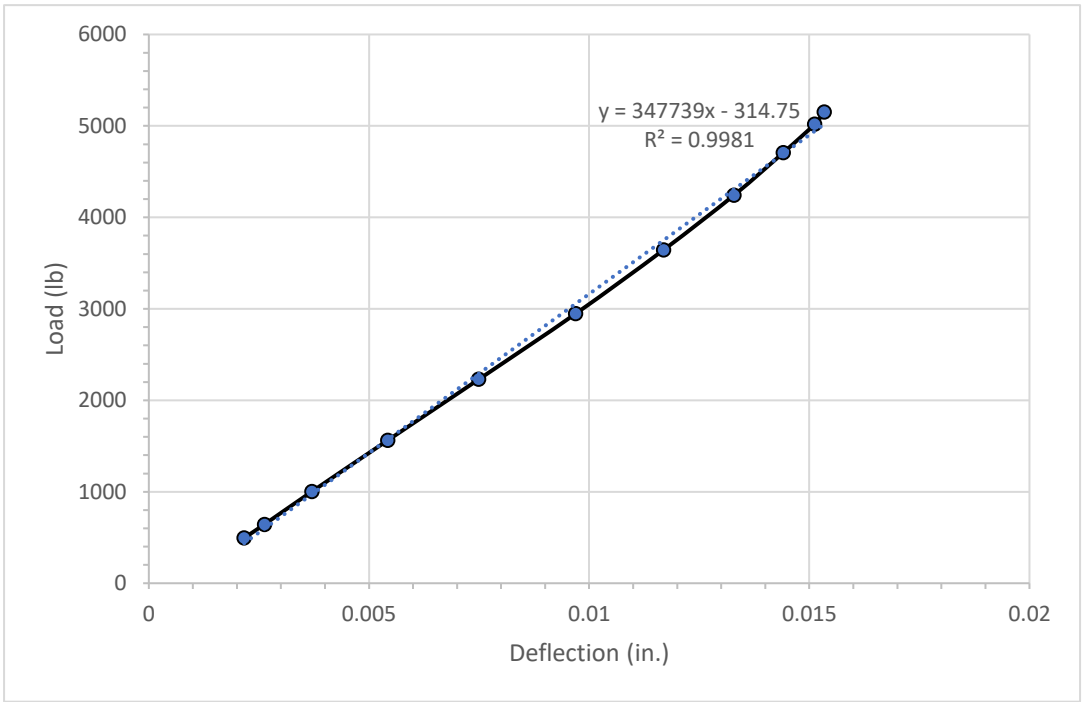

Figure 110: Load vs. deflection for Ductal® slab 3, single load cycle selected from day 23

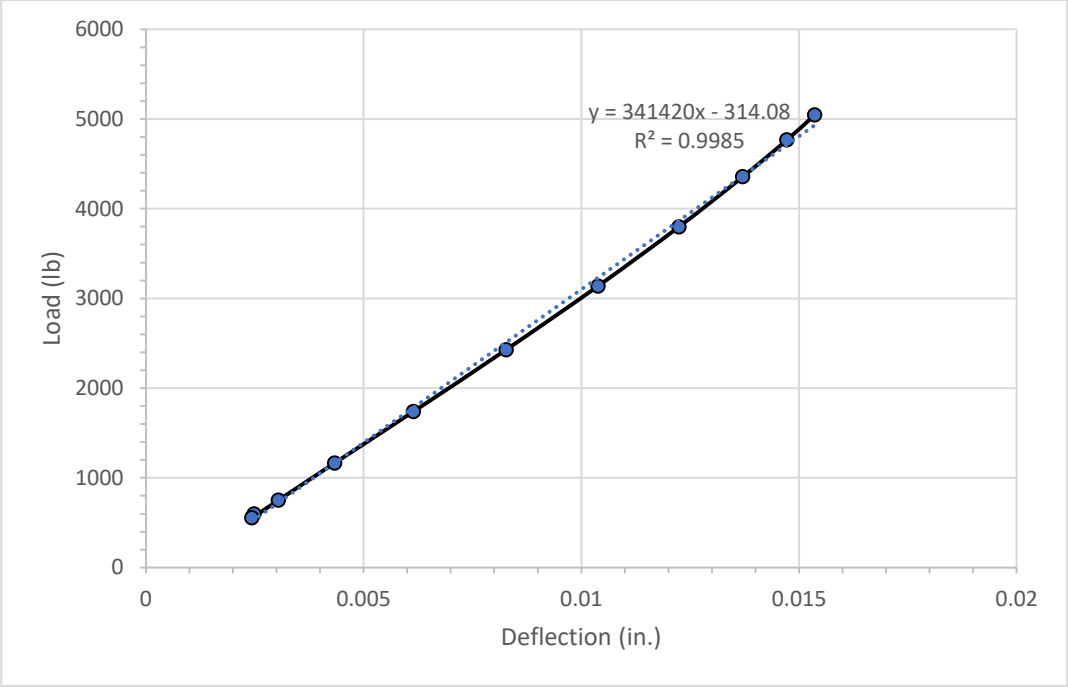

Figure 111: Load vs. deflection for Ductal® slab 3, single load cycle selected from day 25

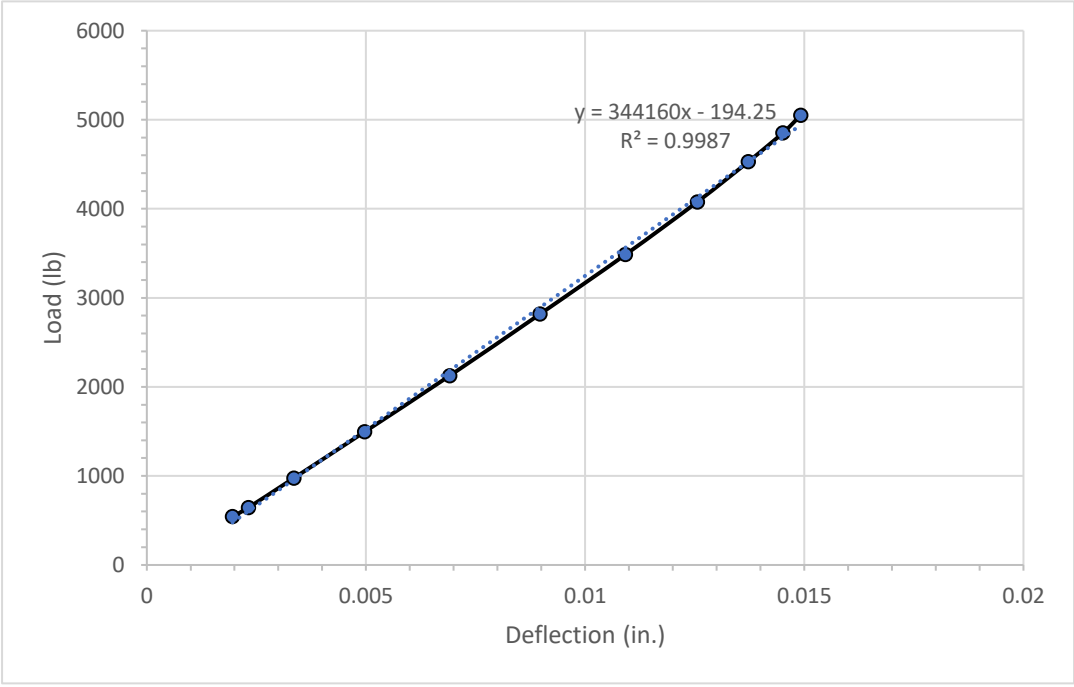

Figure 112: Load vs. deflection for Ductal® slab 3, single load cycle selected from day 27

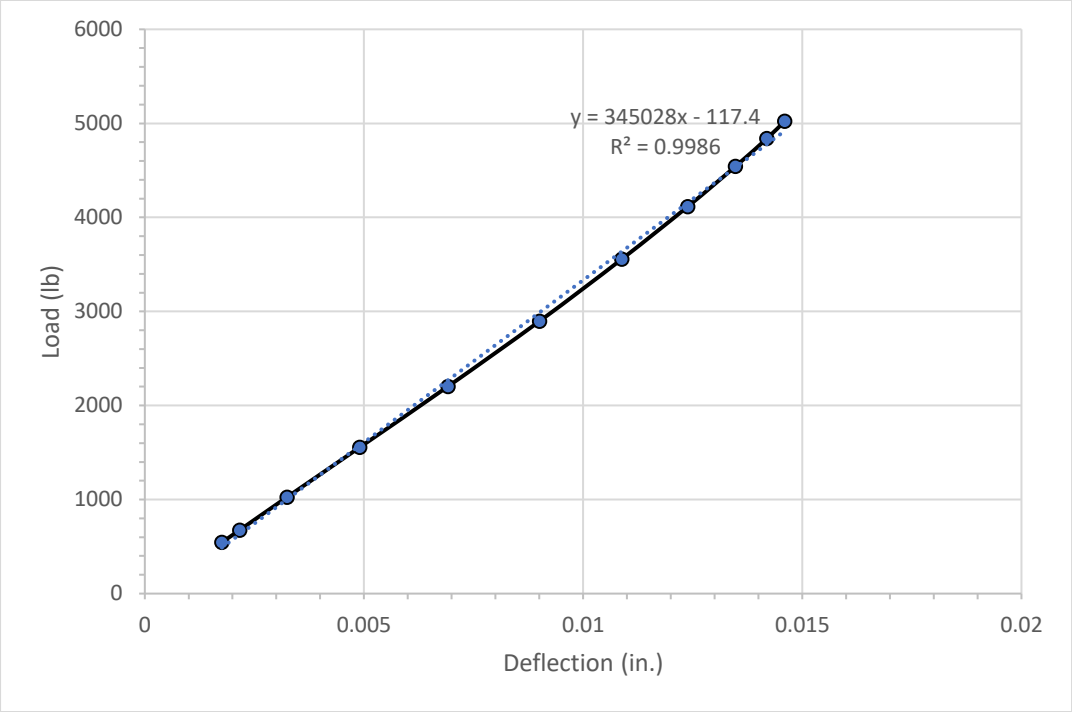

Figure 113: Load vs. deflection for Ductal® slab 3, single load cycle selected from day 29

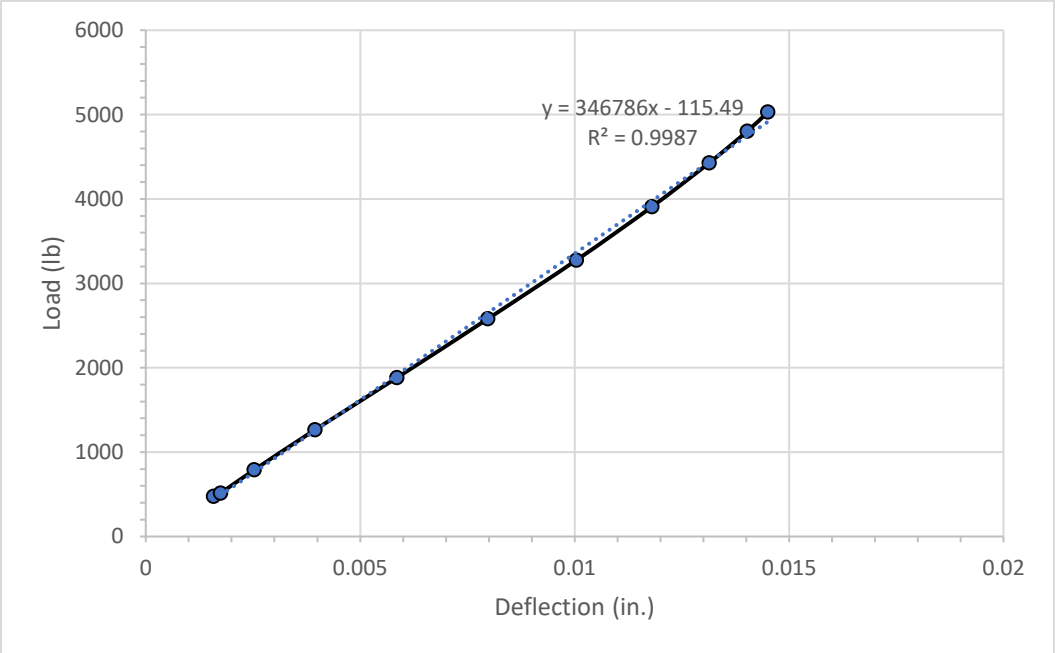

Figure 114: Load vs. deflection for Ductal® slab 3, single load cycle selected from day 31

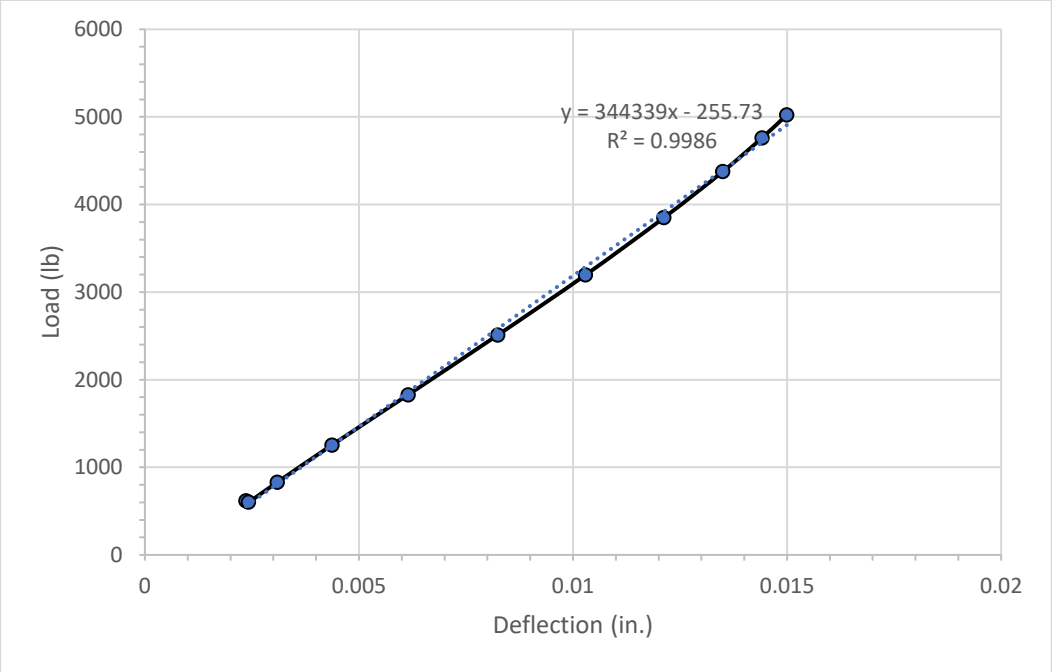

Figure 115: Load vs. deflection for Ductal® slab 3, single load cycle selected from day 33

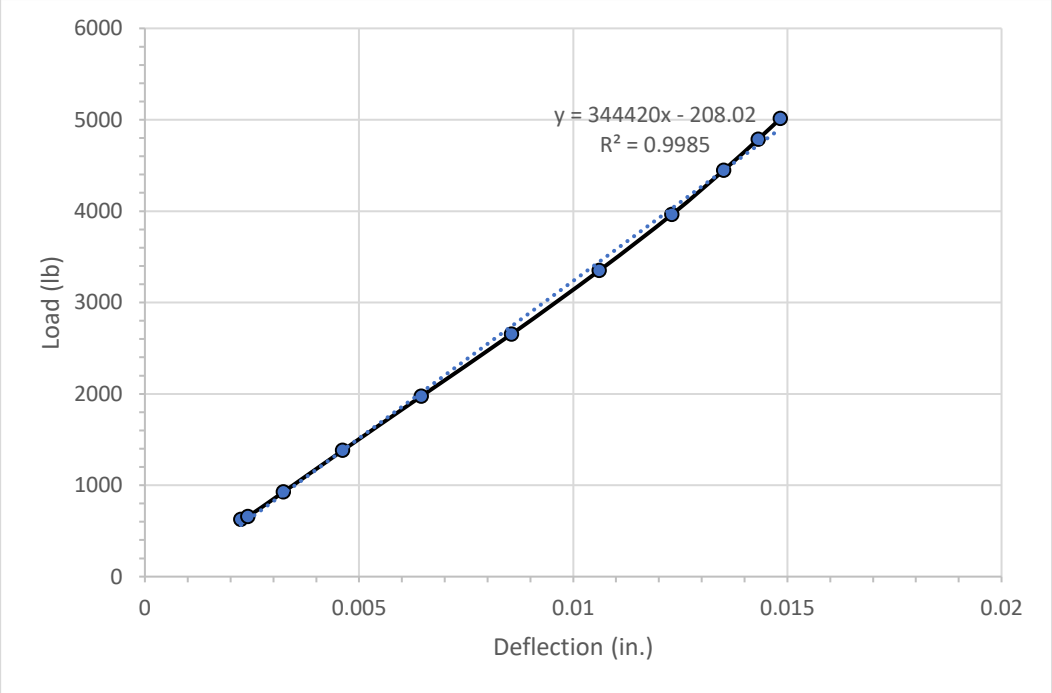

Figure 116: Load vs. deflection for Ductal® slab 3, single load cycle selected from day 35

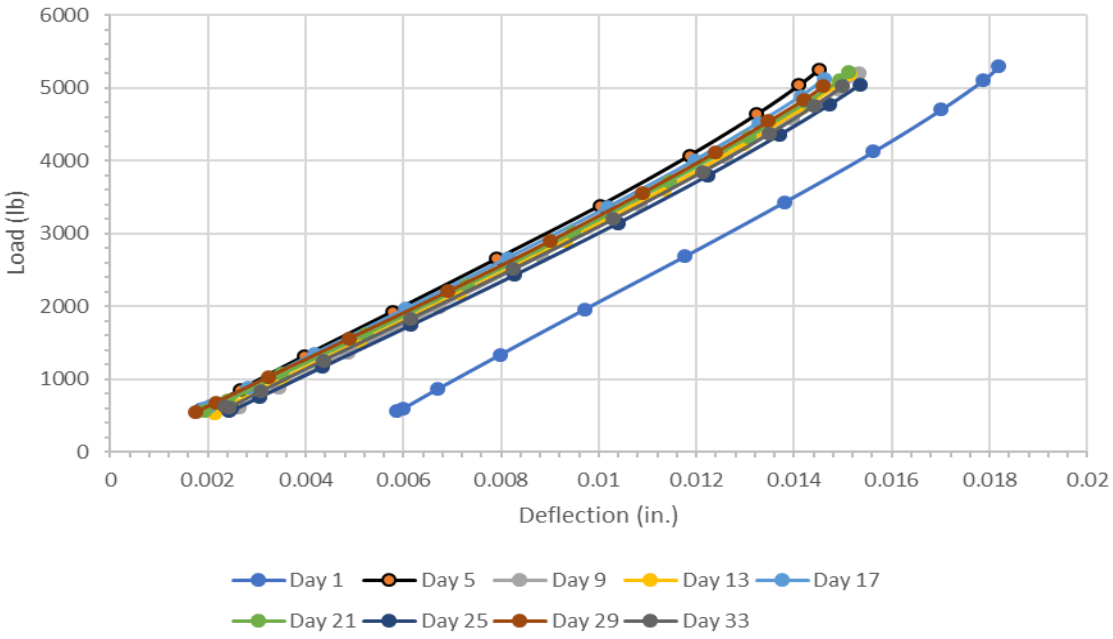

Figure 117: Comparison of load vs. deflection curves of Ductal® for multiple days

Figure 118 shows the stiffness vs. time plot for the 35 days period of cyclic testing. There was a general decrease in stiffness over time steadily. Figure 119 shows residual deflection vs. time plot for 35 days period of cyclic testing. The total residual deflection was 0.012 in.

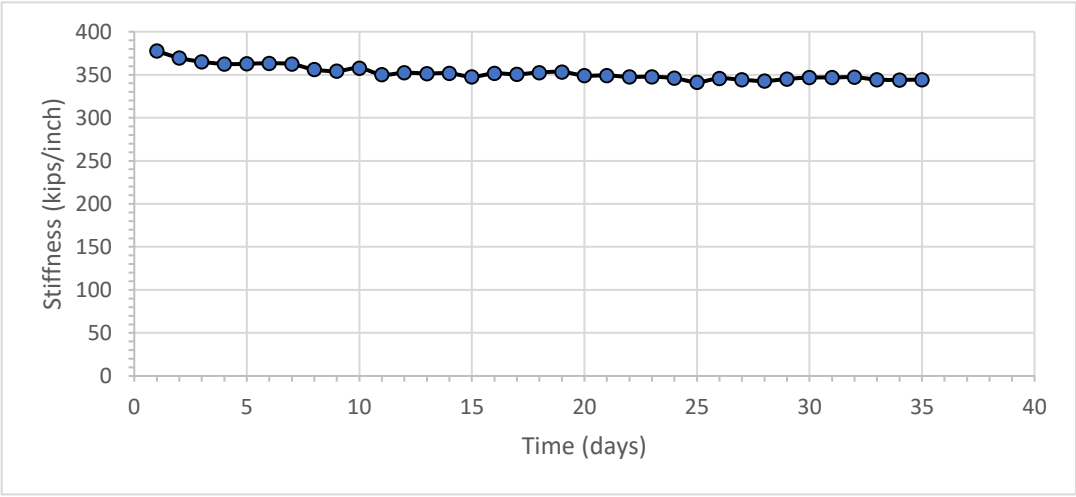

Figure 118: Ductal® slab 3 stiffness over the 35-day loading period

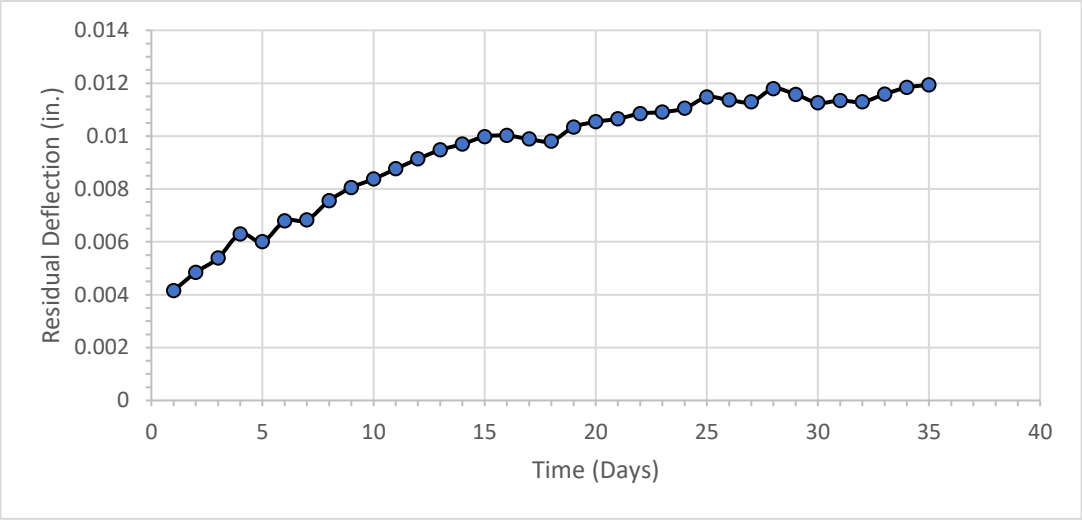

Figure 119: Residual deflection over the course of the 35-day cyclic testing period for Ductal® slab 3

4.7) Comparison of Slabs 1, 2, and 3

4.7.1) Comparison of J3 Slabs 1, 2, and 3

Figure 120 shows J3 UHPC load vs. deflection for the initial loading from the static tests of slabs 1 and 2 and one cyclic load from slab 3. Slab 3 has steeper slop compared to slabs 1 and 2. Slabs 1 and 2 have very similar slope, which demonstrates that they have similar flexural behavior. Slab 3 has a slightly steeper slope than slabs 1 and 2. The trends of all three slabs are similar. Slabs 1 and 2 reached a much higher flexural capacity than anticipated, which can be attributed to UHPC providing additional strength than a monolithic normal concrete slab at the critical section.

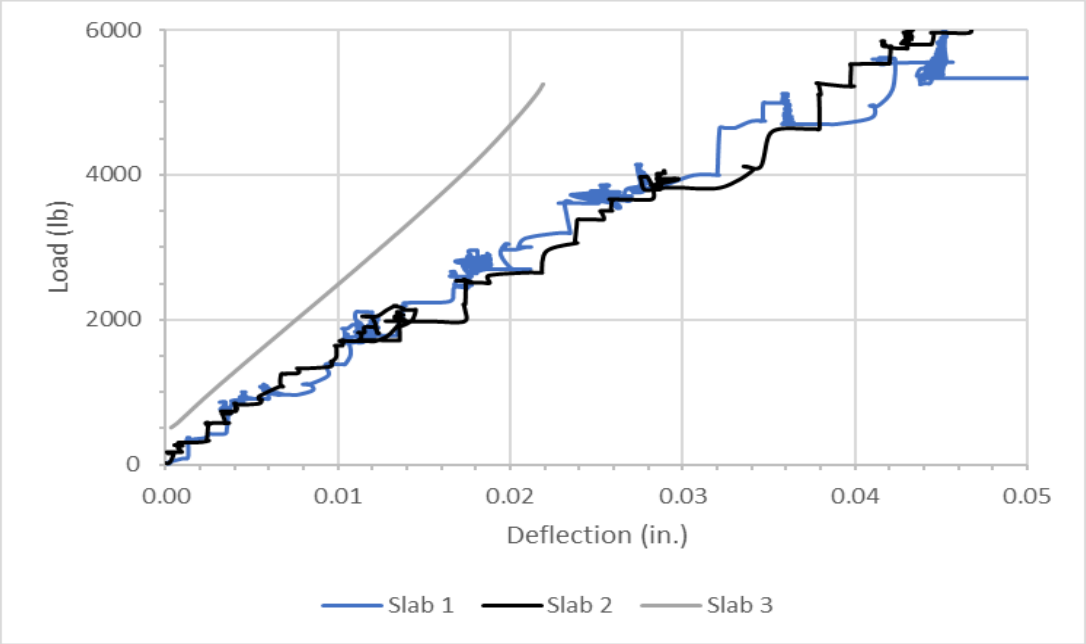

Figure 120: Load vs. deflection curve for initial portion of loading for all 3 slabs (J3)

4.7.2) Comparison of Ductal® Slabs 1, 2, and 3

Figure 121 shows J3 UHPC load vs. deflection for the initial loading from the static tests of slabs 1 and 2 and one cyclic load from slab 3. Slab 3 has steeper slope compared to slabs 1 and 2. Slabs 1 and 2 have very similar slopes, which demonstrates that they have similar flexural behavior. The slab 3 curve is sandwiched between slabs 1 and 2. The trends of all three slabs are similar. Slabs 1 and 2 reached a much higher flexural capacity than anticipated, which can be attributed to UHPC provide additional strength than a monolithic normal concrete slab.

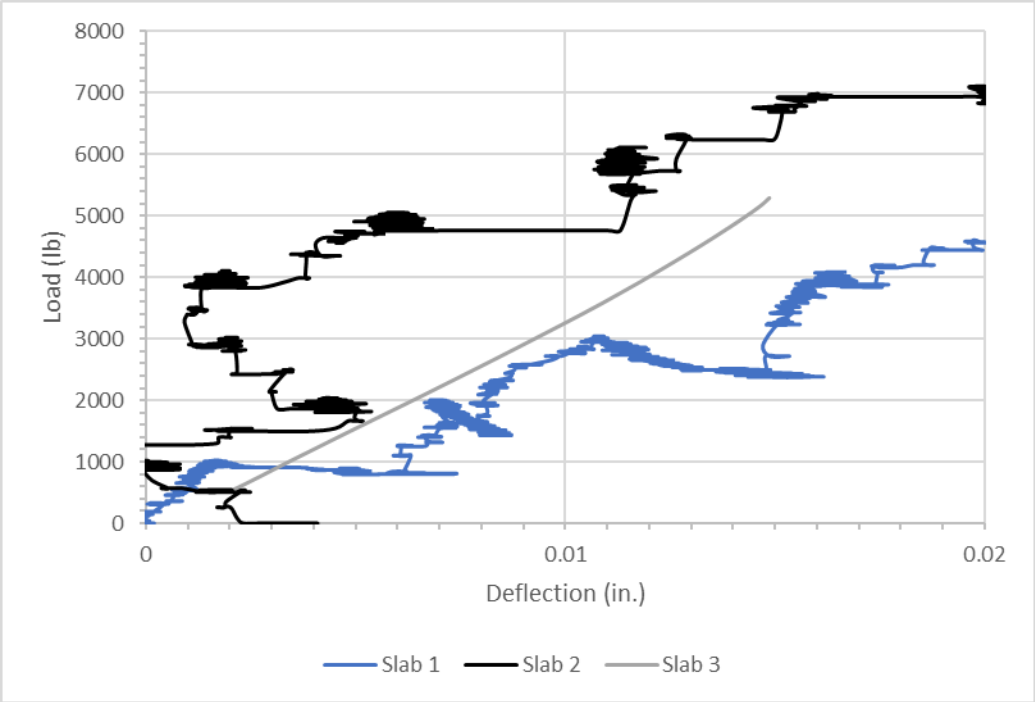

Figure 121: Load vs. deflection curve for initial portion of loading for all 3 slabs (Ductal®)

4.8) Comparison of Results to Coleman (2018) and Funderburg (2018) Studies

The studies conducted by Funderburg (2018) and Coleman (2018) focused on proprietary and non-proprietary UHPC as full-depth joint replacements respectively. Table 6 shows a comparison of cracking and ultimate loads between half-depth and full-depth J3 joints. The cracking load for slab 2 in both cases are less than values for slab 1, however slabs 1 and 2 for each material share the same design and construction. For the half-depth joint, slab 2 may have cracked due to applying cyclic load before switching to static load. For the full-depth joints, slab 2 was inaccurately loaded initially as it was mistakenly loaded constantly instead of being loaded in 1-kip increments (Coleman, 2018). The cracking load for the half-depth joints is approximately half that of full-depth joints. The larger cracking load for the full-depth joints could be attributed to greater volume of UHPC providing additional strength along with the smaller total interface between the conventional concrete and UHPC. The ultimate load for slab

1 has similar values. For slab 2, the half-depth joint has 7% more ultimate load than the full-depth joint, which may have been caused by inaccurate loading on the slab 2 full-depth joint. The average ultimate load for the half-depth J3 joints (33.8 kips) is only 4% greater than ultimate load of full-depth J3 joints (32.3 kips).

Table 6: Comparison of cracking and ultimate loads (kips) between half-depth and full depth J3 joints

	Half-depth J3 Joints	Full-depth J3 Joints
Slab 1 Cracking Load	5.9	10.5
Slab 2 Cracking Load	4.0	8.2
Average Cracking Load	5.0	9.4
Slab 1 Ultimate Load	35.0	34.3
Slab 2 Ultimate Load	32.5	30.3
Average Ultimate Load	33.8	32.3

Table 7 shows a comparison of cracking and flexural moments between half-depth and full-depth J3 joints since the span length of the half-depth and full-depth tests differed slightly. The average cracking moment for the full-depth J3 joints (19.0 kip-ft) is 53% greater than the average cracking moment for the half-depth J3 joints (8.9 kip-ft). The average maximum flexural moment for the full-depth J3 joints (65.4 kip-ft) is 7% greater than ultimate moment of half-depth J3 joints (60.6 kip-ft).

Table 7: Comparison of cracking and flexural moments (kip-ft) between half-depth and full depth J3 joints

	Half-depth J3 Joints	Full-depth J3 Joints
Slab 1 Cracking Moment	10.6	21.3
Slab 2 Cracking Moment	7.2	16.6
Average Cracking Moment	8.9	19.0
Slab 1 Flexural Moment	62.8	69.5
Slab 2 Flexural Moment	58.3	61.4
Average Flexural Moment	60.6	65.4

Table 8 shows a comparison between the half-depth and full-depth Ductal® joints from the Funderburg (2018) study. The cracking loads for the half-depth joints are greater than half of the cracking loads of the full-depth joints. The larger cracking load for the full-depth joints could be attributed to greater volume of UHPC providing additional strength and the smaller total area of interface between the conventional concrete and the UHPC. There is not much difference in the ultimate loads for both cases. The average ultimate load of the half-depth Ductal® joints (35.9 kips) is only 2% less than ultimate load of the full-depth Ductal® joints (36.7 kips).

Table 8*: *Comparison of cracking and ultimate loads (kips) between half-depth and full depth Ductal® joints

	Half-depth Ductal® Joints	Full-depth Ductal® Joints
Slab 1 Cracking Load	7.5	10.9
Slab 2 Cracking Load	7.0	13.1
Average Cracking Load	7.3	12.0
Slab 1 Ultimate Load	35.8	36.2
Slab 2 Ultimate Load	36.0	37.2
Average Ultimate Load	35.9	36.7

Table 9 shows a comparison of cracking and flexural moments between half-depth and full-depth Ductal® joints since the span length of the half-depth and full-depth tests differed slightly. The average cracking moment for the full-depth Ductal® joints (24.3 kip-ft) is 46% greater than average cracking moment for the half-depth J3 joints (13.1 kip-ft). The average flexural moment for the full-depth J3 joints (74.4 kip-ft) is 13% greater than ultimate moment of half-depth J3 joints (64.4 kip-ft).

From Tables 6 and 8, the ultimate load of the half-depth J3 joints can be compared to that of half-depth Ductal® joints. The average ultimate load of the half-depth J3 joints (33.8 kips) is only 6% less than ultimate load of half-depth Ductal® joints (35.9 kips).

From Tables 7 and 9, the ultimate flexural moment of the half-depth J3 joints can be compared to that of half-depth Ductal® joints. The average ultimate flexural moment of the half-depth J3 joints (60.6 kip-ft) is only 6% less than ultimate moment of the half-depth Ductal®

joints (64.4 kip-ft). The cracking moment for the half-depth joints is approximately half that of full-depth joints.

Table 9: Comparison of cracking and flexural moments (kip-ft) between half-depth and full depth Ductal® joints

	Half-depth Ductal® Joints	Full-depth Ductal® Joints
Slab 1 Cracking Moment	13.5	22.1
Slab 2 Cracking Moment	12.6	26.5
Average Cracking Moment	13.1	24.3
Slab 1 Flexural Moment	64.2	73.3
Slab 2 Flexural Moment	64.6	75.4
Average Flexural Moment	64.4	74.4

5) Findings, Conclusions, Recommendations, and Future Work

The purpose of this study was to explore the feasibility of using the alternative UHPC mix design (J3) developed in the Looney et al. (2019) study and compare to the proprietary LafargeHolcim product Ductal®. Another primary purpose was to analyze performance of half-depth UHPC slab joints to determine if they are comparable to full-depth joints in performance. This section summarizes the findings, conclusions, and recommendations from this research study.

5.1) Findings

The following findings were identified throughout the course of this research study:

- Heat curing of UHPC increased the early age compressive strength and accelerated setting time.
- The ultimate flexural load capacity of J3 slab joint 1 (35.0 kips) exceeded the calculated flexural load capacity of a monolithic conventional concrete slab of the same size (27.3 kips).
- The ultimate flexural load capacity of J3 slab joint 2 (32.5 kips) exceeded the calculated flexural load capacity of a monolithic conventional concrete slab of the same size (27.3 kips).
- The ultimate flexural load capacity of Ductal® slab joint 1 (35.8 kips) exceeded the calculated flexural load capacity of a monolithic conventional concrete slab of the same size (27.3 kips).

- The ultimate flexural load capacity of Ductal® slab joint 2 (36.0 kips) exceeded the calculated flexural load capacity of a monolithic conventional concrete slab of the same size (27.3 kips).
- The average ultimate load of the half-depth J3 joints (33.8 kips) was approximately 4.5% greater than ultimate load of full-depth J3 joints (32.3 kips).
- The average ultimate load of half-depth Ductal® joints (35.9 kips) was only 2.2% less than ultimate load of full-depth Ductal® joints (36.7 kips).
- The average ultimate load and average flexural moment of half-depth J3 joints were only 6% less than ultimate load of the half-depth Ductal® joints.
- The average cracking load and moment of the full-depth J3 joints were 2.1 times greater than the average cracking load of the half-depth J3 joints.
- The average cracking load of full-depth Ductal® joints was 1.7 times greater than the average cracking load of the half-depth Ductal® joints.
- The average cracking moment for the full-depth J3 joints (19.0 kip-ft) was 53% greater than the average cracking moment for the half-depth J3 joints (8.9 kip-ft).
- The average ultimate flexural moment for the full-depth J3 joints (65.4 kip-ft) was 7% greater than the ultimate load of the half-depth J3 joints.
- The average cracking moment for the full-depth Ductal® joints (24.3 kip-ft) was 46% greater than the average cracking moment for the half-depth J3 joints (13.1 kip-ft).
- The average ultimate flexural moment for the full-depth J3 joints (74.4 kip-ft) was 13% greater than the ultimate moment of the half-depth J3 joints (64.4 kip-ft).

5.2) Conclusions

Based on the results of the testing described in this study, the following conclusions were made:

- Heat curing of UHPC is necessary to increase early age compressive strength of the material.
- The ultimate flexural load capacity of all slabs (both J3 and Ductal® UHPC joints) exceeded the calculated failure load of a monolithic conventional concrete, indicating that UHPC joint provided additional strength to the slab.
- The half depth slabs have a lower cracking load than the full-depth slabs in general.
- The flexural strength of the half-depth J3 slab joints in this study is comparable to those of half-depth Ductal® slab joints.
- The flexural strength of the half-depth J3 slab joints in this study is comparable to those of full-depth J3 slab joints in the Coleman (2018) study.
- The flexural strength of half-depth Ductal® slab joints in this study is comparable to those of full-depth Ductal® slab joints in the Funderburg (2018) study.
- The cracking load of all the half-depth UHPC slab joints tested was less than the calculated cracking load for a monolithic conventional concrete slab.
- The interface between the UHPC (J3 and Ductal®) and conventional concrete was observed to be a weak point.
- The flexural stiffness measured for the cyclically loaded slab 3 (J3 and Ductal®) steadily decreased throughout the course of cyclic loading.

- The flexural stiffness of the cyclically loaded J3 slab joint sharply decreased when the magnitude of the maximum cyclic load was increased. The magnitude of the maximum cyclic load was not increased for the Ductal® slab joint cyclic test.
- The UHPC alternative, J3, is an acceptable substitute for the proprietary product, Ductal® based on flexural strength for half-depth joints.
- The J3 half-depth joints could potentially be an acceptable substitute for full-depth J3 joints based on flexural strength. However, if half-depth joints are subjected to constant fatigue load, their performance may be reduced relative to full-depth joints due to their lower cracking load.
- The Ductal® half-depth joints could potentially be an acceptable substitute for full-depth Ductal® joints. However, if half-depth joints are subjected to constant fatigue load, their performance may be reduced relative to full-depth joints due to their lower cracking load.

5.3) Recommendations and Future Work

Based on the results of this research, the following recommendations are suggested for potential future projects:

- The remainder of the J3 slab 3 static and cyclic testing should be completed to accurately characterize and compare to the other slab joints in this study. In addition, comparison studies can be made with full-depth J3 slab joints tested in the Coleman (2018) study.
- The remainder of the Ductal® slab 3 static and cyclic testing should be completed to accurately characterize and compare to the other slabs in this study. In addition, comparison studies can be made with full-depth Ductal® slab joints tested in the Funderburg (2018) study.

- Additional studies on bond strength and performance of UHPC repair joints could potentially optimize the joint detail and mechanical properties of the joints.
- The UHPC alternative, J3, is a suitable repair material for bridge joints and can potentially be used instead of Ductal® in certain applications. Further research should be conducted to refine the mix design, identify the best method of applying heat curing, identify the best method for testing bond strength, and identify the best methods for determining other mechanical properties.

References

"Analysis Reveals 58,495 U.S. Bridges Are Structurally Deficient." (2020), *American Society of Civil Engineers (ASCE)*. Accessed May 9, 2020. https://www.asce.org/magazine/20160315-analysis-reveals-58,495-u-s--bridges-are-structurally-deficient/.

Arun Murugesan. (2014), "An Overview of Interface Behaviour between Concrete to Concrete." *International Journal of Advanced Structures and Geotechnical Engineering*, 03(02), 2014.

Coleman, R. (2018), "Comparative Study of Surface Preparation and Bond Angle Combinations for Bridge Repair Using Ultra-High Performance Concrete Alternative" M.S. Thesis, the University of Oklahoma, Norman, OK.

"Field Testing of an Ultra-High Performance Concrete Overlay." (2020), *U.S. Department of Transportation/Federal Highway Administration*. Accessed May 8, 2020. https://www.fhwa.dot.gov/publications/research/infrastructure/structures/bridge/17096/002.cfm.

Funderburg, C. (2018), "Evaluation of Surface Preparation And Bond Angle Combinations For Bridge Joint Replacement Using Ultra-High Performance Concrete" M.S. Thesis, the University of Oklahoma, Norman, OK.

Graybeal, B. (2010), "Behavior of Field-Cast Ultra-High Performance Concrete Bridge Deck Connections Under Cyclic and Static Structural Loading," FHWA-HRT-11-023, Federal Highway Administration, McLean, VA.

Graybeal, B. (2014), "Design and Construction of Field-Cast UHPC Connections," FHWA-HRT-14-084, Federal Highway Administration, McLean, VA.

Júlio, E. N., Branco, F. A., and Silva, V. D. (2004), "Concrete-to-concrete bond strength. Influence of the roughness of the substrate surface." *Construction and Building Materials*, 18(9), 675–681.

Looney, T., McDaniel, A., Volz, J., and Floyd, R. (2019), “Development and Characterization of Ultra-High Performance Concrete with Slag Cement for Use as Bridge Joint Material”, *British Journal of Civil and Architecture Engineering*, 1(2), 1-14.

Peters, W. (2018), "Oklahoma DOT Implementation of UHPC: Projects, Future Plans, and Interactive Discussion," Ultra-High Performance Concrete Connections for Prefabricated Bridge Elements Workshop, Oklahoma City, OK, October 10, 2018.

“Policy Statement 208 - Bridge Safety.” (2020), *American Society of Civil Engineers (ASCE)*. Accessed May 8, 2020. https://www.asce.org/issues-and-advocacy/public-policy/policy-statement-208---bridge-safety/.

Tayeh, B. A., Abu Bakar, B. H., Megat Johari, M. A., and Voo, Y. L. (2013), “Evaluation of bond strength between normal concrete substrate and ultra-high performance fiber concrete as a repair material,” *Procedia Engineering*, 54, 554-563.

Wang, R., Xiaojian, G., Huanghuang, H., and Guangshuai, H. (2017), “Influence of Rheological Properties of Cement Mortar on Steel Fiber Distribution in UHPC.” *Construction and Building Materials* 144, 65–73. doi:10.1016/j.conbuildmat.2017.03.173.

Yazıcı, H., Yiğiter, H., Karabulut, A. Ş., and Baradan, B. (2008), “Utilization of fly ash and ground granulated blast furnace slag as an alternative silica source in reactive powder concrete.” *Fuel*, 87(12), 2401–2407.

Yu, R., Spiesz, P. R., and Brouwers, H. J. H. (2014), “Mix design and properties assessment of Ultra-High-Performance Fibre Reinforced Concrete (UHPFRC)”. *Cement and Concrete Research*, 56, 29-39. https://doi.org/10.1016/j.cemconres.2013.11.002

Zhang, G., Ying, Z., and Yangyang, Z. (2018), “Fatigue Tests of Concrete Slabs Reinforced with Stainless Steel Bars.” *Advances in Materials Science and Engineering*, 2018, 1–5. doi:10.1155/2018/5451398.

Appendix A: Additional Photos of Specimens and Test Setup

Figure 122: Steel fibers added to UHPC mixture

Figure 123: UHPC being mixed using large horizontal axis high-shear mixer

Figure 124: UHPC inside concrete transfer bucket

Figure 125: UHPC flow test using mortar flow table

Figure 126: UHPC cylinders being ground plane for compression testing

Figure 127: UHPC cylinders after compressive strength test

Figure 128: Conventional concrete panel after removing wooden form

Appendix B: Calculations

Cracking Moment and Corresponding Load

$$M_{cr} = \frac{f_r I_s}{y_t}$$

where

$f_r = 7.5\sqrt{f'_c} = 7.5\sqrt{4000psi} = 474.3\ psi$

$I_s = \frac{bh^3}{12} = \frac{(48\ in.)(8\ in.)^3}{12} = 2{,}048\ in.^4$

$y_t = 4\ in.$

Hence,

$$M_{cr} = \frac{f_r I_s}{y_t} = \frac{(474.3\ psi)(2{,}048\ in.^4)}{(4\ in.)} = 242{,}863\ lb \cdot in = 20.24\ kip \cdot ft$$

To find the corresponding point load for a non-symmetric simple span of length L = A+B:

$$P = \frac{ML}{AB} = \frac{(20.24\ kip \cdot ft)(7.45\ ft)}{(4.23\ ft)(3.16\ ft)} = 11.1\ kips$$

Note that

M_{cr} = cracking moment, lb-in.

f_r = modulus of rupture of concrete, psi

I_s = moment of inertia of gross section of slab about cetroidal axis, in.^{4}

b = width of compression face of member, in.

$h =$ overall depth of member, in.

$y_t =$ distance from the centroid of the cross section to the tension face, in.

$f'_c =$ compressive strength of concrete taken as 4000 psi

Flexural Capacity and Corresponding Load

Assuming both layers of steel are in tension during loading,

$$M_n = A_{s1} f_y \left(d_1 - \frac{a}{2}\right) + A_{s2} f_y \left(d_2 - \frac{a}{2}\right)$$

where

$A_{s1} = A_{s2} = 4(0.31\ in.^2) = 1.24\ in.^2$

$f_y = 60\ ksi$

$d_1 = 6.063\ in.$

$d_2 = 2.44\ in.$

$$a = \frac{2A_s f_y}{0.85 f'_c b} = \frac{2(1.24\ in.^2)(60\ ksi)}{0.85(6\ ksi)(48\ in.)} = 0.61\ in.$$

$$c = \frac{a}{\beta_1} = \frac{0.61\ in.}{0.85} = 0.72\ in.$$

Checking the assumption that the steel yields:

$$\varepsilon_{s1} = \frac{0.003}{c}(d_1 - c) = \frac{0.003}{0.72}(6.063 - 0.72) = 0.022 > 0.00207$$

$$\varepsilon_{s2} = \frac{0.003}{c}(d_1 - c) = \frac{0.003}{0.72}(2.44 - 0.72) = 0.0072 > 0.00207$$

Hence,

$$M_n = (1.24\ in.^2)(60\ ksi)\left[\left(6.063\ in. - \frac{0.61\ in.}{2}\right) + \left(2.44\ in. - \frac{0.61\ in.}{2}\right)\right]$$

$$= 587.2\ kip \cdot in = 48.9\ kip \cdot ft$$

To find the corresponding point load for a non-symmetric simple span of length L = A+B:

$$P = \frac{ML}{AB} = \frac{(48.9\ kip \cdot ft)(7.45\ ft)}{(4.23\ ft)(3.16\ ft)} = 27.3\ kips$$

Note that

$M_n =$ nominal flexural strength at section, lb-in.

$A_{s1} =$ area of the bottom layer of longitudinal tension reinforcement, in.^{2}

$A_{s2} =$ area of the top layer of longitudinal tension reinforcement, in.^{2}

$f_y =$ specified yield strength of reinforcement, ksi

$d_1 =$ distance from extreme compression fiber to centroid of bottom layer of longitudinal tension reinforcement, in.

$d_2 =$ distance from extreme compression fiber to centroid of top layer of longitudinal tension reinforcement, in.

$\varepsilon_{s1} =$ value of net tensile strain in the bottom layer of longitudinal tension reinforcement, unitless

$\varepsilon_{s1} =$ value of net tensile strain in the top layer of longitudinal tension reinforcement, unitless